UNIVERSITÀ DI CAMERINO

SCHOOL OF ADVANCED STUDIES IN PHARMACEUTICAL SCIENCES
XXI CYCLE

IMPACT OF SOLID STATE PROPERTIES OF SODIUM NAPROXEN HYDRATES ON THEIR TECHNOLOGICAL PERFORMANCE

By

Ledjan MALAJ

ACADEMIC DISSERTATION

ITALY, JANUARY 2009

Supervisor: Prof. Ass. Piera DI MARTINO
Department of Chemical Sciences
Faculty of Pharmacy
University of Camerino
Camerino, Italy

Course
Coordinator: Prof. Piero ANGELI
Department of Chemical Sciences
Faculty of Pharmacy
University of Camerino
Camerino, Italy

Final Exam Committee: Prof. Stavros Malamataris
Department of Pharmaceutical Technology
School of Pharmacy
Aristotle University of Thessaloniki
Thessaloniki, Greece

Prof. Mariapia Abbracchio
Department of Pharmacological Sciences
University of Milan
Milan, Italy

Prof. Carlo Melchiorre
Department of Pharmaceutical Sciences
University of Bologna
Bologna, Italy

TO ELA & ANRI

SUMMARY

Sodium naproxen, a member of the class of non-steroidal anti-inflammatory drugs (NSAIDs), exists in one anhydrous form and four hydrated ones: one monohydrate, two dihydrate and one tetrahydrate. Sodium naproxen (SN) forms can be summarised as follows:

- *the anhydrous sodium naproxen (ASN) is the commercialised form;*
- *the monohydrated sodium naproxen (MSN), is obtained by dehydration of the dihydrated sodium naproxen (DSN), according to Kim and Rousseau (2004);*
- *the dihydrated sodium naproxen (DSN) is obtained by exposing the ASN to 55% RH according to Di Martino et al. (2001);*
- *the dihydrated sodium naproxen (CSN) is obtained by crystallizing sodium naproxen from water, according to Di Martino et al. (2001) and Kim and Rousseau (2004);*
- *the tetrahydrated form (TSN) is obtained by exposing the ASN at 75% RH according to Di Martino et al. (2007).*

The hydration state of SN may strongly influence its physico-chemical and technological properties and consequently its bioavailability. Water exposure during storage or pharmaceutical processing can cause changes in the crystal lattice of the starting material. Therefore, a profound understanding and characterisation of SN solid state and phase transitions throughout storage or processing are important in predicting and defining its technological performance.

In fact, it was observed that following wet granulation process by high-shear mixer-granulator, the drug hydrated to the tetrahydrated form. Performing two different drying procedures, granules of different water content and crystallographic characteristics were obtained. This means that differences in drying procedures could lead to products of different crystallographic properties. The behaviour under compression revealed that one

of the batches offered the best tabletability and compressibility. These results make it possible to state that differences in the crystallographic properties and water content of sodium naproxen are such that different hydration/drying processes can alter the drug crystal form and thus the tabletability of the resulting granules.

Next, the water uptake of ASN during storage was evaluated. A correlation between water uptake by ASN at two different relative humidities and modifications in tableting and densification behaviour under hydration exists. Models for the hydration kinetics of ASN at 55% and 86%, corresponding to the formation of the dihydrated and tetrahydrated forms respectively, were evaluated assuming Eyring's dependence on temperature. Tabletability, compressibility, compactibility and densification behaviour were determined using an instrumented single punch tablet machine.

Kinetic data is consistent with a model where water molecules enter the crystal preferentially along hydrophilic tunnels existing in the crystal structure and corresponding to the propionate side chain. Water inclusion perturbs the crystallographic structure, causing slight structural changes according to the amount and associated to an increase in entropy. The interposition of water molecules between SN molecules weakens intermolecular bonds, and these sites can behave like sliding planes under compression. Such structural changes may explain the improved compression behaviour and modified densification propensity mechanism. Kinetic data describing the water hydration mechanism of ASN explains in an original way the improved tableting and densification properties under hydration.

Because different hydration/dehydration processes can alter the drug crystal form, the isothermal dehydration of some of SN hydrates was observed by thermogravimetry at several temperatures. The rate of water removal from the crystal was used to determine the mechanism of dehydration in the solid state, by fitting results with selected expressions corresponding to the most common solid-state processes. The water loss was then evaluated according to Eyring's equation, and both changes in activation enthalpy (ΔH^*) and activation entropy (ΔS^*) were estimated from rate constant values. Experiments made it possible to distinguish different dehydration mechanisms for these hydrate forms, and in particular, to discern the dehydration behaviour of CSN and DSN dihydrate forms. These

results add new evidence supporting the X-ray powder diffraction study and showing different patterns for these two forms. X-ray powder diffractometry evaluation of the phase transitions occurring during dehydration of these two dihydrate forms showed that they vary according to dehydration temperature.

To finalize our study, the technological and mechanical properties of several solid forms of SN were investigated. Particular attention has been made in order to reduce differences, among the samples, in crystal habit, particle size and distribution, amount of absorbed water, so that only the hydration degree and the crystalline structure might affect the technological behaviour of powders. Thus, the compression behaviours were determined by using an instrumented single punch tablet machine and evaluated through the tabletability, compressibility and compactibility analysis. The results showed that the compression ability was influenced by the hydration degree and the crystalline form. In general, the tabletability was mainly due to the ability of particles to close up by establishing numerous bonds.

Keywords: Sodium naproxen; Hydrates; Hydration; Dehydration; Wet granulation; High-Shear Mixer-Granulator; Tabletability; Compressibility; Densification; Thermal analysis, X-ray powder diffraction.

TABLE OF CONTENTS

I. INTRODUCTION

I.1. AIMS OF THE STUDY

ASN can be differently hydrated or dehydrated according to the vapour pressures during storage and pharmaceutical processing. The hydration/dehydration processes promote changes in crystallographic structure. The changes in crystallographic structure can influence drug performance, such as mechanical behaviour, stability, dissolution rate and often bioavailability. Because of this, the physico-chemical drug metastability must be fully evaluated before and during the technological development.

The main objective of this thesis was to investigate the influence of the solid state properties on the technological performance of sodium naproxen in its different hydrate forms. In addition, it is essential to carefully evaluate if changes in the experimental procedures of technological processes or storage conditions may affect the physico-chemical stability of the hydrate forms.

Several objectives may be therefore sequentially considered:

- Demonstrate that technological processes such as wet-granulation/drying procedures can strongly influence the crystallographic form of SN.
- Prove that differences in compression behaviour of SN can be ascribed to hydration degree, so that the behaviour of the active raw material under compression will be examined at different hydration degrees.
- Explore the mechanism of crystal hydration from anhydrous SN to DSN and TSN.
- Analyse the effect of hydration on the compression properties and densification mechanism of SN powders.
- Establish a relationship between the hydration of SN at different relative levels of humidity and its tableting and densification behaviour.
- Investigate if differences in tableting and densification behaviour result from the mechanisms of water inclusion inside the crystal and the consequent perturbations caused by them.
- Clarify the dehydration mechanism of some of the hydrated forms of SN.

- Describe differences between the two dihydrate forms of SN obtained by two different procedures (hydration at a relative humidity of 55% and crystallization from water).
- Describe the phase transitions during dehydration according to the starting material and the experimental temperature.
- Clarify the effect of water inclusion in the crystal lattice and the effect of crystalline structure on the compression behaviour of sodium naproxen.

I.2. SOLID STATE IN PHARMACEUTICAL SCIENCES

Solid is the most commonly encountered phase in pharmaceutical practise (Cui, 2007). The accurate choice and the fully characterization of the solid phase influence the quality of manufacturing process, the performance and the bioavailability of the final dosage form of the drug.

Solid phase can be classified, based upon the order of molecular packing, into two major types of subphases that are crystalline form and amorphous form (Figure 1.1).

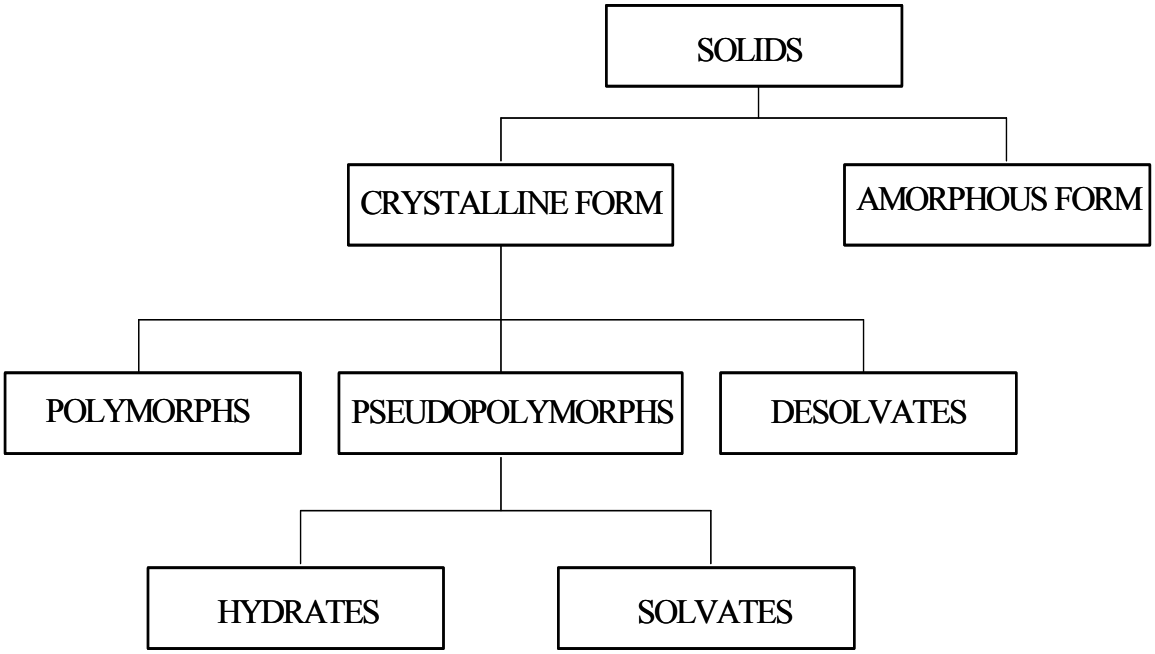

Figure 1.1.

Schematic representation of solid state forms.

When applied to solids, the adjective, crystalline, implies an ideal crystal in which the structural units, termed unit cells, are repeated regularly and indefinitely in three dimensions in space (Figure 1.2.a and 1.2.b). The unit cell has a definite orientation and shape defined by the translational vectors, *a*, *b*, and *c*, and hence has a definite volume, *V*, that contains the atoms and molecules necessary for generating the crystal.

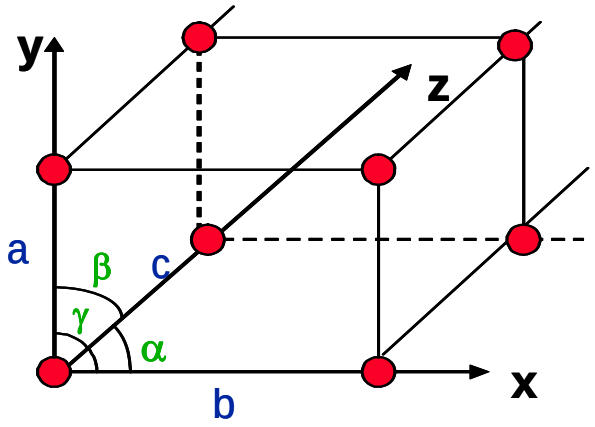

(a)

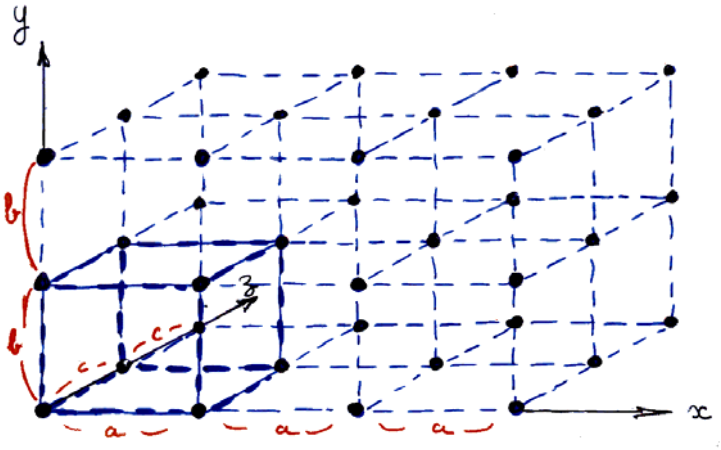

(b)

Figure 1.2

Unit cell with cell dimensions (a) and three dimensional structural organization of a crystalline lattice (b).

Each crystal can be classified as a member of one of seven possible crystal systems or crystal classes (Table 1.1) that are defined by the relationships between the individual dimensions, *a*, *b*, and *c*, of the unit cell and between the individual angles, a, b, and γ of the unit cell (Brittain, 1999).

Table 1.1

Seven crystal systems

Crystal System	**Axial lengths and angles**
Cubic	$a = b = c$
	$\alpha = \beta = \gamma = 90°$
Tetragonal	$a = b \neq c$
	$\alpha = \beta = \gamma = 90°$
Orthorhombic	$a \neq b \neq c$
	$\alpha = \beta = \gamma = 90°$
Rhombohedral (Trigonal)	$a = b = c$
	$\alpha = \beta = \gamma \neq 90°$
Hexagonal	$a = b \neq c$
	$\alpha = \beta = 90°, \gamma = 120°$
Monoclinic	$a \neq b \neq c$
	$\alpha = \gamma = 90° \neq \beta$
Triclinic	$a \neq b \neq c$
	$\alpha \neq \beta \neq \gamma \neq 90°$

The structure of a given crystal may be assigned to one of the seven crystal systems, to one of the 14 Bravais lattices, and to one of the 230 space groups (Kim, 2005).

All the 230 possible space groups, their symmetries, and the symmetries of their diffraction patterns are compiled in the International Tables for Crystallography (Hahn, 1987).

Crystalline solids exist in three groups that are polymorphs, solvates or hydrates, and desolvates.

I.3. POLYMORPHISM AND POLYMORPHS

Polymorphism is the case in which one type of molecule can arrange into different crystalline forms. Polymorphs have different relative intermolecular and/or interatomic distances as well as unit cells, resulting in different physical and chemical properties such as density, hardness, tabletability, refractive index, melting point, enthalpy of fusion, vapor pressure, solubility, dissolution rate, other thermodynamic and kinetic properties and even color. The different crystal structures in polymorphs arise when the drug substance crystallizes in different crystal packing arrangements and/or different conformations. The occurrence of polymorphism is quite common among organic molecules, and a large number of polymorphic drug compounds have been noted and catalogued (Kuhnert-Brandstatter, 1971; Borka et al., 1990; Giron, 1995).

Furthermore, stresses during processing, such as drying, grinding, milling, wet granulation, oven drying and compaction, are reported to accelerate the phase transitions in pharmaceutical solids. The degree of polymorphic conversion will depend on the relative stability of the phases in question, and on the type and degree of mechanical processing applied. Keeping these factors in mind, it is desirable and usual to choose the most stable polymorphic form of the drug in the beginning and to control the crystal form and the distributions in size and shape of the drug crystals during the entire process of development. The presence of a metastable form during processing or in the final dosage form often leads to instability of drug release as a result of phase transformation (Rodriguez-Hornedo, 1992).

I.4. HYDRATES AND SOLVATES

Hydrates and solvates are formed by two compounds, when solvent molecules are present in the crystal lattice, leading to molecular adducts with the host molecules, which is different from polymorphs. Adducts frequently crystallize easier because two molecules often can pack together with less difficulty than single molecules. Since property changes by solvent-incorporation are analogous to polymorphism, the phenomenon of crystal solid adducts that possess solvents is called pseudopolymorphism and the compounds are called "pseudopolymorphs", in a sense to show their similarity to the "real" polymorphs (Bechtloff et al., 2001).

If the solvent is water, the molecular adducts are termed hydrates. Hydrates are especially relevant for pharmaceutical development because water is prevalent in manufacturing dosage forms.

The pharmaceutical importance of crystalline hydrates is summarized by Morris (Morris et al., 2001). The physicochemical stability and/or bioavailability of pseudopolymorphs may become a serious problem during new drug development. To prevent possible problems, the drug substance guideline of the United State Food and Drug Administration (FDA) states that «for approval of a new drug, "appropriate'' analytical procedures need to be used to detect polymorphs, hydrates and amorphous forms of the drug substance and also stresses the importance of controlling the crystal form of the drug substance during the various stages of product development» (Byrn et al., 1995). For example, study of the bioavailability of ampicillin has shown that blood serum concentrations of ampicillin by the anhydrous form were higher and reached earlier than those by the trihydrated form (Carstensen et al., 1993). It was deduced from the results of experiments that the differences of blood serum concentrations of ampicillin between the anhydrate and the trihydrate result from the differences in the aqueous solubility of those two forms.

Bulk drug substances are produced by several consecutive processes and unintentional interconversion among pseudopolymorphs may happen very frequently during the processes. For example, crystallization for the purpose of separation,

purification, or simply solidification can lead to the production of hydrated forms. Since the formation of pseudopolymorphs is affected by variables such as temperature, pressure, and polarity of solvents, changing operating variables during crystallization may result in transformation between pseudopolymorphs. Some anhydrous substances that yield hydrates are tamoxifen (Kojima et al., 2007), ampicilline, nitrofurantoine (Kojima et al., 2008), azythromicin (Gandhi et al., 2002).

Solvates may be formed when a pure organic solvent or a mixture of solvents is used as solvent for crystallizing the compound. Guillory et al. (1999) have discussed the various methods of preparation of hydrates and solvates in detail. Because solvates behave similarly to hydrates, common analytical techniques can be used for characterization of solvates and hydrates.

Drying process is usually employed to remove solvent-residues from crystals after crystallization.

If hydrated forms are wet and they are introduced into the drying process, not only solvents on the surface of the forms but also solvents incorporated in the lattice structures may be evaporated. Therefore, drying may result in the transformation of a hydrated form into a new form with a lower degree of hydration (Jørgensen et al., 2002; Morris et al., 2001; Airaksinen et al., 2003).

Removal of solvent from the crystals by drying may have an effect on the interconversion from one form to the other one. Zhu and Grant (2001) have studied the dehydration behaviour of nedocromil magnesium pentahydrate.

Some hydrated compounds may convert to an amorphous form upon dehydration and some may become chemically labile. For example, cephradine dihydrate dehydrates to become amorphous and undergoes subsequent oxidation (Haleblian et al., 1969). Dihydrophenylalanine anhydrate (Oberholtzer et al., 1979; Threlfall, 1995) crystallizes as prism-shaped crystals from ether and it is stable to oxidation; however, the dihydrated form grows as needle-like crystals and these crystals oxidize in air producing 70% phenylalanine in 10 minutes.

Changes in hydration state of crystalline drugs substances and excipients may occur frequently throughout the various steps of the manufacturing process or during storage and consequently the final product quality will not be the same as predicted.

Morris states that "substances may hydrate/dehydrate or solvate/desolvate in response to changes in environmental conditions, processing, or over time in a metastable thermodynamic state" (Morris et al., 1993).

In fact, technological processes, such as aqueous granulation, particle size reduction, film coating, and tablet compression all provide opportunities to "trap" a compound in a metastable form that may "relax" to a more stable form during the life of a dosage form. Alternatively, a kinetically favoured but thermodynamically unstable form may be converted during these processes to a more stable and less soluble form.

The phase transformations associated with exposure to water, such as during solubility measurements, wet granulation processes, dissolution studies and accelerated stability tests are likely to occur via solution mediation. Solution mediated phase transformations depend upon the solution phase to provide the mobility necessary to rearrange in the most stable form and hence are much faster than solid-state transformations. The rate of a solution-mediated transformation is proportional to the solubility of the species involved.

Temperature, pressure and relative humidity may increase the rate of phase transformation of hydrates by inducing mobility in the system. Solution-mediated phase transformations have been reported for many hydrate systems, such as theophylline crystals (Rodriguez-Hornedo et al., 1992), eprosartan mesylate (Sheng et al., 1999) and nedocromil sodium (Khankari et al., 1998).

Several authors have described the influence of the different steps of manufacturing and of storage conditions on the phase transitions of the drugs. For example, Otsuka et al. have demonstrated that wet granulation process causes the transformation of carbamazepine anhydrous forms to carbamazepine dehydrate form (Otsuka et al., 1999).

Sometimes, mechanical grinding of organometallic pseudopolymorphs using a mortar and pestle to prepare samples for powder X-ray diffraction experiments help water molecules become inserted into crystal lattice structures (Sukenik et al., 1975).

According to the study on transitions of carbamazepine (Shalaev et al., 1997), it was found that compression causes the instability of the dihydrated crystalline form.

Wöstheinrich and Schmidt (2001) reported that, during spray granulation, thiamine hydrochloride transforms to a monohydrate and during the final drying loses its water, and a dehydrated anhydrate is obtained. When a dehydrated anhydrate is exposed to ambient conditions during tabletting, again the monohydrate is formed. After storage for four months at room temperature the monohydrate converts to a hemihydrate. As a result, the tablet hardness and disintegration times are increased.

High humidity conditions during storage provide the crystallisation of theophylline monohydrate, which has a lower dissolution rate, in tablets (Herman et al., 1989; Ando et al., 1992; Adeyeye et al., 1995) and pellets (Herman et al., 1988; Herman et al., 1989).

Other examples have been reported for nitrofurantoin and caffeine, where the phase transformation to a hydrate form occurs in high humidity (Shefter and Highuchi, 1963; Otsuka et al., 1991; Ando et al., 1992).

Another consideration is the frequency with which hydrates are encountered in the pharmaceutical practise. Focusing on active drug substances, it is estimated that approximately one-third of the pharmaceutical actives are capable of forming crystalline hydrates (Stahl, 1980). The water molecule, because of its small size, can easily fill structural voids and, because of its multidirectional hydrogen bonding capability, is also ideal for linking a majority of drug molecules into stable crystal structures (Byrn et al., 1999). The mere presence of water in a system is not a sufficient reason to expect hydrate formation, because some compounds, though they are soluble in water, do not form hydrates. It is the activity of water in the medium that determines whether a given hydrate structure will form.

Apart from identifying and characterizing the phases during various stages of drug development, it is very important to gain an understanding of the dehydration/hydration mechanisms and kinetics. Many models have been developed to account for the dehydration kinetics of the crystalline hydrates (Byrn, 1982). These all assume certain

geometry and rely on some consistency of the system as the process proceeds. The dehydration kinetics to some extent will also depend upon the class of the hydrate system to which the drug belongs, particle size and morphology.

I.4.1. Classification of hydrates

Water molecule is small enough to fill the empty spaces formed when larger molecules are packed, and it interacts through hydrogen bonds to overcome some of the entropy of mixing. Crystalline hydrates have been classified by either structure or energetics aspects (Falk et al., 1973). The classification of crystalline hydrates of pharmaceutical interest by their structural characteristics is the most common, intuitive and useful approach.

Based in their structural aspects crystalline hydrates have been classified into three classes (Table 1.2) and these three classes are discernible by the commonly available analytical techniques (Morris, 1999).

Table 1.2

Classification of crystalline hydrates

Class	**1**	**2**	**3**
Description	Isolated lattice sites	Lattice channels a. Expanded channels b. Lattice planes c. Dehydrated hydrates	Metal-ion coordinated water

The first class, *isolated site hydrates*, represents the structures with water molecules that are isolated and kept from contacting other water molecules directly in the lattice structure. Therefore, water molecules exposed to the surface of crystals may be easily lost. However, the creation of holes that were occupied by the water molecules on the surface of

crystals does not provide access for water molecules inside the crystal lattice. The analyses of the hydrates in this class show sharp Differential Scanning Calorimetry (DSC) endotherms, a narrow Thermogravimetry (TGA) weight loss range and sharp O-H stretching frequencies in the infrared spectrum. The characterization of cephradine dehydrate (Florey, 1973), an example of this class of hydrates, was particularly important for understanding and illustrating this hydrate class.

The class two, *channel hydrates,* has water molecules structured in channels. The water molecules in this class lie continuously next to the other water molecules, forming "channels" through the crystal. The TGA and DSC data show interesting characteristics of channel hydrate dehydration. Early onset temperature of dehydration is expected and broad dehydration is also characteristic for the channel hydrates. This is because the dehydration begins from the ends of channels that are open to the surface of crystals. Then, dehydration keeps on happening until all water molecules are removed through the channels. Ampicillin trihydrate and theophilline belong to this class and are described by Byrn (Byrn, 1982) using light microscopy. As the crystal is heated on the microscope hot stage, the dehydration appears as a progressive darkening from the ends of the crystal toward the center. As the dehydration process continues, the crystal may change its structure or become amorphous.

Class two channel hydrates are subdivided in three subclasses:

a) expanded channels,
b) lattice planes,
c) dehydrated hydrates.

The expanded channel hydrates may take up additional moisture in the channels when exposed to high humidity and the crystal lattice may expand. The lattice expansion can give changes in the dimensions of the unit cell. This is expressed in the XRPD as slight shifts in some or all the scattering peaks. Chromylin sodium (Cox et al., 1971) is an example of this behavior.

Some hydrates have water molecules in two-dimensional order or plane and they are called planar hydrates. Examples of this structure are sodium ibuprofen and nedocromil zinc (Zhu et al., 1997). In both cases water is ion associated. In the case of nedocromil zinc,

the long axis of the crystal is perpendicular to the hydration plane and was observed to dehydrate primarily along the planar axis.

Dehydrated hydrates are obtained when dehydration leaves an intact anhydrous structure that is very similar to the hydrated structure but with lower density. If there already an anhydrous crystalline form of the molecule exists, the dehydrated hydrate is classified as polymorph. Dehydrated hydrates may in principle belong to any of the classes discussed above or may be a class their selves.

Ion-associated hydrates belong to the third class of hydrates. Hydrates contain metal-ion coordinated water and the interaction between the metal ions and water molecules is the major force in the structure of crystalline hydrates. The metal–water interactions may be quite strong relative to the other non-bonded interactions and, therefore, dehydration occurs at very high temperatures (Dzidic et al., 1970). In TGA and DSC thermograms, very sharp peaks corresponding to dehydration of water bonded with metal ions are expected at high temperatures.

I.5. NAPROXEN AND SODIUM NAPROXEN

Sodium naproxen (sodium salt of (S)-(+)-6-methoxy-α-methyl-2-naphtalene-acetic acid) is a non-steroidal anti-inflammatory drug (NSAID). The compound (Figure 1.3) is an arylacetate derivative which consists of aromatic moiety and propionate side chain, and it has an asymmetric carbon at the side chain (Kim et al., 1990).

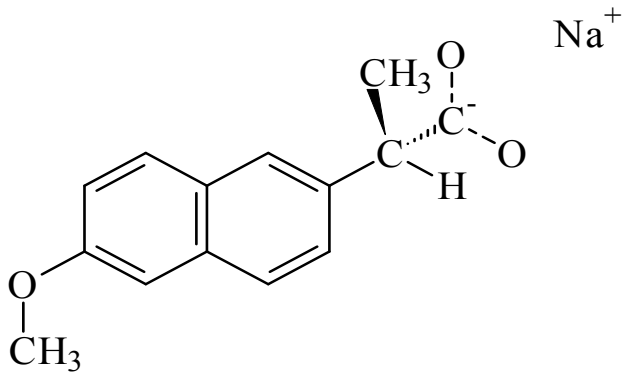

Melting point = 244-246°C

MW = 252,24

pK_a = 4,15

Figure 1.3

Chemical structure of sodium naproxen.

Sodium naproxen is a white to creamy crystalline powder. Soluble in water and in methyl alcohol; sparingly soluble in alcohol; very slightly soluble in acetone; practically insoluble in chloroform and in toluene (USP, 27th Edition).

Naproxen was introduced to the market by Syntex in 1976 (Harrington, 1997).

It is used in musculoskeletal and joint disorders such as ankylosing spondylitis, osteoarthritis, and rheumatoid arthritis including juvenile idiopathic arthritis. It is also used in dysmenorrhoea, headache including migraine, postoperative pain, soft-tissue disorders, acute gout, and to reduce fever.

Naproxen is usually given by mouth as the free acid or as the sodium salt because the salt has much higher solubility in water than its acid free form. The doses in the

manufacturers product information are expressed in terms of the free acid or the sodium salt as appropriate for an individual preparation. Each 550 mg of naproxen sodium is approximately equivalent to 500 mg of naproxen.

I.5.1. Pharmacokinetics

Naproxen and naproxen sodium are readily absorbed from the gastrointestinal tract (Martindale, 2005). Peak plasma concentrations are attained about 1 to 2 hours after ingestion of naproxen sodium and in about 2 to 4 hours after ingestion of naproxen. Food reduces the rate but not the extent of absorption. Naproxen and naproxen sodium are also well absorbed rectally.

At therapeutic concentrations naproxen is more than 99% bound to plasma proteins. Plasma concentrations of naproxen increase proportionally with dose up to about 500 mg daily; at higher doses there is an increase in clearance caused by saturation of plasma proteins. Naproxen diffuses into synovial fluid; it crosses the placenta and is distributed into breast milk in small amounts. Naproxen has a plasma elimination half-life of about 13 hours. About 95% of a dose is excreted in urine as naproxen and 6-*O*-desmethylnaproxen and their conjugates. Less than 5% of a dose appears in the faeces.

Sodium naproxen exists in an anhydrous form and the following four hydrated ones: one monohydrate, two dehydrate, and one tetrahydrate.

I.5.2. Sodium naproxen anhydrous and hydrate forms

SN is commercialized in its anhydrous form. The anhydrous form was described by Kim et al. (2004). The asymmetric unit of anhydrous sodium naproxen, contains two independent anions, denoted A and B, and two cations. In the anhydrous material, the Na^+ ion is four-coordinate. It has four nonequivalent $Na^{\cdots}O$ bonds that involve the carboxy groups of four different naproxen anions.

The evidence of the existence of hydrated forms of sodium naproxen is connected with previous studies performed in our laboratories (Pharmaceutical Technology Laboratories, University of Camerino) under the guidance of Prof. Piera Di Martino.

Di Martino et al. (2001) described the formation of a dihydrate form of SN by both crystallization in water and hydration of the anhydrous form at a RH>55% and the evidence that two water molecules were bound to one SN molecule was established by elemental analysis. This technique was revealed fundamentally to quantify the number of water molecules bonded in the dihydrate SN, because other techniques such as KFT and TG do not allow to distinguish absorbed and bonded water since water loss already occur at temperatures close to room temperature.

Di Martino et al. (2007) described the hydration of the anhydrous SN to a tetrahydrate form by exposure at a RH>75%.

The two previously cited studies proved that water absorption clearly promoted changes in the crystallographic structure of the SN, and that the two different hydrate structures may be formed during the hydration process, according to the RH%. In addition, it has been proven that the water seemed to be weakly bonded in the crystal structure, as demonstrated by the relatively low desolvation temperatures. This statement is in accordance with Allen et al. (1978) who suggested that water released at low temperature has very weak interaction with nearby molecules in the crystal lattice. The fact that the interaction of the carboxylate group with water in the forms obtained at 55% and 75% RH was probably rather weak was equally confirmed by solid-state ^{13}C-NMR results (Di Martino et al., 2007).

Kim et al. (2004) described the development of a monohydrate form of SN (MSN) by dehydration of a dihydrate form crystallized from water. The monohydrated form of SN was prepared by drying the dihydrate in a dessicator for 2 days. This form also appeared as an intermediate during the dehydration of the dihydrate and the tetrahydrate forms obtained respectively at 55 and 75% RH followed by X-ray powder diffractometry.

Summarizing, in this study the following SN forms have been described:

a) the anhydrous sodium naproxen (ASN);

b) the monohydrated sodium naproxen (MSN), obtained by dehydrating the dihydrated sodium naproxen (DSN), according to Kim and Rousseau (2004);
c) a dihydrated sodium naproxen (DSN) obtained by exposing the ASN at 55% RH according to Di Martino et al. (2001);
d) a dihydrated sodium naproxen (CSN) obtained by crystallizing sodium naproxen from water, according to Di Martino et al. (2001) and Kim and Rousseau (2004);
e) the tetrahydrated form (TSN) obtained by exposing the ASN at 75% RH according to Di Martino et al. (2007).

II. MATERIALS AND METHODS

II.1. MATERIALS

Sodium naproxen (SN) (Eur. Ph. 5th Ed.; USP, 27th Edition) was kindly supplied by A.C.R.A.F. (Ancona, Italy) in its anhydrous form (anhydrous sodium naproxen, ASN). To avoid unwanted hydration, ASN was stored in a desiccator in the presence of diphosphore pentaoxyde (Sigma Aldrich, Stenheim, Germany).

The mean particle diameter determined by laser diffraction method by the supplier was 22.82 ± 14.38 μm.

During the present study, four different hydrated forms of sodium naproxen were used:

- One dihydrated form (CSN) was obtained by crystallizing ASN from water (Di Martino et al., 2001). 25 g of sodium naproxen were dissolved under continuous stirring in 250 ml of demineralised water at a constant temperature of 333 K. The obtained solution was left to cool down spontaneously to 277 K under continuous stirring until crystallization occurred. The obtained crystals were then filtrated under vacuum filter and dried under room conditions.
- The second dihydrated form (DSN) was obtained by exposing the ASN at a relative humidity of 55 ± 2%, according to the following method: 1.5 g of ASN powder were placed as a thin layer in a container in its turn placed in a sealed box where a RH% of 55% was produced by a supersaturated solution of magnesium nitrate in water. The RH% was checked by a thermohygrometer (Universal Enterprise Inc., Cambiago, Milano, Italy). The sealed box was stored at 298 ± 0.5 K in an incubator (Velp Scientifica, FTC 90E, Usmate, Italy). The sample was periodically weighted until equilibrium weight was reached (approximately 7 days).
- The monohydrated form (MSN) was obtained by dehydrating the CSN under desiccation, slightly modifying the method described by Kim and Rousseau (2004). Briefly, the monohydrated form was obtained by drying 5 g of CSN in a desiccator under vacuum for 2 days at 298 K. The hydration state was checked by STA analysis.

- The tetrahydrated form (TSN) was obtained by exposing the ASN at a RH of 75 ± 2% according the following method: 1.5 g of ASN powder were placed as a thin layer in a container in its turn placed in a sealed box where a RH% of 75% was produced by a supersaturated solution of sodium chloride in water. The RH% was checked by a thermohygrometer (Universal Enterprise Inc., Cambiago, Milano, Italy). The sealed box was stored at 298 ± 0.5 K in an incubator (Velp Scientifica, FTC 90E, Usmate, Italy). The sample was periodically weighted until the equilibrium weight was reached (approximately 10 days).

All the powders were sieved in order to collect the same granulometric fraction 50-100 μm.

Other materials used during this study were: magnesium stearate A.C.E.F. (Fiorenzuola d'Arda, Piacenza, Italy), povidone (Kollidon® K30, BASF, Ludwigshafen, Germany), microcrystalline cellulose (MC) (Vivapur® 101, Ph. Eur., USP, J. Rettenmaier & Söhne, Rosemberg, Germany); the particle size distribution of the latter substance given by the supplier was as follows: less than 1% > 250 μm, 24% > 75 μm, 68% > 32μm.

II.2. ISOTHERMAL WATER SORPTION EXPERIMENTS

Appropriate amounts of ASN were stored in an incubator (Velp Scientifica, FTC 90E, Usmate, Italy) at 298 K. Powders were in turn placed in several boxes under appropriate RH%, obtained with saturated salt solutions, which generated a controlled water vapour pressure (Figure 2.1)

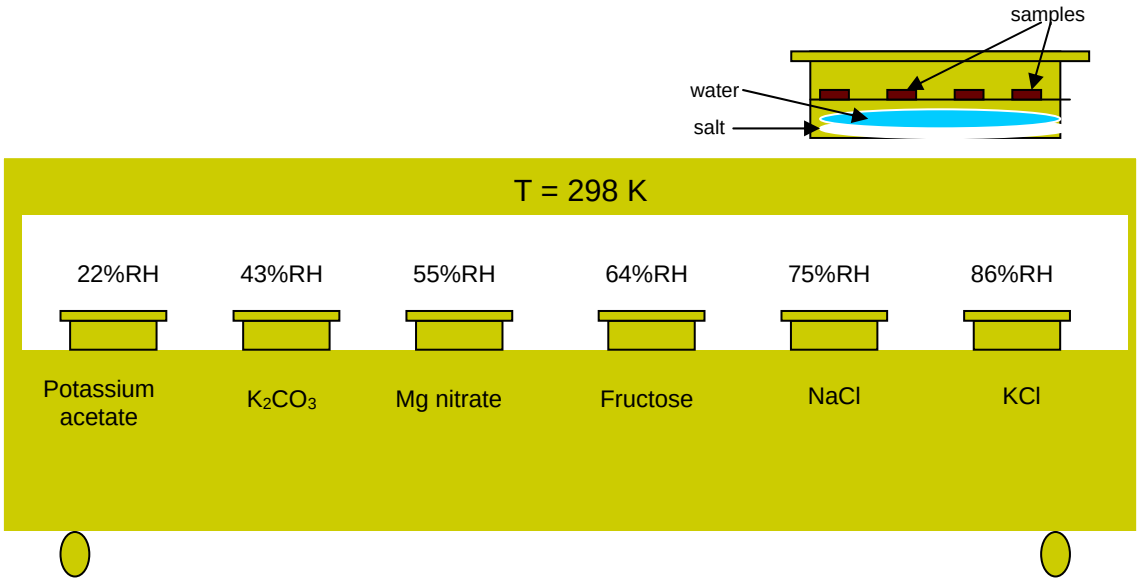

Figure 2.1

Representation of the isothermal water sorption experiment

Experimental RH% was checked with a thermohygrometer (Universal Enterprise Inc., Cambiago, Italy). Hydration was followed by a discontinuous procedure, i.e. by taking and weighing samples at regular intervals until reaching equilibrium weight (Kontny and Zografi, 1995). Weight was checked every 10 days for three months. Assays were carried out in triplicate. Water uptake was calculated as a percentage of the initial mass of ASN. Sorption isotherms at 55% and 86% RH were established in the same experimental conditions, by weighing the samples twice daily. The powders recovered under hydration were used for the compression and densification study. The criteria for water uptake and water content were quite different because the mass of dried sample was

used as reference in the first case, while the mass of humid product was used in the second. Target values are indicated in Table 2.1.

Table 2.1

Target values of water uptake and water content.

Formula	Molecular weight	Water uptake (%)	Water content (%)
$C_{14}H_{13}O_3Na$	252	-	-
$C_{14}H_{13}O_3Na \cdot 0.5H_20$	261	3.57	3.45
$C_{14}H_{13}O_3Na \cdot 1.0H_20$	270	7.14	6.66
$C_{14}H_{13}O_3Na \cdot 1.5H_20$	279	10.71	9.67
$C_{14}H_{13}O_3Na \cdot 2H_20$	288	14.28	12.50
$C_{14}H_{13}O_3Na \cdot 3H_20$	306	21.43	17.64
$C_{14}H_{13}O_3Na \cdot 4H_20$	324	28.57	22.22

II.3 STUDY OF HYDRATION KINETICS

An experimental procedure similar to that previously described for the isothermal water sorption experiments was carried out to study hydration kinetics. The ASN powder was stored at two different RHs, 55% and 86%, at several temperatures (288, 293, 298, 303 and 308 K) and generated in the appropriate saturated salt solutions. With the same discontinuous procedure as previously described, changes in weight were continuously and

regularly checked until equilibrium was reached. The 55% and 86% RH values were used because they led respectively to the dihydrated form (DSN) and the tetrahydrated form (TSN).

II.4 DETERMINATION OF PARTICLE SIZE AND MORPHOLOGY

For routine control of powder particle size, the measurement of the Ferret's diameter of 500 particles determined by an optical microscope supplied with an objective of 100x (Leitz Ortholux II Pol-Bk, Wetzlar, Germany) was used. For more accurate particle size determination and for characterization of particle morphology the analysis by means of the Scanning Electron Microscopy (SEM) (Stereoscan 360, Cambridge Instruments, Cambridge, United Kingdom) was preferred. Samples were mounted on a metal stub with a double-sided adhesive tape and then recovered under vacuum with a gold layer of thickness of 200 Å using a metallizer (Balzer MED 010, Linchestein). Again, particle size was determined by counting Ferret's diameter of 500 particles under SEM.

II.5 SIMULTANEOUS THERMAL ANALYSIS (STA)

Simultaneous Thermal Analysis (STA) enables to simultaneously analyse a sample for change in weight (Thermogravimetric analysis, TGA) and change in enthalpy flow (Differential Scanning Calorimetry, DSC). In this text, the acronyms TGA-STA and DSC-STA will be used to refer to TGA and DSC obtained from STA. The analysis was performed with a Simultaneous Thermal Analyser (STA 6000, Perkin Elmer, Inc., Waltham, MA, USA), under nitrogen atmosphere (20 mL/min) in 0.07 ml open aluminium oxide pans. STA was calibrated for temperature and heat flow with three standard metals (tin, indium and zinc), taking into account their expected melting temperatures (505.08, 429.75, 692.68 K respectively) and for weight with an external Perkin Elmer standard (Calibration Reference Weight P/N N520-0042, Material lot 91101 GB, Weight 55.98 mg,

01/23/08 VT). Calibration was repeatedly checked to assure deviation ≤ ± 0.3 K. Two different analyses were performed: a scanning analysis and an isothermal analysis. In the first case, samples (approximately 10 mg) were tested in quadruplicate by heating from 293 to 393 K at a heating rate of 10 K min^{-1}. In the second case, the isothermal dehydration experiments were performed at 295, 298, 301, 304, 307 and 310 K. During experiments, the STA furnace was heated in absence of the sample to reach the required temperature.

After this, once the sample was introduced in the apparatus, a short period was required to stabilize the balance prior to data collection, during which some dehydration occurred, accounting for slightly lower than expected values of weight loss, especially at higher temperatures. This phenomenon has been previously described by Taylor and York (1998). In the present study, this fact is of particular importance because, as previously stated (Di Martino et al., 2001) desolvation of hydrated forms of SN already occurs close to room temperature. Thus, during the equilibration phase of the STA microbalance, a certain amount of water can be lost when the sample is subjected to the anhydrous nitrogen gas flux, before the analysis is actually started.

II.6 DIFFERENTIAL SCANNING CALORIMETRY (DSC)

Differential Scanning Calorimetry (DSC) analysis was also performed on a Pyris 1 (Perkin Elmer, Co. Norwalk, USA) equipped with a cooling device (Intracooler 2P, Cooling Accessory, Perkin Elmer, Co. Norwalk, USA). A purge of dry nitrogen gas (20 mL/min) was used for all runs. DSC was calibrated for temperature and heat flow using a pure sample of indium and zinc standards, respecting the same criteria previously described for STA. Sample mass was about 3-4 mg and aluminium perforated pans were used (Di Martino et al., 2001). Each run was performed in triplicate from 293 K to 553 K at a heating rate of 10 K/min. To avoid confusion with DSC-STA results, this last technique will be identified as conventional DSC.

II.7 X-RAY POWDER DIFFRACTION (XRPD)

X-ray powder diffractometry (XRPD) was used to follow changes in the crystalline phase during dehydration processes. For this purpose, a Philips PW 1730 (Philips Electronic Instruments Corp., Mahwah, NJ, USA) as X-ray generator for Cu Kα radiation ($\lambda_{\alpha 1}$ = 1.54056 Å, $\lambda_{\alpha 2}$ = 1.54430 Å) was used. The experimental X-ray powder patterns were recorded on a Philips PH 8203. The goniometer supply was a Philips PW 1373 and the channel control was a Philips PW 1390. Data were collected in the discontinuous scan mode using a step size of 0.01° 2θ. The scanned range was 2° to 40° (2θ).

II.8 PARTICLE WETTABILITY

Particle wettability was determined by the capillary rise wetting method, based on Washburn's equation, the theoretical basis of which was reported by Lazghab et al. (2005). An appropriate quantity of particles was packed into a glass cylinder in order to obtain reproducible bed porosity. The tube (12 cm long and 1 cm internal diameter), closed on one end with a sintered glass filter, was then joined to a scale (1/100000 precision), and then the solvent was placed in a container positioned under the tube and brought in contact with the filter. The tube was weighed every second until the particle bed became saturated, that is, when the mass ceased to increase. The rate of liquid penetration through the powder bed was used to calculate the contact angle (Lazghab et al., 2005).

II.9 WET GRANULATION

Wet granulation was performed in a high-shear mixer-granulator (Romaco, Lucca, Italy) equipped with a 2.6 L capacity vertical bowl, with a 3-blade impeller that can rotate at an interval speed of 50-1500 rpm, and with a vertical chopper that rotates at a fixed

speed of 6000 rpm. The binder liquid was added through a spray nozzle placed at the top of the bowl cover, with constant feeding of the liquid ensured by a peristaltic pump. The temperature inside the bowl was kept constant by water circulating in a jacket, and a temperature probe facilitated temperature control inside the bowl. Three different granule batches were produced: a drugless (placebo) batch and two medicated batches (MB). The placebo batch was composed of 5% povidone and 95% microcrystalline cellulose. The two medicated batches (MB), batch A and batch B, were obtained from the same wet granule batch, which will be indicated as the wet medicated batch (WMB). Medicated batches A and B also included 5% povidone, but instead of the 95% microcrystalline cellulose in the placebo, they contained 40% of this substance and 55% of ASN. The wetting liquid, a 5% W/W solution of povidone in water, was added to the placebo and the MB for the granulation, in quantities of 70 ml/100g of solid weight and 35ml/100g of solid weight respectively. Granulation conditions are summarized in Table 2.2, where granulation parameters are indicated for dried mixing, liquid addition, and proper granulation. The same granulation procedure was always used for all three batches in order to avoid variables caused by differences in process (Table 2.2) (Holm, 1997). Two liters of powder were processed in the bowl.

Table 2.2

Experimental conditions used during wet granulation in the high-shear mixer-granulator

Granulation phases	**Time (sec)**	**Impeller speed (rpm)**	**Temperature (K)**	**Chopper (rpm)**	**Vacuum**
Dried mixing	100	300	298	No	No
Liquid addition	300	600	298	No	No
Granulation	900	600	298	6000	No

The initial densities of powder mixes before granulation were 0.3605 and 0.4423 g/cm^3 respectively for placebo and MB formulations.

The power consumption profile was recorded for each formulation during the granulation process, as the granulating liquid was being added, until the overwetting point (paste formation) was reached. The power consumption of the impeller was recorded with Labtech® Realtime Vision Version 3.0 (1998) software and expressed in comparison with the granulating liquid amount. The stages of wet granulation are explained afterwards in results section. The stage III corresponds to the agglomeration stage of wet granules.

II.10 CHARACTERIZATION OF PHYSICAL PROPERTIES OF GRANULES

The degree of liquid saturation percentage (DLS%) of wet granules was determined according to Saleh et al. (2005) through the calculation of the granule apparent density, which represents the ratio of the mass of a binder-free granule to its volume including the intra-particle voids. To measure this parameter, a sample of wet granules was subdivided into narrow size fractions by screen sieving. Each fraction was analyzed separately as follows: a significant sample of wet granules (at least 200) was counted and oven-dried at 323 K for 24h. It must be specified that granules recovered after this drying procedure are composed of SN that is not completely dehydrated (as proven by the presence of some typical peaks of SN hydrated forms, as explained later). Assuming that the selected granules were spherical particles of homogeneous density and diameter, the granule apparent density, ρ_g, was calculated by equation (1):

$$\rho_g = \frac{6}{n\pi d^3}\left[m_d - \frac{c}{c-1}\left(m_w - m_d\right)\right] \quad (1)$$

where n is the number of particles in the analyzed sample, c is the mass fraction of the dry material in the granulating liquid, d is the mean particle size of the examined granule population, and m_w and m_d are masses of wet and oven-dried samples, respectively.

The intra-particle void fraction was calculated by equation (2)

$$\chi = 1 - \frac{\rho_g}{\rho_s} \tag{2}$$

where ρ_s is the true density of the dry powder, experimentally measured using a helium pychnometer (Accupyc 1330, Micromeritics, Norcross, USA).

The DLS of granules was defined as the portion of the overall intra-particle space occupied by the granulating liquid, and was calculated according to equation (3).

$$DLS = \frac{c+1}{\left[\left(\frac{m_d}{m_w - m_d}\right) - c\right]} \times \frac{\rho_g}{\rho_l \chi} \tag{3}$$

ρ_l is the density of granulating liquid.

This study assessed two different drying procedures with a high-shear mixer-granulator, after preliminary examinations showed that drying by oven or dessicator was not satisfactory.

Our first procedure, used with both the placebo and batch A, consisted of drying granules under vacuum at room temperature (298 K) in the high-shear mixer-granulator, while the second procedure (batch B) employed the same equipment, method, and time, but at a temperature of 313 K. According to these procedures, the chopper was stopped, the impeller blade velocity was lowered to 100 rpm in order to limit friction forces acting on particles, and the temperature inside the bowl was checked and set to 298 K for the placebo batch and medicated batch A, while a temperature of 313 K was used for medicated batch B. Next, the batches were subjected to the drying phase under vacuum for 1800 sec.

Once dried, granules were sieved according to the method <786> of the USP 27 through sieves of the following ISO nominal aperture: 1000, 800, 710, 630, 500, 355, 250, 180 μm. Fractions higher than 1000 μm and those lower than 180 μm were discarded.

The appropriate drying period of time was evaluated, taking into account the loss on drying percentage LOD(%) and the friability index (FI). Before deciding upon the above-described drying methods and the period of 1800 seconds, a number of methods and times were tested, taking into account the loss on drying percentage LOD(%) and the friability index (FI). Our preliminary assays established that drastic drying conditions and increasing drying time did not decrease LOD(%), but dramatically increased FI (results not given). The mechanical action on the granule surface promotes its pulverization. In the attempt to produce granules containing a completely anhydrous sodium naproxen form, we examined such drying tools as a tray-oven (without vacuum) and a desiccator (under vacuum) to. In the case of the oven, we found that T > 333 K caused darkening of the granule surface. So, for our experiments, we fixed a limit temperature of 323 K, which was also used for DLS% calculation. The drying in the desiccator resulted unsatisfactory as well, as it was slow and inefficient. With both drying methods, the granules still contained hydrated forms of sodium naproxen in the granule core, as proven by X-ray powder diffraction study, which revealed the presence of some peaks of the hydrated forms. All drying experiments in static bed gave resistant granules.

These preliminary examinations assessing the oven and the dessicator did not indicate them as a viable drying method for this study, and so for the final experiments we settled on the high-shear mixer-granulator, with the advantage to complete the process in the same apparatus.

II.11 TECHNOLOGICAL PROPERTIES OF GRANULES

The loss on drying percentage (LOD%) was determined with a thermal scale (Scaltec Instruments, SMO 01, Göttingen, Germany), by heating an appropriate amount of ground granules at 393 K until a constant weight was attained. Results are the mean of four measurements and are calculated on wet basis.

True particle densities, necessary to determine the tablet porosity during compression and densification, were measured using a helium pychnometer (Accupyc

1330, Micromeritics, Norcross, USA) with a cell of 10 cm^3. The particle density represents the mean of ten measurements. Each sample was analyzed three times and the result is the mean of three different determinations.

Porosity was determined with an Autopore 9220 mercury porosimeter (Micromeritics, Norcross, USA). An intrusion measure was executed into the range between 3.45 kPa and 414 MPa. Results are the mean of 10 measurements.

Friability was determined three times with a standard rolling-drum apparatus (Tecnogalenica, Milano, Italy) in conformance with the European Pharmacopoeia 5.3 edition (2006) (described in the "Friability of uncoated tablets" section). Granules, of sieving fraction of 180-1000 μm, were subjected to 200 rotations in the apparatus, and passed again through the 180 μm sieve. The Friability Index (FI) expresses the ratio between the broken granules mass passed through the 180 μm sieve, and initial granule mass: the more the FI approaches 1, the more friable the granules.

Bulk and tapped densities were determined by measuring the volume of carefully weighed samples. Carr's Index (1965a, 1965b) was determined from initial and tapped sample volumes (Tecnogalenica, Milano, Italy).

II.12 STUDY OF COMPRESSION PROPERTIES OF GRANULES

The compression study was performed on a high tech mini rotary press (Piccola 10, Ronchi, Milano, Italy) equipped with a computerized control system to detect and analyze force-signals (pressing force and ejection force) and with ten flat 11.28 mm-diameter punches. Magnesium stearate addition directly to the granules as lubricant was eschewed for fear that it might influence the results; hence, a discontinuous compression procedure was chosen and samples were manually introduced into only one die. Die and punches were pre-lubricated with a 1% magnesium stearate suspension in ethanol 96% (v/v). The granule mass was always constant in order to obtain 1000 mg tablets. The force at the upper punch was progressively increased and recorded. Results for each compression force were the mean of five measurements. Thickness and diameter of intact ejected tablets were

measured with a manual micrometer (Mitutoyo, Japan) immediately after ejection. Tablet porosity was calculated from tablet dimensions, mass, and powder density. Crushing force was measured immediately after compression with a tablet strength tester (Erweka, type TBH30, Germany). Tensile strength Q (Fell and Newton, 1970) was calculated according to equation 4:

$$Q = \frac{2H}{\pi dt} \quad (4)$$

where H is the tablet crushing strength, d the diameter and t the thickness of the tablet.

II.13 STUDY OF COMPRESSION PROPERTIES OF POWDERS

Compression was carried out in an instrumented single punch tablet machine (Frogerais OA, Vitry, France), equipped with flat punches of 11.28 mm in diameter.

Two sets of tablets were prepared for each powder. The powder mass was adapted so as to reach a maximal compression pressure of 150 ± 5 MPa (first set, to study tabletability and compressibility) or a porosity value of 10 ± 0.1% (second set, to study compactibility) (Joiris et al., 1998; Sun and Grant, 2001). Results are the mean of five measurements. The die depth was fixed at 10.00 mm and the upper punch displacement for an empty die at 7.50 mm. External lubrication was obtained by compressing microcrystalline cellulose along with 1% W/W magnesium stearate. For each tablet, an appropriate amount of powder was weighed and introduced manually into the die. The machine was started and measures were recorded at a frequency of 2000 Hz. The length of pressure application on the powder (compression and decompression) was about 150 ms.

Once recovered, mass, thickness and crushing strength of tablet were measured, with scales (Precisa XT220 A), a micrometer (Mitutoyo, Japan) and a strength tester (Tablet Tester 8M, Schleuniger, Switzerland) respectively. Correction of displacement

transducer data for machine looseness and punch deformation was carried out according to Juslin and Paronen (1980).

Pressure transmission through the powder bed in the die was estimated by comparing maximal compression pressures on the upper and lower punches. Transmission coefficient corresponds to the ratio of lower punch and upper punch values.

Once recovered, mass, thickness and crushing strength of tablets were measured. Tensile strength was determined as previously.

II.14 STUDY OF THE DENSIFICATION BEHAVIOUR

The densification behaviour of powders was studied using Heckel's equation (1961):

$$\ln \frac{1}{1-D} = KP + A \qquad (5)$$

where D is the relative density of the compressed powder bed at applied pressure P. K is the slope of the straight linear portion of Heckel's plot and the reciprocal of K is the mean yield pressure (P_Y).

The constant A is the sum of two densification terms:

$$A = \ln\left(\frac{1}{1-D_0'}\right) + B \qquad (6)$$

According to Doelker (1994), D_0' corresponds to the relative density of the powder at the moment when the last recorded applied pressure is still nil and B is the densification due to particle fragmentation.

Constants *A* and *B* can be expressed as relative densities using:

$$D_A = 1 - e^{-A} \tag{7}$$

$$D_B' = D_A - D_0' \tag{8}$$

Heckel's profiles were established from single compression cycles on tablets compressed approximately at 150 MPa. Parameters P_Y, D_A, D_0', D_B' were calculated using a precompression pressure value of 2.0 MPa. Several methods have been described to select a linear region of the Heckel function in order to determine Heckel constants.

Following Paronen and Ilkka (1996), we selected a range of measurement points where the linear regression coefficient was as high as possible. This corresponded for both samples to the 50 to 100 MPa range, with coefficient values superior to 0.998. Each value is a mean of five measurements.

Total elastic recovery (TER) was calculated according to Armstrong and Haines-Nutt (1974):

$$TER = \left[\frac{(t_2 - t_1)}{t_1} \right] \times 100 \tag{9}$$

where t_1 is the minimal thickness of the powder bed in the die and t_2 is tablet thickness.

Tablet porosity (ε) was calculated from weight, volume and apparent powder density. Minimal porosity (ε_{min}) refers to powder porosity when maximal compression force was applied during each compression cycle. It was determined from weight, die dimensions and apparent powder density using a helium pychnometer (Accupic 1330, Micromeritics, Norcross, USA), with a cell of 10 cm^3. Results are the mean of 10 measurements. Densities of ASN, DSN and TSN were respectively 1.377 ± 0.008, 1.343 ± 0.006 and 1.337 ± 0.005. The density of intermediate hydrates was calculated by averaging apparent powder densities as a function of water content.

RESULTS AND DISCUSSION

III. PHYSICO-CHEMICAL AND TECHNOLOGICAL PROPERTIES OF SODIUM NAPROXEN GRANULES PREPARED IN A HIGH-SHEAR MIXER-GRANULATOR

IV. INFLUENCE OF CRYSTAL HYDRATION ON THE MECHANICAL PROPERTIES OF SODIUM NAPROXEN

V. MECHANISMS FOR DEHYDRATION OF THREE SODIUM NAPROXEN HYDRATES

VI. MECHANICAL PROPERTIES OF DIFFERENT ANHYDROUS AND HYDRATED FORMS OF SODIUM NAPROXEN

III. PHYSICO-CHEMICAL AND TECHNOLOGICAL PROPERTIES OF SODIUM NAPROXEN GRANULES PREPARED IN A HIGH-SHEAR MIXER-GRANULATOR

Tablets of anhydrous sodium naproxen were produced by wet granulation using a high-shear mixer-granulator. Drug hydrated to the tetrahydrated form, as observed by X-ray powder diffractometry. After wet granulation, authors performed then two different drying procedures, obtaining granules of different water content and crystallographic characteristics. The first procedure dried granules in the high-shear mixer-granulator by applying vacuum at room temperature (batch A), while the second employed the same apparatus and time, under vacuum at 313 K (batch B). X-ray powder diffractometry revealed that the sodium naproxen contained in batch A granules was a mixture of dihydrated and tetrahydrated forms, (as demonstrated by the coexistence of peaks typical of both hydrated forms), while that of batch B granules was a mixture of monohydrated and tetrahydrated forms. This means that differences in drying procedures could lead to products of different crystallographic properties. The behaviour under compression was evaluated, revealing that batch A offered the best tabletability and compressibility. These results make it possible to conclude that differences in the crystallographic properties and water content of sodium naproxen are such that different hydration/drying processes can alter the drug crystal form and thus the tabletability of the resulting granules.

III.1 WET GRANULATION AND TECHNOLOGICAL CHARACTERIZATION OF GRANULES

XRPD studies (Figure 3.1) revealed the suitability of the excipients chosen for this study, in particular, their compatibility with the raw material in the granulations.

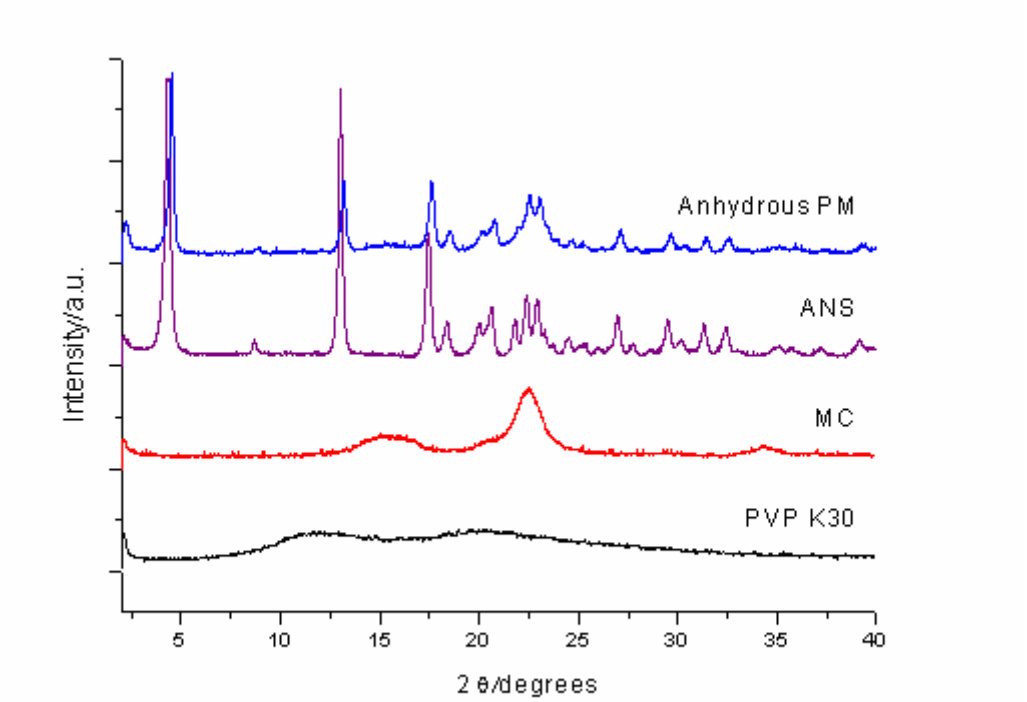

Figure 3.1

XRPD patterns of the starting materials anhydrous sodium naproxen (ASN), microcrystalline cellulose (MC), povidone (PVP K30) and of the physical mixture (PM) of MC (40%) and PVP K30 (5%).

Povidone's XRPD patterns are typical for an amorphous material, with two broad flat curves without crystalline peaks. Similarly, the XRPD patterns of MC show wide reflections characteristic of this material: one broad flat curve and one sharper peak were observed at the angular ranges of 12-18° 2θ and 20-24° 2θ respectively. The XRPD patterns of SN, the raw material used for the present study, comply with those of the

anhydrous form, as confirmed by comparing them with known patterns (Di Martino et al., 2007).

In the same Figure, the XRPD patterns of the mixture with the same dry composition as that used for wet granulation are given and compared to the XRPD patterns of ASN.

The presence of excipients does not significantly interfere with the ASN patterns: we can only observe a slight decrease in peak intensity, a slight baseline curvature between 13-16° 2θ, due to the presence of the first flat curve of the MC, and a broadening of peaks between 21-24° 2θ, due to the overlap with the broad peak of MC.

Predicting the appropriate amount of liquid to add to powders for wet granulation is important but difficult, because suitable moisture content varies with pharmaceutical formulation and powder characteristics.

Crystal structure, water solubility, porous structure, and the ability to form crystal hydrates are factors determining the mechanism of water absorption in the solid (Dawoodbhai and Rhodes, 1989) and thus the amount of water required for wet granulation.

In the present study, the appropriate amount of granulating liquid was determined through the power consumption method used by Leuenberger (1982). The granulating liquid, composed of a 5% W/W solution of povidone in water, was progressively added through constant feeding, while each batch was processed in the high-shear mixer-granulator.

In Figure 3.2, power consumption profiles (PCP) of both placebo and WMB are reported. For each graph, four stages are indicated, according to Betz et al. (2003).

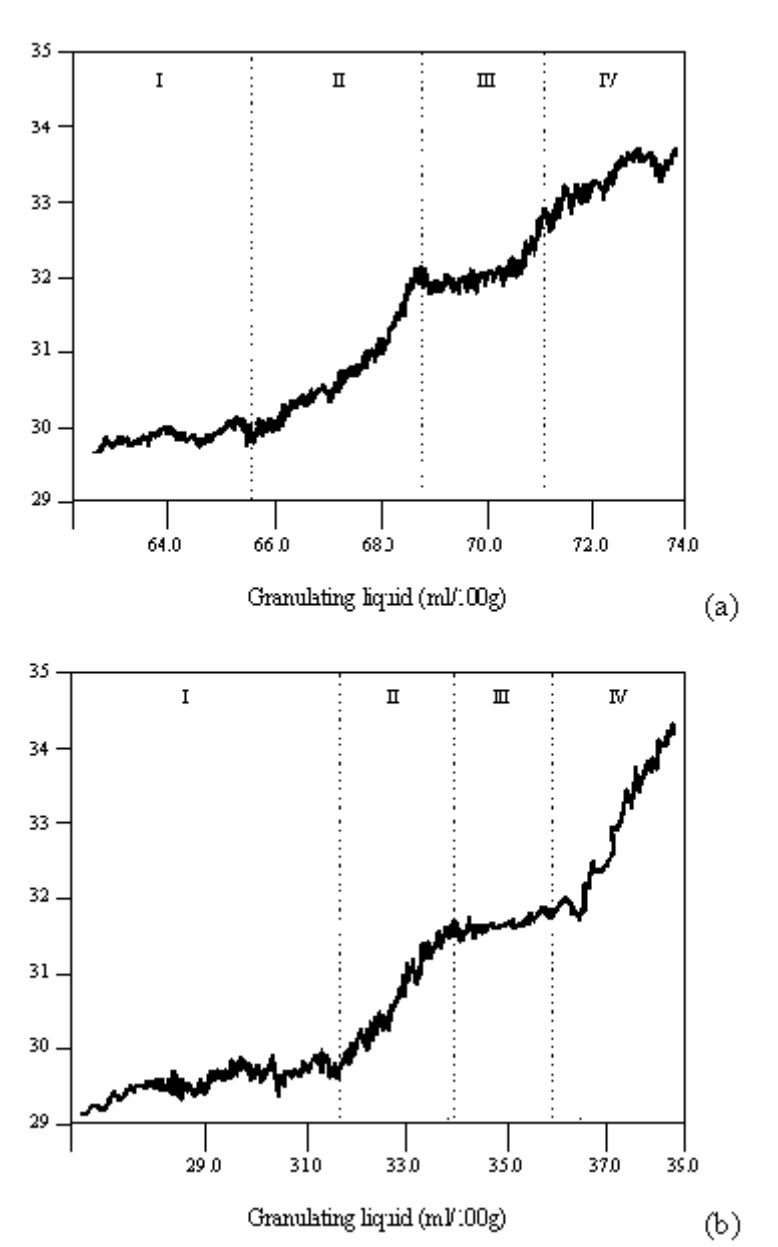

Figure 3.2

Power consumption profiles (PCP) for placebo (a) and wet medicated batch (WMB) (b). (stages I-IV are explained in the text).

Stage I corresponds to initial liquid/powder mixing, while in stage II we can observe a progressive increase of work done by the impeller, due to the increased resistance exerted by the mass under wetting. During this phase the build up of liquid bridges between the powder particles begins and the first granules are formed (pendular phase). Stage III, the plateau region, when the granulating liquid is added and fills more inter-particle voids, is

considered appropriate for getting usable granules. In stage IV with the increase of water there is a consequent abrupt increase of resistance by the wet mass. Stage III corresponds to the funicular state. The capillary state is reached at the end of the stage IV. After these four stages, the water content dramatically increases with a loss of mass consistency. The length of stage III is different for the placebo and the medicated batch: for placebo, the appropriate liquid amount ranges approximately between 69-71 ml every 100 g of powder, while less liquid is necessary when SN is introduced into the formula. In this case, a quantity of 34-36 ml every 100 g of powder is necessary to reach the plateau region. Because the high water solubility of SN reduces the granulation liquid amount, a fact confirmed by the results of wettability studies. Contact angles (θ) of placebo and medicated batch are 45.00 ± 2.37 and 21.00 ± 1.24 respectively. Contact angle can be considered a measure of particle wettability (Ebube et al., 1997; Simons et al., 2004; Rondeau, 2003; Pont et al., 2001; Zhang et al., 2002) such that the lower the contact angle, the higher the wettability. Particle wettability is higher for the medicated batch because of the presence of SN as a highly hydrophilic drug, which can partially dissolve in water and partially absorb water in its crystalline lattice, in spite of the lower quantity of granulating liquid. These results are also supported by the DLS%, which reflects particle wettability, and thus particle hydrophilicity. In Figure 3.3a, the mean granule size, *d*, is expressed as a function of the DLS%; it shows the granule growth with the increase of granulating liquid addition. Placebo granules grow faster than those in the WMB, in which the SN, which is soluble in the binder liquid, keeps granule growth under control. In Figure 3.3b, the DLS% is expressed as a function of the percentage of the mass ratio between the introduced liquid and the total dry powder (L/S %). The DLS% increases according to the granulating liquid amount and reflects the results of the PCP.

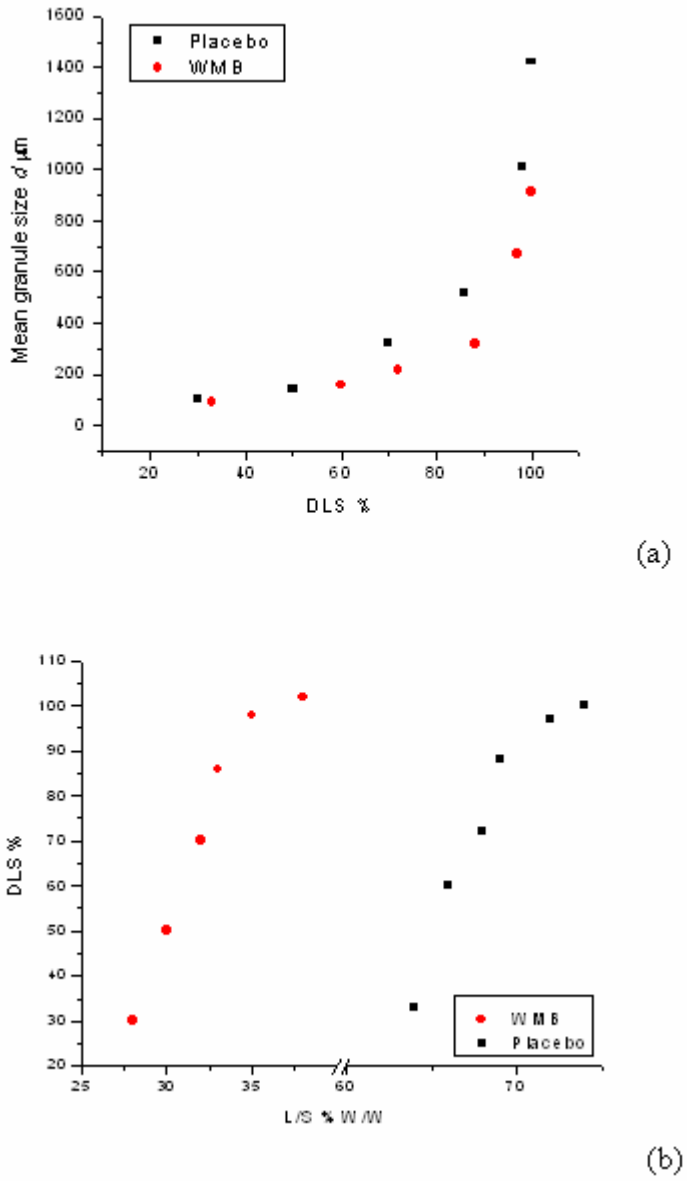

Figure 3.3

Mean particle size of granules expressed as a function of the degree of liquid saturation DLS% (a) and DLS% expressed as a function of the percentage of liquid introduced to the total dry powder (L/S%) (b), for the placebo and wet medicated batch (WMB).

According to a few preliminary assays, the liquid amount was fixed as 70 and 35 ml for every 100 g of powder, respectively for placebo and MB. Some additional details, particularly regarding the reason for choosing this liquid amount for the medicated batch, will be given below.

When wet granules were analysed by XRPD, no differences were identified for the placebo batch, whether powder was dried or wetted (results not given). On the contrary, WMB exhibited significant changes, with an alteration of the typical ASN patterns, and the appearance of the pattern typical of the tetrahydrated form. In Figure 3.4, the XRPD patterns of wet granules are compared to both the anhydrous physical mixture and tetrahydrated sodium naproxen (TSN). In this case, this analysis revealed that the tetrahydrated form of wet granules was pure, and no peaks related to different SN forms were present. TSN was previously described by Di Martino et al. (2007). This hydrated form was obtained by exposing the ASN to a temperature of 298 K at an RH% higher than 75%. The hydration of SN to TSN has not been yet described by any alternative methods.

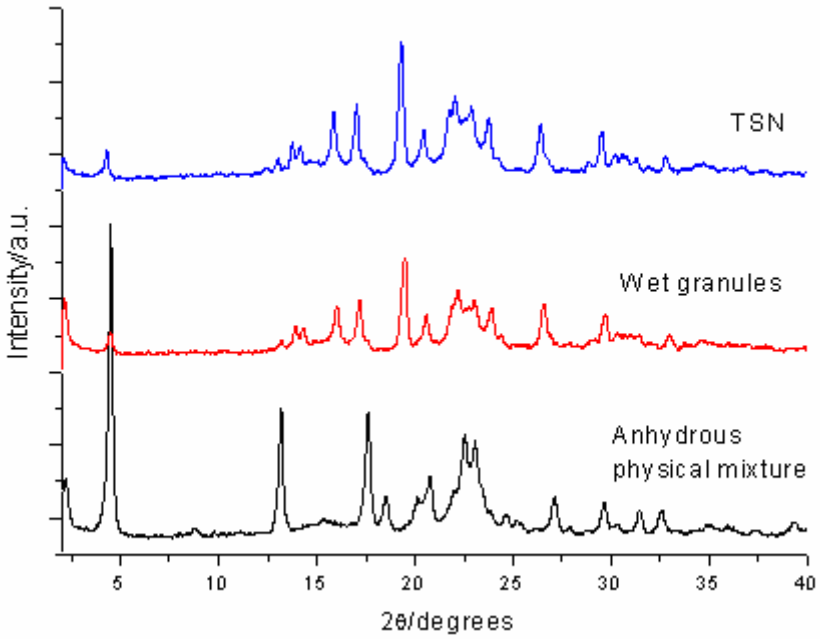

Figure 3.4

XRPD patterns of physical mixture, before wetting and after wetting. The latter is done in comparison with that of pure tetrahydrated form (TSN).

During preliminary studies devoted to establish the granulating liquid amount at the steady flow stage and assess the influence of phase conversion, several experiments were carried out by checking XRPD patterns in relation to the granulating liquid amount.

Within this scope, experiments were performed to determine whether the patterns had typical diffraction peaks of each crystalline form in a zone where no peaks of the other forms existed: 18.5 (2θ) and 19.5 (2θ) were chosen respectively for ASN and TSN. Peak intensities were evaluated and expressed as percentages with respect to the maximum intensity of the same peak when form was pure. Figure 3.5 represents results of three different experiments and shows that the progressive decrease of ASN peak intensity is accompanied by a concomitant increase of TSN peak intensity.

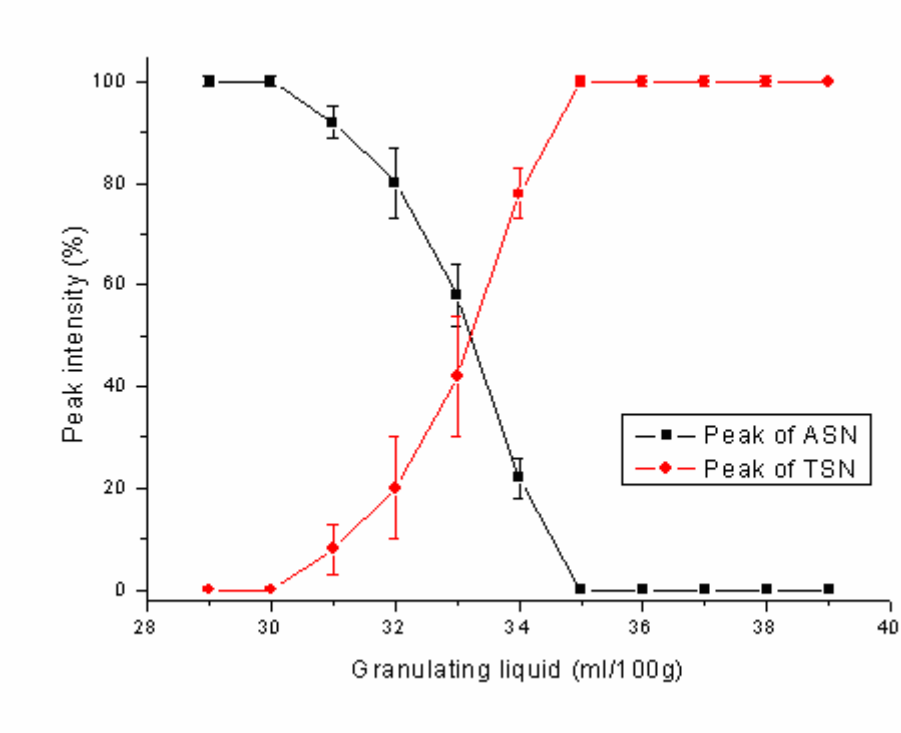

Figure 3.5

XRPD peak intensity percentage versus granulating liquid amount. The analyzed peaks are positioned at 18.5 (2θ) and 19.5° (2θ) for ASN and TSN respectively.

This means that during this transition, no other phases appeared that were different from ASN and TSN forms. The 35ml/100g amount of granulating liquid was the minimum amount required to obtain the pure tetrahydrated form. Since 35ml/100g also corresponds to the required liquid addition for funicular state, it was selected for further granulations.

The WMB was halved and the resulting batches A and B subjected to different drying procedures, as previously described. The XRPD patterns of batch A were compared

to those of different SN forms, such as ASN, monohydrated sodium naproxen (MSN), dehydrated sodium naproxen (DSN), and tetrahydrated sodium naproxen (TSN). Results are given in Figure 3.6, where some typical peaks were assigned to specific SN forms.

In particular, the peaks at 3.98, 11.77, 21.60 and 24.36 (2θ) could be clearly identified as DSN, and those at 17.07 and 20.42 (2θ) were identified as the TSN form.

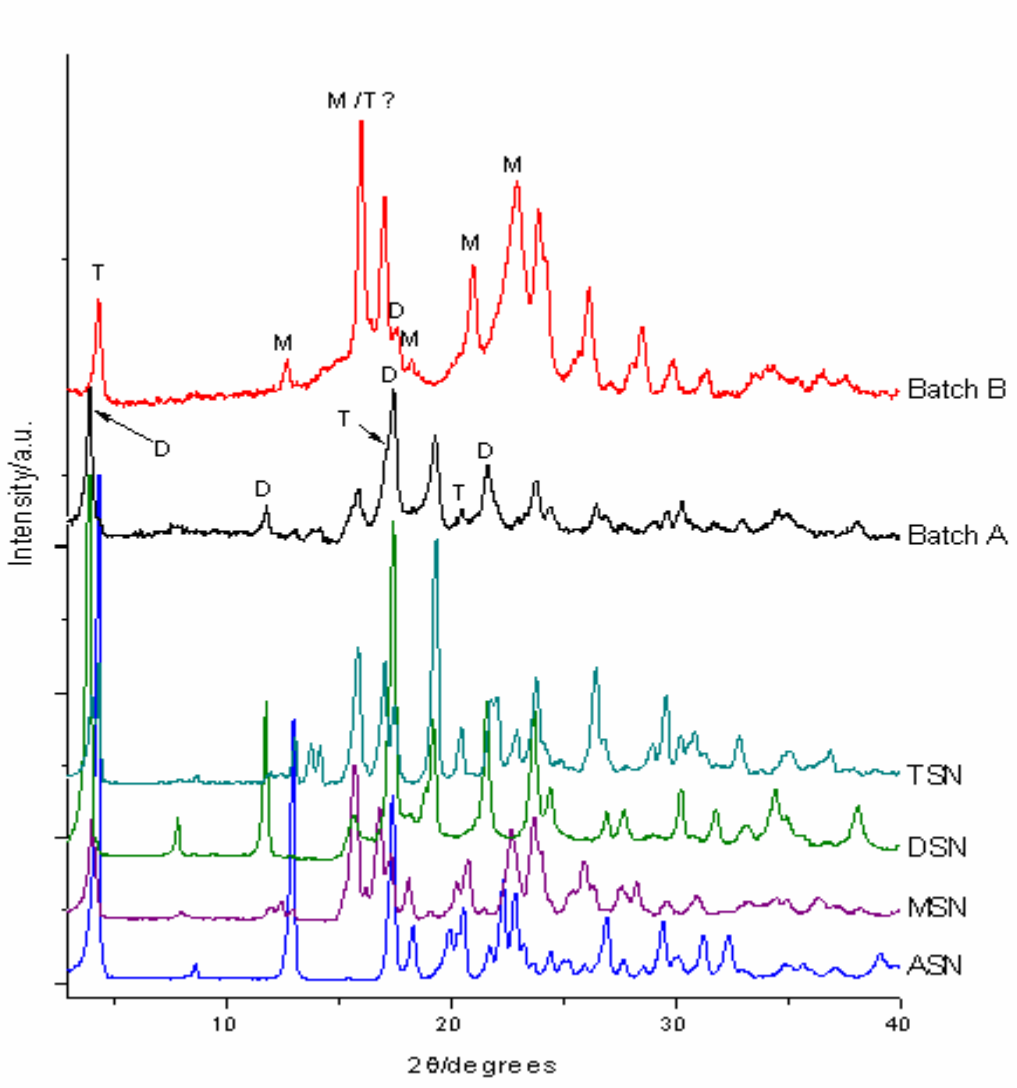

Figure 3.6

XRPD patterns of medicated batches dried under vacuum at 298 (batch A) and 313 K (batch B), and XRPD patterns of sodium naproxen anhydrous (ASN), monohydrate (MSN), dihydrate (DSN) and tetrahydrate (TSN).

It must also be noted that the ASN form was present only in traces, because typical and intensive peaks of this form are only distinguishable as very small peaks. Other peaks could not be identified as any form, because they are common to all hydrated forms: 15.90, 19.29 and 23.77 (2θ). In any case, it is significant that these peaks were absent in the ASN form. These observations lead to the conclusion that batch A was mainly composed of a mixture of DSN and TSN.

As previously explained, batch B was dried with the second procedure, and subsequently its crystallographic characteristics were analysed and typical patterns were compared to those of known SN structures. Some peaks (12.69, 18.26, 20.95, 22.90 2θ) could be easily identified as MSN, a form previously described in the literature (Kim and Rousseau, 2004; Kim et al., 2005; Di Martino et al., 2007).

In addition, the peak at 15.97 (2θ) could be clearly identified as either MSN or TSN.

The possibility that traces of TSN were present in this batch was corroborated by the presence of a peak at 4.29 (2θ), typical of either the ASN or TSN. Because of the absence of typical and intensive ASN peaks, it was possible identify as the peak at 4.29 (2θ) to TSN. These observations allowed the conclusion that in batch B, SN mainly existed as MSN with some traces of TSN.

In concluding this paragraph, it is necessary to clarify that all other attempts to obtain completely dehydrated granules, in which sodium naproxen was present only in its anhydrous form, were unsuccessful. In fact, the use of more drastic drying conditions such as higher temperature or prolonged drying time yielded highly friable granules, drying the granule surface, but leaving the core hydrated. This fact was proven by sieving the granules, separating the powder produced from the granule surface from the intact granules, and analyzing them by XRPD: while the powder generated from the granule surface was characterized by ASN peaks, the core of the granules were still characterized by peaks consistent with hydrated forms.

III.2 TECHNOLOGICAL CHARACTERIZATION OF GRANULES

The three granule batches were analysed for LOD(%), porosity, FI, density, and flowability, and results are indicated in Table 3.1.

Table 3.1

Technological properties of granules of the three different batches. Results refer to the sieved granule fraction of 180-1000 μm.

	Placebo	**Batch A**	**Batch B**
LOD (%)	2.32 ± 0.37	7.20 ± 0.93	4.50 ± 0.29
Porosity (%)	42.28 ± 3.27	47.23 ± 4.98	49.33 ± 5.37
Friability index	0.55 ± 0.15	0.38 ± 0.09	0.48 ± 0.28
App. particle density (g/cm^3)	1.430 ± 0.001	1.484 ± 0.001	1.473 ± 0.002
Bulk density (g/cm^3)	0.68 ± 0.12	0.75 ± 0.15	0.72 ± 0.11
Tapped density (g/cm^3)	0.77 ± 0.53	0.81 ± 0.36	0.79 ± 0.24
Carr's Index	11.54	7.70	8.86

In spite of the higher granulating liquid amount added to the placebo formula, the LOD(%) (2.32 ± 0.37) for this formulation was lower than that of both MBs. In fact, batch A and batch B exhibited a LOD(%) of 7.20 ± 0.93 and 4.50 ± 0.29 respectively, the expression of the different hydration degrees reached at the end of drying procedure, reflecting the ability of SN to keep water in its crystalline lattice by forming hydrates. Granule porosity % reflected the DLS% and the drying degree, with batch B > batch A > placebo.

During the wetting phase, SN is hydrated to the tetrahydrated form with the consequence of a change in the crystallographic structure. The subsequent drying process promotes further crystallographic changes and escaping water yields place to pores. This explains the higher porosity % of medicated batches with the respect to placebo batch. The higher porosity % of batch B compared to batch A was due to the more drastic drying conditions, that gave rise to the development of a more porous structure.

Drying also influenced friability, as FI ranked in the order: placebo > batch B > batch A. In this case, an higher friability index is associated to a lower water content (LOD%).

Granule particle density, determined by helium pychnometry, is given in Table 3.1 and here compared to that of starting materials, microcrystalline cellulose (1.5578 ± 0.0002 g cm^{-3}) and anhydrous sodium naproxen (1.351 ± 0.001 g cm^{-3}). The apparent particle density of placebo batch, mainly composed of MC, is anyway lower than that of pure MC, because of the presence of povidone (apparent particle density 1.1755 ± 0.0002 g cm^{-3}).

Differences in apparent particle densities with medicated batches reflect differences in batch composition (placebo and medicated batches) and, more particularly, differences in the degree of drug hydration: the SN hydration results in an increase of apparent particle density as a consequence of a change in crystallographic structure. Initial and tapped densities were ranked in the order: placebo < batch B < batch A. The Carr's Indexes were always very good and appropriate for free flowing materials such as granules.

Granule size distribution is given in Figure 3.7, which shows similar behaviour for the three batches.

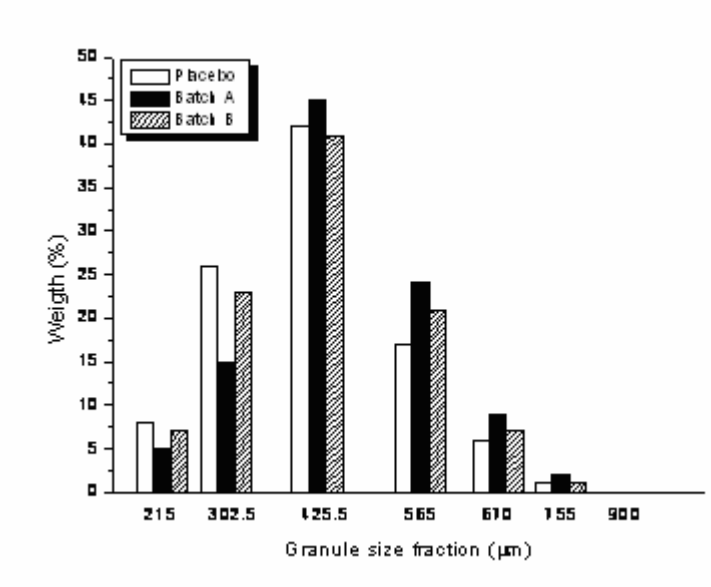

Figure 3.7

Granule size distribution of the three granule batches determined by the sieve method.

The three granule batches compressed in the rotary press exhibited different compression ability (Figure 3.8). The latter was evaluated in terms of tabletability, which is the capacity of a material to give tablets of specified strength under the effect of compression pressure (Joiris et al., 1998). It is expressed in Figure 3.8a as tablet tensile strength versus compression pressure.

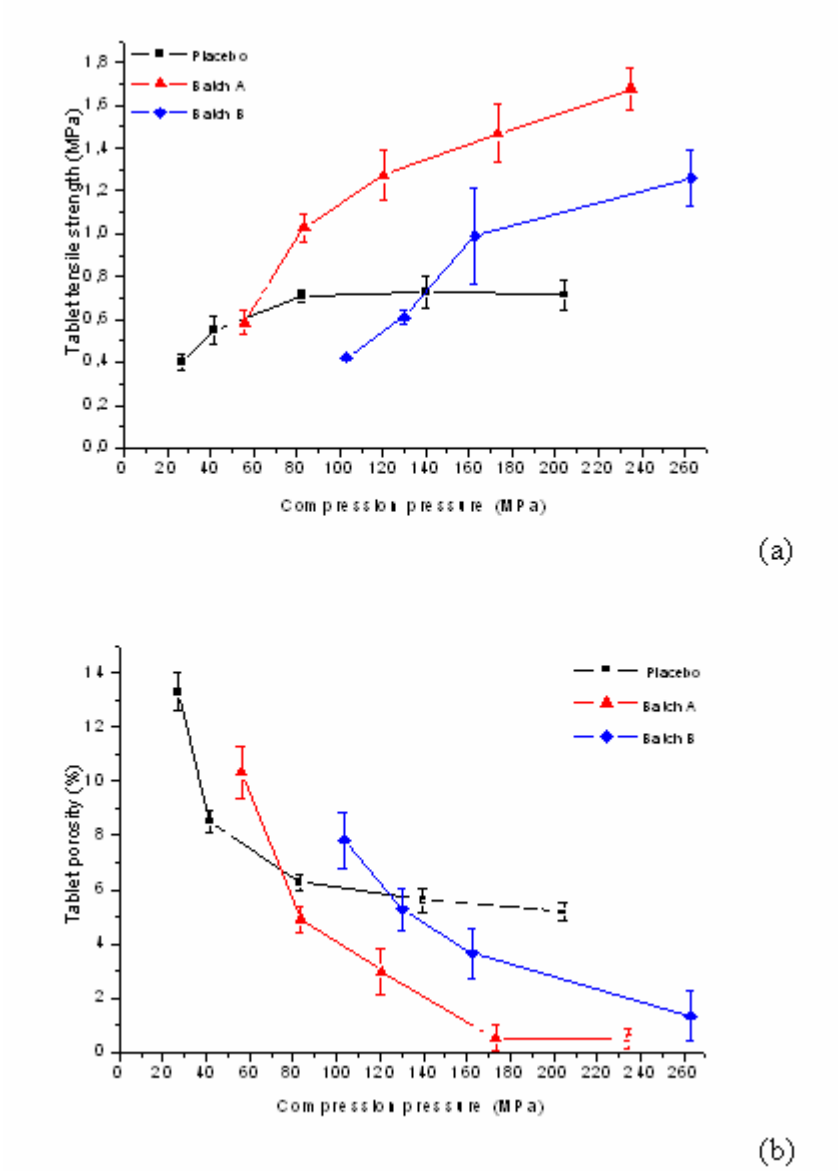

Figure 3.8

Tensile strength (a) and tablet porosity (b) versus compression pressure for placebo and medicated batches.

The tabletability of the three batches can be evaluated as a function of compression pressure range. In our experiments, the placebo batch, composed for the most part of MC (95%), exhibited the highest tabletability only at low compression pressures. In fact, in the compression range of 28-52 MPa, only the placebo gave tablets of sufficient tensile strength, while both medicated batches required higher compression pressures to yield tablets of appreciable strength. Tensile strength of placebo tablets progressively increased

only up to 80 MPa, after which the tensile strength remained constant whatever the compression pressure. At pressures over 80 MPa, the placebo exhibited no change in tabletability, in spite of the excellent compression properties of MC when used as diluent in direct compression (Dreu et al., 2005).

Batch A exhibited the best compression behaviour in the pressure range between 60 and 230 MPa: tabletability was good and tablet tensile strength increased proportionally with the increments in compression pressure reaching satisfying tablet tensile strengths.

Batch B exhibited very poor tabletability for compression pressures lower than 100 MPa: it was impossible to recover tablets, because they were too soft. It exhibited lower tabletability than the placebo batch in the compression pressure range of 100-140 MPa, but its tabletability was higher than that of the placebo for compression pressures over 140 MPa. Comparison of batches A and B tabletability shows the best tabletability of batch A. For example, to get tablets of 1.0 MPa tensile strenght, batch A must be compressed at a compression pressure of 70 MPa, while a compression pressure of 150 MPa is necessary for the batch B. In addition, it must be noted that the maximum recorded tablet tensile strength for batch B was 1.2 MPa at a compression pressure of 260 MPa, compared to 1.6 MPa for batch A obtained at a compression pressure of 240 MPa.

Tabletability is strongly related to compressibility, which is the ability of a material to undergo a reduction in volume as a result of an applied pressure (Joiris et al., 1998). This is expressed in Figure 3.8b as tablet porosity versus compression pressure. Here we can observe that for the placebo batch, porosity diminished markedly as compression pressure increased (with a total porosity reduction of 60%). The two medicated batches exhibited similar behaviour in reducing volume under compression, although batch A tablet porosity was always the lowest one, confirming better tableting performance than batch B. Batch A underwent a total porosity reduction of about 95%, while batch B underwent a total porosity reduction of 88%. Batch B required higher compression pressures to reach tablet porosity similar to that of batch A.

IV. INFLUENCE OF CRYSTAL HYDRATION ON THE MECHANICAL PROPERTIES OF SODIUM NAPROXEN

The aim of the study presented in this chapter is to establish a correlation between water uptake by anhydrous sodium naproxen (ASN) at two different relative humidities and modifications in tableting and densification behaviour under hydration.

Water uptake was evaluated at different relative humidities. Models for the hydration kinetics of ASN at 55% and 86%, corresponding to the formation of the dihydrated and tetrahydrated forms respectively, were evaluated assuming Eyring's dependence on temperature. Tabletability, compressibility, compactibility and densification behaviour were determined using an instrumented single punch tablet machine.

Kinetic data are consistent with a model where water molecules enter the crystal preferentially along hydrophilic tunnels existing in the crystal structure and corresponding to the propionate side chain. Water inclusion perturbs the crystallographic structure, causing slight structural changes according to the amount and associated to an increase in entropy. The interposition of water molecules between sodium naproxen molecules weakens intermolecular bonds, and these sites can behave like sliding planes under compression. Such structural changes may explain the improved compression behaviour and modified densification propensity mechanism. Kinetic data describing the water hydration mechanism of ASN explains in an original way the improved tableting and densification properties under hydration.

IV.1 ISOTHERMAL WATER SORPTION EXPERIMENTS

Results of isothermal water sorption experiments on ASN at 298 K are given in Figure 4.1.

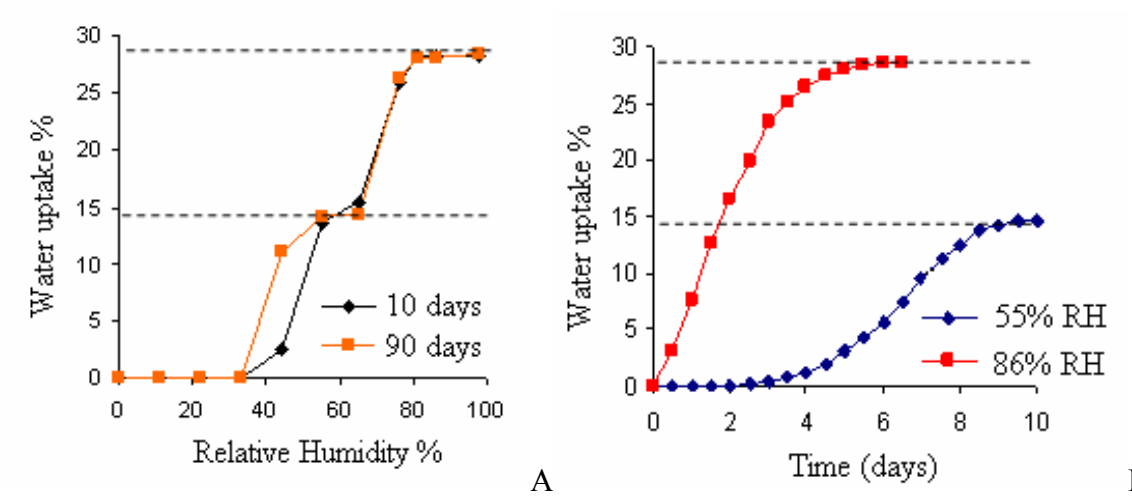

Figure 4.1

Sodium naproxen water uptake expressed versus relative humidity % (A) and versus time (B).

For relative humidity (RH) lower than 55%, water uptake was very low after 10 days of exposure. A weight increase corresponding to 2 water molecules for one ASN molecule was noted. This was followed by a rather short plateau, then a second water uptake corresponding to two additional water molecules at 76% RH, and finally by a plateau above 76% RH. These results are in agreement with those of Di Martino et al. (2007). The first plateau corresponds to the formation of dihydrated sodium naproxen (DSN), while the second one corresponds to that of tetrahydrated sodium naproxen (TSN). It should be noted that the curve obtained after 90 days at different RH% is identical, with the exception of the dot at 43%, where water uptake considerably increased with time due to the slow formation of the dihydrated form at this RH% value. This phenomenon was previously described by Kontny and Zografi (1995) for other hydrated systems. The kinetics of water uptake at 298 K at RHs of 55% and 86% are given in Fig. 4.1b. At 55%

RH, DSN formation required a latency period of some days. At 86% RH, TSN formation started immediately and was more rapid.

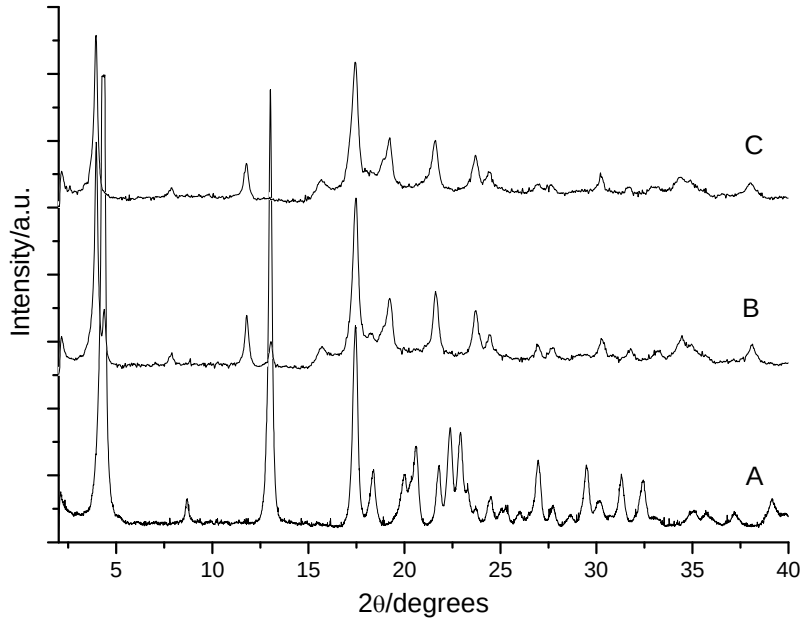

(a)

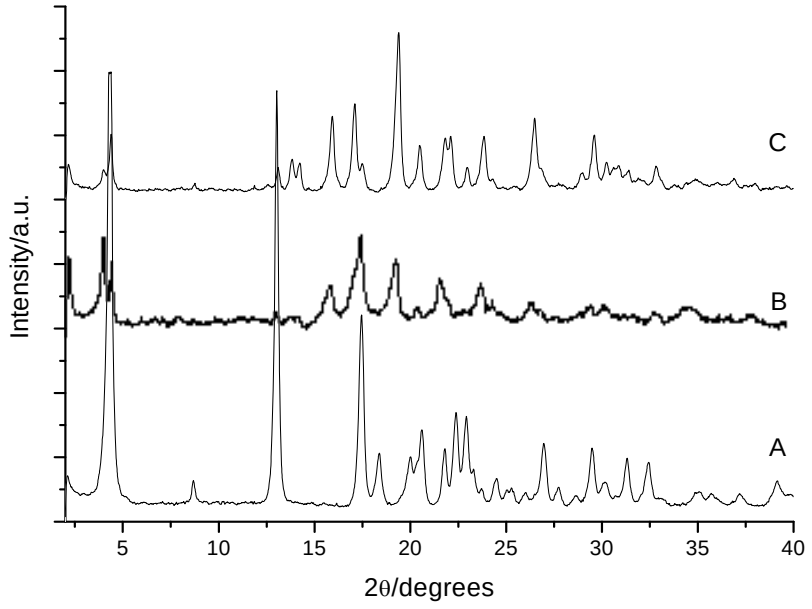

(b)

Figure 4.2

XRPD patterns of powders under hydration. (a) ASN starting material (A), after 6 days of exposure to 55% RH (50% hydration) (B), and completely hydrated DSN powder (C).
(b) ASN starting material (A), after 2 days of exposure to 86% RH (50% hydration) (B), and completely hydrated TSN powder (C).

These curves were used to prepare the samples for tableting experiments. Powders under hydration were checked by XRPD. These analyses showed that, at an RH of 55%, when water uptake was not still complete, powders were composed of a mixture of ASN and DSN, without any intermediate crystalline form, such as for example monohydrate sodium naproxen (MSN).

This result is clearly shown in Figure 4.2a, where XRPD patterns of sodium naproxen exposed to 55% RH are presented when hydration was at 50%, as well as those of ASN, the starting material, and DSN, the completely hydrated form.

The intermediate form is clearly composed of a mixture of the two pure forms (ASN and DSN), and no peaks of any other forms, such as MSN, were visible. Peak intensities are proportional to water sorption and results concord with previously published data (2007), showing that typical ASN peaks progressively decrease as DSN peaks appear, without any other different forms. Similarly, at an RH of 86%, when water uptake was not still complete, powders were composed of a mixture of ASN and TSN, without any intermediate crystalline form such as, for example, MSN or DSN, as can be seen in Figure 4.2b. These results are in agreement with those of Di Martino et al. (2007).

Figure 4.3 shows the particle morphology of ASN, the starting material, and of the completely hydrated and now pure forms, DSN and TSN. This evaluation, together with particle size, is important particularly afterwards, when interpreting compression and densification behaviour. Particles are irregular with smoothed edges; there are no obvious differences between the three products and hydration does not seem to affect particle morphology.

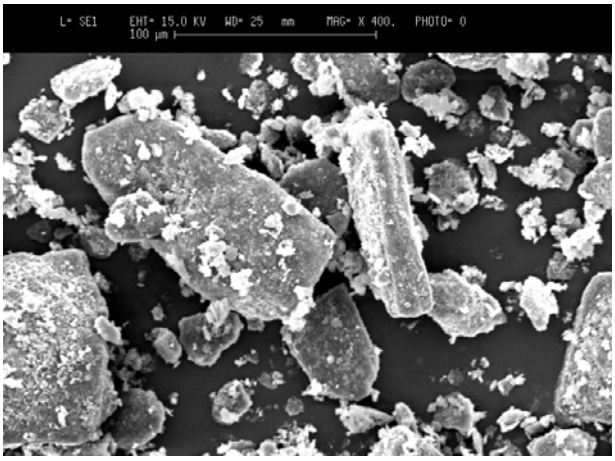

(a)

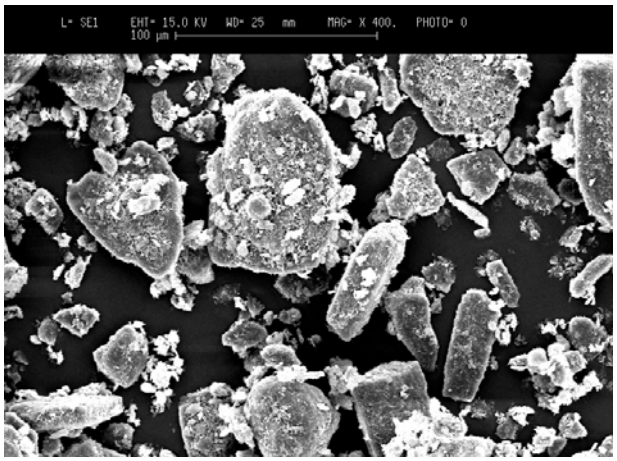

(b)

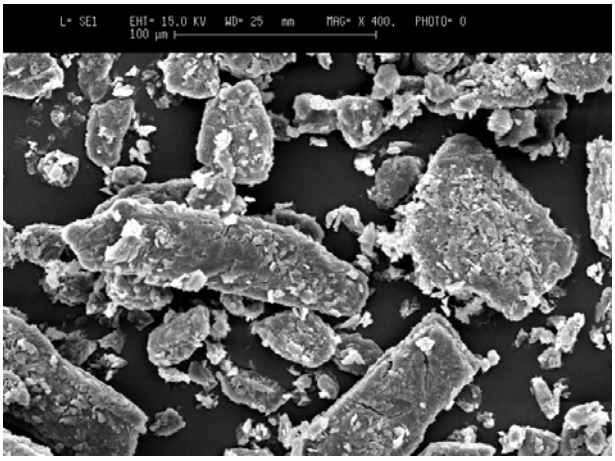

(c)

Figure 4.3

SEM microphotographs of ASN (a), completely hydrated DSN after exposure to 55% RH (b), completely hydrated TSN after exposure to 86% RH (c)

Particle sizes and distributions are given in Figure 4.4. No differences occurred as a consequence of hydration and slight variations among the three products are not statistically relevant.

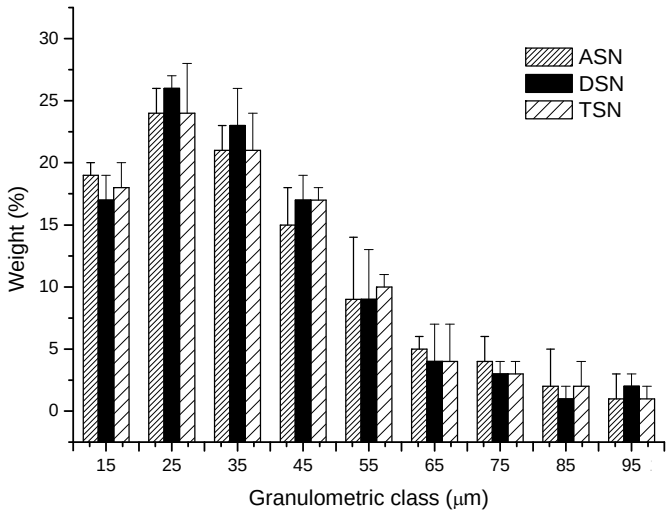

Figure 4.4

Particle size and distribution of sodium naproxen particles. ASN: anhydrous sodium naproxen; DSN: dihydrated sodium naproxen; TSN: tetrahydrated sodium naproxen.

IV.2 STUDY OF HYDRATION KINETICS

To describe the process of water addition into the crystal, the following general equation was considered:

$$\frac{d\alpha}{dt} = k(T) \cdot f(\alpha) \tag{10}$$

where *k(T)* is the rate constant at temperature *T* and α , the fractional degree of reaction, represents the fraction of water added at time *t*, that is:

$$\alpha = \frac{M}{M_T} \tag{11}$$

where *M* is the mass of water in the sample at time *t* and M_T is the total mass of water in the sample at the end of hydration. The relationship between α and time is embodied in the function $f(\alpha)$, which in turn depends on the reaction model followed by water addition.

Integration of equation (10) at constant temperature gives:

$$\int_0^1 \frac{d\alpha}{f(\alpha)} = g(\alpha) = \int_0^t k(T) \cdot dt = k(T) \cdot t \tag{12}$$

The rate constant *k(T)* may be considered as follows, based on Eyring's dependence on *T*:

$$k(T) = \frac{k_B T}{h} exp\left(\frac{\Delta S^*}{R}\right) exp\left(\frac{-\Delta H^*}{RT}\right) \tag{13}$$

where ΔS^* is the activation entropy, ΔH^* is the activation enthalpy, *R* is the gas constant, k_B is Bolzmann's constant and *h* is Planck's constant.

Both ΔS^* and ΔH^* can be estimated from rate constant values determined by isothermal measurements (at several temperatures), provided $g(\alpha)$ is known. Table 4.1 gives selected expressions (Šesták and Gunnar, 1971; Dong et al., 2002) for $g(\alpha)$ corresponding to the most common solid-state processes.

Table 4.1

Algebraic expressions corresponding to the most common mechanism generally used to describe changes in solid state (Šesták and Gunnar, 1971; Dong, et al, 2002).

Model	$g(\alpha)$	**Mechanism (description of equation)**
A2	$[-\ln(1-\alpha)]^{\frac{1}{2}}$	one-dimensional growth of nuclei (Avrami-Erofeyev equation, n=2)
A3	$[-\ln(1-\alpha)]^{\frac{1}{3}}$	two-dimensional growth of nuclei (Avrami-Erofeyev equation, n=3)
A4	$[-\ln(1-\alpha)]^{\frac{1}{4}}$	three-dimensional growth of nuclei (Avrami-Erofeyev equation, n=4)
R1	α	one-dimensional phase boundary reaction (zero-order mechanism)
R2	$1-(1-\alpha)^{\frac{1}{2}}$	two-dimensional phase boundary reaction (contracting cylinder)
R3	$1-(1-\alpha)^{\frac{1}{3}}$	three-dimensional phase boundary reaction (contracting sphere)
D1	α^2	one-dimensional diffusion
D2	$(1-\alpha)\ln(1-\alpha)+\alpha$	two-dimensional diffusion
D3	$\left[1-(1-\alpha)^{\frac{1}{3}}\right]^2$	three-dimensional diffusion (Jander's equation)
D4	$\left(1-\frac{2}{3}\alpha\right)(1-\alpha)^{\frac{2}{3}}$	three-dimensional diffusion (Ginstling-Brounshtein equation)

Table 4.2

Eyring's parameters for hydration process.

					Eyring plot		
Hydration Condition	**Model**	***T* (°C)**	***K* (sec^{-1})**	***r***	**ΔH^* ($kJ\ mol^{-1}$)**	**ΔS^* ($J\ K^{-1}\ mol^{-1}$)**	***r***
55% RH First step	D1	15	$7.590 \cdot 10^{-9}$	0.942	122.4	+30.8	0.910
		20	$9.780 \cdot 10^{-8}$	0.947			
		25	$9.722 \cdot 10^{-8}$	0.898			
		30	$1.886 \cdot 10^{-7}$	0.970			
		35	$3.670 \cdot 10^{-7}$	0.950			
55% RH Second step	A2	15	$3.05 \cdot 10^{-6}$	0.978	5.0	-332.6	0.999
		20	$3.12 \cdot 10^{-6}$	0.984			
		25	$3.21 \cdot 10^{-6}$	0.965			
		30	$3.37 \cdot 10^{-6}$	0.974			
		35	$3.65 \cdot 10^{-6}$	0.992			
86% RH	A2	15	$2.88 \cdot 10^{-6}$	0.996	24.1	-266.5	0.992
		20	$3.69 \cdot 10^{-6}$	0.998			
		25	$4.51 \cdot 10^{-6}$	0.996			
		30	$5.06 \cdot 10^{-6}$	0.994			
		35	$6.06 \cdot 10^{-6}$	0.989			
86% RH	R2	15	$1.39 \cdot 10^{-6}$	0.997	22.0	-280.2	0.997
		20	$1.69 \cdot 10^{-6}$	0.995			
		25	$2.02 \cdot 10^{-6}$	0.996			
		30	$2.27 \cdot 10^{-6}$	0.988			
		35	$2.75 \cdot 10^{-6}$	0.985			

Plots were placed according to kinetic equations shown in Table 4.1 and their conformity assessed by the least-square method. The function that best fitted the hydration

data was selected, and the corresponding values of *k* were determined. By fitting Eyring's expression to these values the activation enthalpy and entropy of the process could be determined.

Table 4.2 and Figure 4.5 give the results of ASN hydration at two different relative levels of humidity and at different temperatures.

At 55% RH, reaction occurred in three stages (Figure 4.5a).

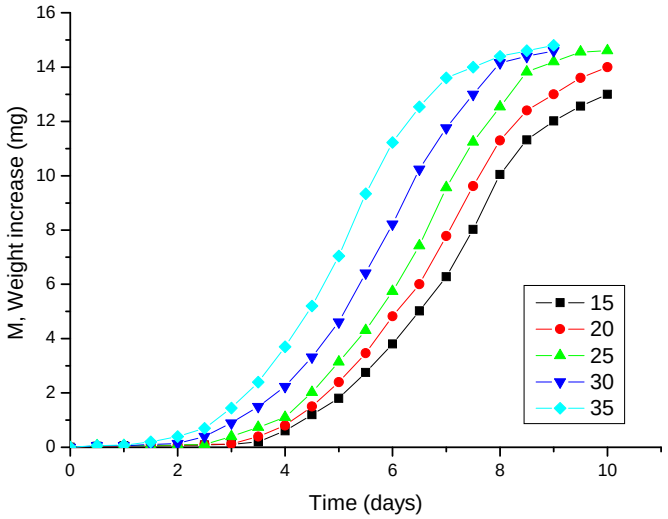

(a)

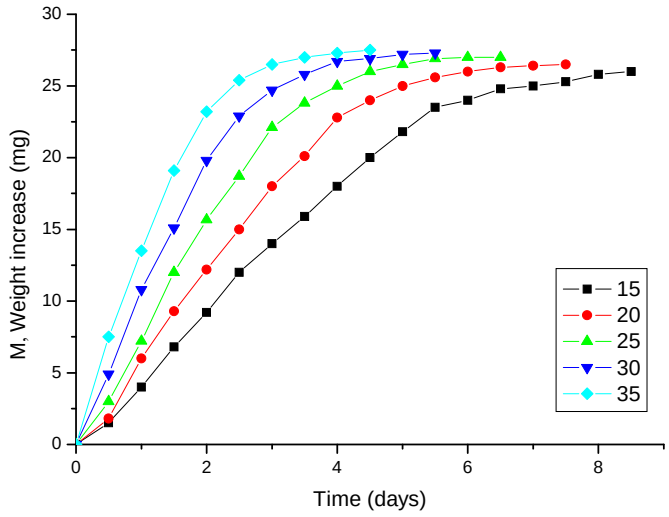

(b)

Figure 4.5

Sodium naproxen hydration rate at different experimental temperatures. (a) NS exposed to 55% RH; (b) NS exposed to 86% RH.

The induction period of nucleation, which is the initial reaction step, was rather long in time, but insignificant in weight increase. During the subsequent stage at the interface, i.e. the acceleratory period, weight increased with time, and this was followed by a decay period. The experimental *M* versus *t* curves had a sigmoid shape. Values suggest that hydration proceeded according to the model reported in Table 4.2. In the present case, such curves could only fit one of the models reported in Table 4.1 and so fitting was performed separately for the induction period and for the acceleratory-decay period. The first hydration period involved a D1 model, i.e. one-dimensional diffusion. When a gas molecule is fixed to a solid substratum, the ΔS^* should be negative, because the gas molecule loses degrees of translation freedom. However, a positive and non-negligible ΔS^* was obtained during the induction period, meaning that the freedom degrees of the activated state compensated for the loss of freedom degrees by water. Enthalpy value (ΔH^*) was high, suggesting that introduction of the water molecule greatly modified the rigid structure of the crystal. Eyring's parameters suggest that the entry of the water molecule alters the crystalline form towards a more expanded structure, in which the hydrated solid has more freedom degrees than the anhydrous one.

The second stage of the hydration reaction is best described by an A2 model (Avrami-Erofeyev equation, n=2), which indicates that reaction is controlled by one-dimensional growth of nuclei. ΔS^* (–332.7 J K^{-1} mol^{-1}) was now negative and reflected the expected entropy loss of water molecules entering the solid. On the other hand, the enthalpy change (ΔH^* = 5.0 kJ mol^{-1}) was much lower than during the induction period, suggesting that there was little enthalpic hindrance to the growth of the new phase.

To sum up, the hydration process for ASN exposed to 55% RH occurred in two steps: firstly, water molecules diffused inside the crystal, accessing through hydrophilic sites present in the crystal (1st step corresponding to the D1 model and then water reacted with surrounding SN molecules to create new bonds and rearrange molecules (2nd step corresponding to the A2 model).

A rather different reaction model is involved when the solid is exposed to 86% RH (Table 4.2, Figure 4.5b). In this case the induction period, if any, was no more than a few

hours, i.e. shorter than the time interval chosen for the experimental design. Two different reaction models gave a very good fit for $g(\alpha)$ versus t:

a) the one-dimensional growth of nuclei (Avrami-Erofeyev equation, n=2), i.e. the same involved in the second stage of hydration at 55% RH and

b) the two-dimensional phase boundary reaction (contracting cylinder, R2 model).

The ΔS^* values for the two models, both negative and quite similar to each other, were similar to that found for the second hydration stage at 55% RH. Also the ΔH^* values were quite similar to each other (respectively 24.1 or 22.0 kJ mol^{-1}), but higher than the value found for the second hydration stage at 55% RH. Then at 86% RH, when four water molecules rather than two entered the lattice, hydration was accompanied by a greater enthalpy change, probably due to more notable crystallographic changes.

To sum up, and by analogy with hydration results at 55% RH, the R2 model (two dimensional phase boundary reaction) seems the most probable mechanism, because again it implies water diffusion through pre-existing hydrophilic channels, then the association of water with polar groups capable of forming hydrogen bonds with water.

IV.3 COMPRESSION BEHAVIOUR

Before compression, all the hydrated powders were analysed by TGA to verify whether hydration occurred as expected. It should be noted that in the case of sodium naproxen TGA does not make it possible to distinguish between bound and absorbed water.

This fact has also been previously highlighted by Kim et al. (2005) and Di Martino et al. (2001) and is due to the fact that the loss of bound water starts at quite low temperatures close to those favouring the loss of absorbed water.

All the tested products showed very favourable behaviour under compression and no capping, sticking or seizing problems arose during the present study.

Results are given in Figure 4.6a (tabletability), 4.6b (compressibility), 4.6c (compactibility). In these Figures, the unit used to represent the amount of water is the

Mean Stoichiometric Coefficient (MSC), which is, the number of water molecules per molecule of SN. It is of paramount importance to keep in mind that this number is a mean number, because hydrates in formation are mixtures of anhydrous and hydrated forms, and not intermediate hydrates.

The tabletability of ASN was relatively good. The tensile strength after compression at 150 MPa was 1.25 MPa. The values for the hydrated forms were higher: 2.59 MPa for DSN and 3.30 MPa for TSN. Tensile strength of hydrates in formation was proportional to MSC (Figure 4.6a).

At 55% RH, the progressive formation of DSN corresponded to a progressive increase in tablet resistance, indicating a very significant correlation between tabletability and water content. At 86% RH, the progressive formation of TSN yielded a bell trend, with a maximal tensile strength of 3.95 MPa for an MSC of 3. Beyond this point, the increase in water content corresponded to a decrease in tensile strength. The compression behaviour of hydrated samples was compared to that of physical mixtures (PM) prepared by gently mixing different proportions of pure ASN and DSN or pure ASN and TSN in a mortar.

Compression of physical mixtures of ASN and DSN (ASN : DSN of 75 : 25 or 50 : 50), or ASN and TSN (ASN : TSN of 12.5 : 87.5 and 75 : 25), corresponding to MSCs of 0.5 and 1, was then carried out. For the same water amount, the tabletability of physical mixtures was lower than that of hydrates in formation. It is clear that the way in which water is distributed among the particles is fundamental.

In the case of physical mixtures, water is present in one portion of particles, while the other portion is anhydrous. However, in hydrates in formation, the water involved in hydration may be assembled in the periphery of particles, while the centre remains dry. This phenomenon is compatible with the typical structure of “channel hydrates” (Morris, 1999). Kim (2005) observed a similar situation under optical microscopy, but the other way round, during the dehydration of MSN to ASN: there was initial dehydration at the periphery of the particles followed by progression of the phenomenon to the centre of the crystal parallel to the channels.

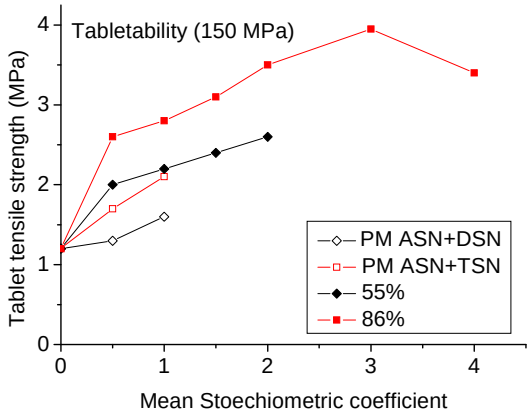

(a)

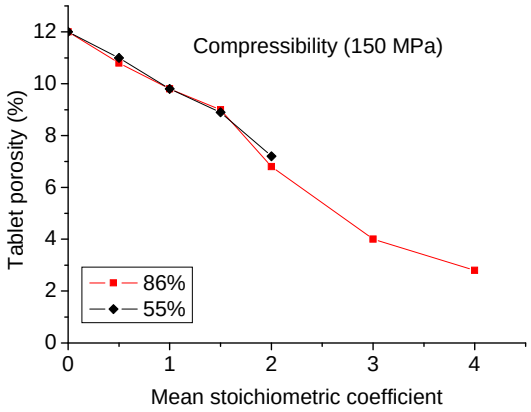

(b)

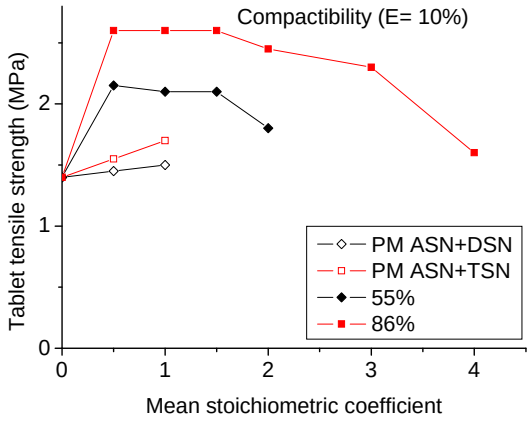

(c)

Figure 4.6

Tabletability (a), compressibility (b) and compactibility (c) of SN hydrated forms. Each point is the mean of five independent determinations and is given with the 95% confidence interval. Solid symbols correspond to hydrates in formation at 55% (blue) and 86% (red). The open symbols correspond to the physical mixtures of ASN and DSN (blue) and ASN and TSN (red).

To have a better understanding of the profiles of tabletability, other representations are required. Tablets can be considered as the dispersion of particles in the air. Their cohesion comes from the intermolecular strength among particles that can act only when distances are very small (Nyström and Karehill, 1996). Any variation in tablet cohesion can thus theoretically be caused either by a modification of interparticle distances or an alteration in the intensity and/or the number of bonds. These phenomena can be explained by interpreting the compressibility and compactibility results.

Water greatly modifies the compressibility of SN. After compression at 150 MPa, tablet porosity changes from 12.1% for ASN to 7.2% for DSN and 2.4% for TSN. The compressibility of hydrates in formation is presented in Figure 4.6b. The porosity of tablets produced at 150 MPa progressively decreases as a function of water content. This porosity reduction is comparable, whatever the water uptake, at 55% or 86%. A Pearson's test carried out on the data shows that a very good correlation exists between tablet porosity and MSC ($r= -0.97$, $p<0.0001$). Compressibility data of physical mixtures is not presented in the same Figure, because it is exactly superposed over that of hydrates in formation.

These results show that SN particles are closer together in water for the same compression pressure. The tabletability of SN is therefore increased by the presence of water. However, such evidence is inadequate to explain the differences observed between DSN and TSN, between hydrates in formation and those between physical mixtures and the bell profile of the tabletability of TSN. This is the reason why it is also essential to consider compactibility, which makes an assessment of the strength of interparticle bonds possible. The basic concept for a compactibility study is to make and compare the mechanical resistance of tablets of the same porosity for any substance under study. As proximity between particles is the same, the differences observed can be attributed to the number and/or intensity of interparticle bonds. For this study therefore, new tablets must be produced and porosity fixed at 10%, a value at which it is possible to recover tablets for any powder under study. The tensile strengths are 1.45, 1.83 and 1.77 MPa respectively for ASN, DSN and TSN at 10% porosity. As these values are quite close, they are not very informative and so the complete profiles of hydrates in formation and of physical mixtures are given in Figure 4.6c. It can be observed that for the very first water content tested

(MSC 0.5), the compactibility of DSN and TSN in formation abruptly increased to reach the values of 2.18 and 2.57 MPa respectively. These values changed little as water content increased, giving the profile of compactibility as a plateau. The last value on each curve (corresponding to DSN and TSN completely formed) was significantly lower, and more pronounced for TSN. In addition, the evolution of compactibility for physical mixtures was completely different and remained intermediate between the values measured for ASN and complete hydrates. All this information is compatible with a hydration model in which water enters into the anhydrous particles through pre-existing channels and thus remains confined at the periphery of the crystals, causing an abrupt modification to particle surface and thus to interparticle bonds. The higher compactibility of TSN in formation compared to DSN may account for its better tabletability. It must be considered that the tetrahydrated form can already be formed at lower RH% (up to 64 %) as proven by water sorption isotherms. Exposure to higher humidity levels (as in the case of 86% RH) can imply that a part of the water is involved in the hydration of the crystal (to form the tetrahydrated structure) and excess water is absorbed inside the tunnels and on the crystal surface.

Consequently, it is possible to assume that at the end of hydration, when the crystalline structure is “saturated”, the available water is adsorbed on the surface of the particles, covering them with a thin film that reduces the possibility of interparticle bonds.

However, as it is impossible to quantify exactly the water absorbed by TGA, as previously explained, this can only be a supposition. Water distribution in physical mixtures is completely different, yielding samples of lower compactibility than that of hydrated forms and practically uninfluenced by mixture composition.

IV.4 DENSIFICATION MECHANISM

The study of the compression behaviour of SN showed that hydration water significantly increased compressibility. The objective of the densification study is to obtain information about the mechanisms related to compressibility changes.

The first step in the study was to identify in which phase (compression or decompression) the compressibility modifications due to hydration take place. Figure 4.7 shows the effect of hydration on the minimal porosity of tablets in formation, at the end of compression phase (Figure 4.7a), and on the elastic recovery of tablets during decompression. Results are given in Table 4.3.

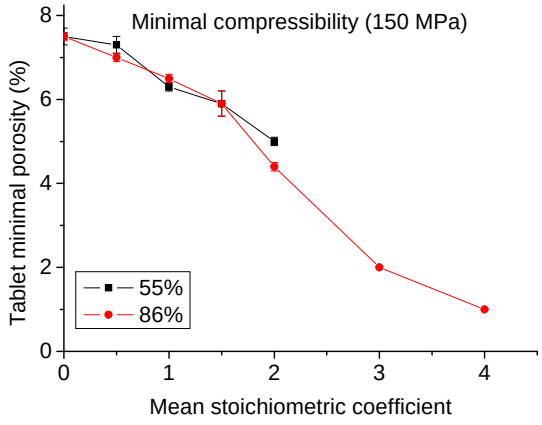

(a)

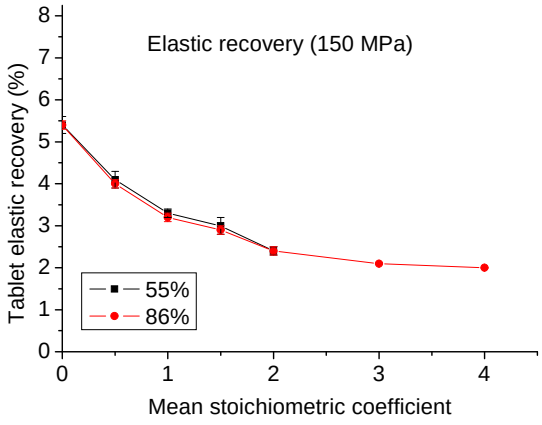

(b)

Figure 4.7

Minimal porosity (a) and elastic recovery (b) expressed versus MSC. Each point is the mean of five independent determinations and is given with the 95% confidence interval. Solid symbols correspond to hydrates in formation at 55% (blue) and 86% (red). The open symbols correspond to the physical mixtures of ASN and DSN (blue) and ASN and TSN (red).

Table 4.3

Compressibility values and Heckel's parameters, expressed with their 95% confidence intervals, of tablets produced at 150 MPa. Each value is the mean of five independent determinations.

RH (%)	MSC	ε (%)	ε_{min} (%)	RE (%)	P_y (MPa)	D_0'	D_B'
55	0	12.1±0.3	7.4±0.3	5.30±0.19	125.1±0.9	0.583±0.002	0.186±0.002
	0.5	10.9±0.3	7.2±0.3	4.12±0.17	113.4±0.9	0.552±0.003	0.179±0.002
	1	9.4±0.2	6.3±0.2	3.44±0.06	104.0±1.0	0.576±0.001	0.152±0.001
	1.5	8.5±0.2	5.7±0.3	3.12±0.08	97.8±0.1	0.584±0.006	0.136±0.006
	2	7.2±0.3	5.0±0.1	2.39±0.05	92.9±1.0	0.605±0.002	0.120±0.001
86	0	12.1±0.3	7.4±0.3	5.30±0.19	125.1±0.9	0.583±0.002	0.186±0.002
	0.5	10.5±0.2	6.9±0.1	4.02±0.20	110.1±0.6	0.566±0.002	0.161±0.001
	1	9.5±0.2	6.5±0.2	3.34±0.09	106.6±1.6	0.572±0.002	0.149±0.003
	1.5	8.7±0.3	5.7±0.4	3.00±0.10	99.4±2.2	0.582±0.004	0.137±0.004
	2	6.6±0.3	4.4±0.2	2.35±0.10	87.3±2.3	0.585±0.003	0.132±0.005
	3	3.8±0.2	1.9±0.1	1.98±0.15	61.4±2.8	0.609±0.003	0.131±0.007
	4	2.4±0.2	0.7±0.2	1.80±0.28	47.6±2.0	0.642±0.003	0.162±0.006

MSC = Mean Stoichiometric Coefficient; ε = tablet porosity; ε_{min} = minimal porosity; P_y = mean yield pressure.

These results clearly show that two different mechanisms contribute to the increase in compressibility. When hydration starts, minimal porosity changes little, while elastic recovery decreases. Afterwards, minimal porosity decreases while elastic recovery levels off at a low value. The limit between these two phases is located at a stoichiometric coefficient of 1.5. It is visible in Figure 4.7b which presents the whole evolution of compressibility. Results corresponding to the same MSC are similar, whether water uptake has occurred at 55% or 86% RH.

The second step in the densification study focuses on the way the particle is deformed during the compression phase. This is done by analysing the parameters of Heckel's equation (Table 4.3).

These values show that ASN particles fragment during compression (high D_B' and P_y) and that they change progressively during hydration, indicating a modification in the densification mechanism, from fragmentation to plastic deformation (lower P_y). With TSN the peculiarity is the association of a high D_B'value to a low P_y value, corresponding to the high compressibility of this product. Results registered during this second part of the work are similar for the common stoichiometric coefficients, independently of the RH% used for water uptake (55 or 86% RH).

Results of the densification study are confirmed by examining the general profiles of Heckel's cycles. The cycles obtained for tablets produced at the same final porosity of 10% are given in Figure 4.8. For low water content, the decrease in the initial curve is clearly evident, and corresponds to the change from volume reduction by fragmentation to plastic deformation. The decrease in elastic recovery is also clearly evident, as can be noted by the decompression phase which becomes more horizontal. For the highest water content, the increased slope in the climbing part of the cycle can be observed with maximal pressure, which becomes weaker and weaker to obtain tablets of 10% porosity.

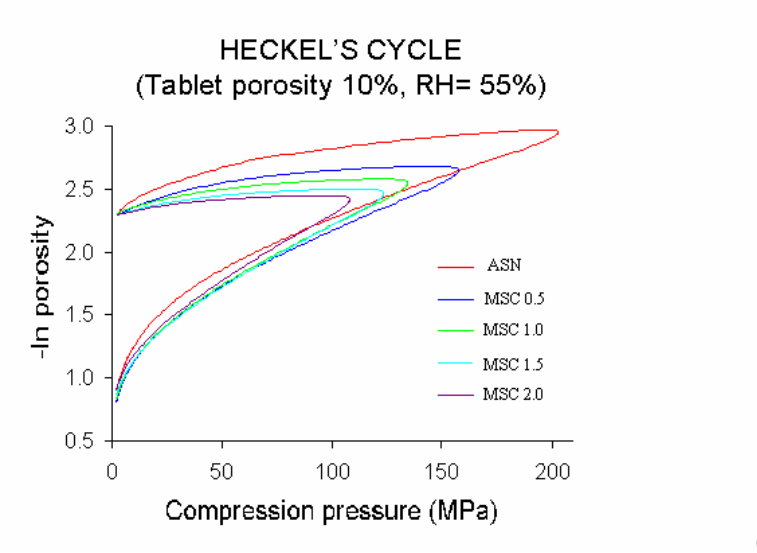

(a)

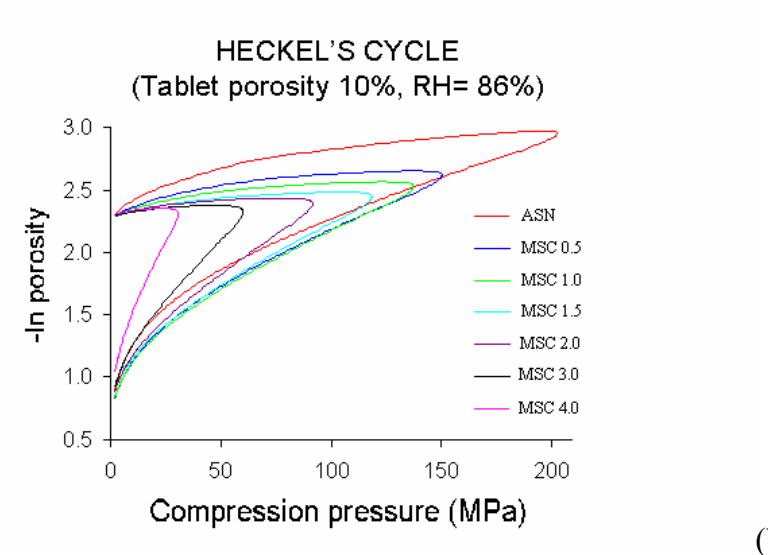

(b)

Figure 4.8

Heckel's cycles for tablets of 10% porosity. Tablets are produced from SN under hydration at 55 (a) and 86% RH (b) RH. Each curve corresponds to whole values recorded while producing one tablet.

Modification in the densification mode is at the origin of the tabletability and compactibility improvement to be seen at the very start of hydration. Indeed, as explained above, the water captured at the initial phase of hydration may be concentrated in the periphery of the crystal. This external zone can become highly deformable, increasing the interparticle contact surface. This hypothesis is compatible with the fact that TSN, which is more plastic than DSN, also displays greater compactibility.

IV.5 RELATIONSHIP BETWEEN HYDRATION AND THE MECHANICAL PROPERTIES OF SN

The crystallographic structure of naproxen acid has been described as monoclinic (Ravikumar et al., 1985; Kim et al., 1987) and the presence of the Na atom in the salified form does not modify this (Kim et al., 1990). The Na atom participates in an "O···Na" type interaction where Na is simultaneously linked to four oxygen atoms forming a tetramer that stabilizes the structure (Kim et al., 1990). Di Martino et al. (2001, 2007) have classified the hydrated forms of SN as "channel hydrates" according to Morris (1999).

During the hydration process, water molecule access into the crystal is limited by the presence of some hydrophobic sites, mainly formed by the π cloud of the naphthalene rings. Water molecules can thus move preferentially from the periphery of the crystals along hydrophilic tunnels existing in the crystal structure and corresponding to the propionate side chain. Water molecules can then be easily accommodated between the SN molecules by forming hydrogen bonds with both Na and/or O atoms. The dimensions of the tunnel can be dependent on the number of water molecules placed in the tunnel (two for the dihydrate and four for the tetrahydrated). The conformational changes associated with hydration promote crystallographic modifications. Consistently with this, hydrated forms of sodium naproxen can be considered as "expanded channel hydrates" (Morris, 1999). In this hydrated form, the water molecules converge on channels in the crystal structure, causing the distance between some crystalline planes to be increased proportionally to the amount of water. In this kind of structure, the water molecules are mainly bound together by hydrogen bonds and interact little with the host molecule. Thus, water molecules can easily move into the channel, bringing about easy and progressive hydration or dehydration of the crystals. This can explain the progressive increase in plastic deformation of hydrated forms which is proportional to the increase in water inside the crystal, as well as the modification in the densification mechanism from fragmenting to plastic deformation. This also accounts for the differences between the dihydrated and tetrahydrated forms. The intermolecular spaces occupied by water molecules behave like "sliding planes" for plastic deformation. In a previous study, Sun and Grant (2001)

explained the greater tableting propensity of the monohydrated form of *p*-hydroxybenzoic acid in its anhydrous form through the combination of a larger interparticle bonding area, thanks to the presence of water, and higher bonding strength. In fact, in the monohydrated form, the water molecules fill the spaces between the layers and facilitate the plastic deformation of the crystals by maintaining a larger separation between the zigzag-shaped planes.

V. MECHANISMS FOR DEHYDRATION OF THREE SODIUM NAPROXEN HYDRATES

In the present work, it is observed the isothermal dehydration of some of naproxen hydrates by thermogravimetry at several temperatures. The rate of water removal from the crystal was used to determine the mechanism of dehydration in the solid state, by fitting results with selected expressions corresponding to the most common solid-state processes.

The water loss was then evaluated according to Eyring's equation, and both changes in activation enthalpy (ΔH^*) and activation entropy (ΔS^*) were estimated from rate constant values. Experiments made it possible to distinguish different dehydration mechanisms for these hydrate forms, and in particular, to discern the dehydration behaviour of two different dihydrate forms, one obtained by crystallizing sodium naproxen from water (CSN) and the other obtained after exposure to 55% RH (DSN).

These results add new evidence supporting the X-ray powder diffraction study carried out in this work, showing different patterns for these two forms. X-ray powder diffractometry evaluation of the phase transitions occurring during dehydration of these two dihydrate forms showed that they vary according to dehydration temperature.

V.1 PHYSICAL CHARACTERIZATION OF STARTING SAMPLES

All the samples under study were firstly characterized for their mean particle size, which was as follows:

- ASN: 75.0 ± 2.7 μm;
- MSN: 80.3 ± 4.5 μm;
- DSN: 78.2 ± 3.9 μm;
- CSN: 74.5 ± 1.7 μm;
- TSN: 79.1 ± 2.5 μm.

From these results, it is possible to deduce the very high particle size similarity, aspect of paramount importance to correctly interpret the results presented afterwards.

Anhydrous and hydrated forms of SN have already been described above (Kim and Rousseau., 2004; Di Martino et al., 2007). In Figure 5.1, the results of STA analysis, simultaneously showing TGA and DSC thermograms, are reported for all the forms described previously

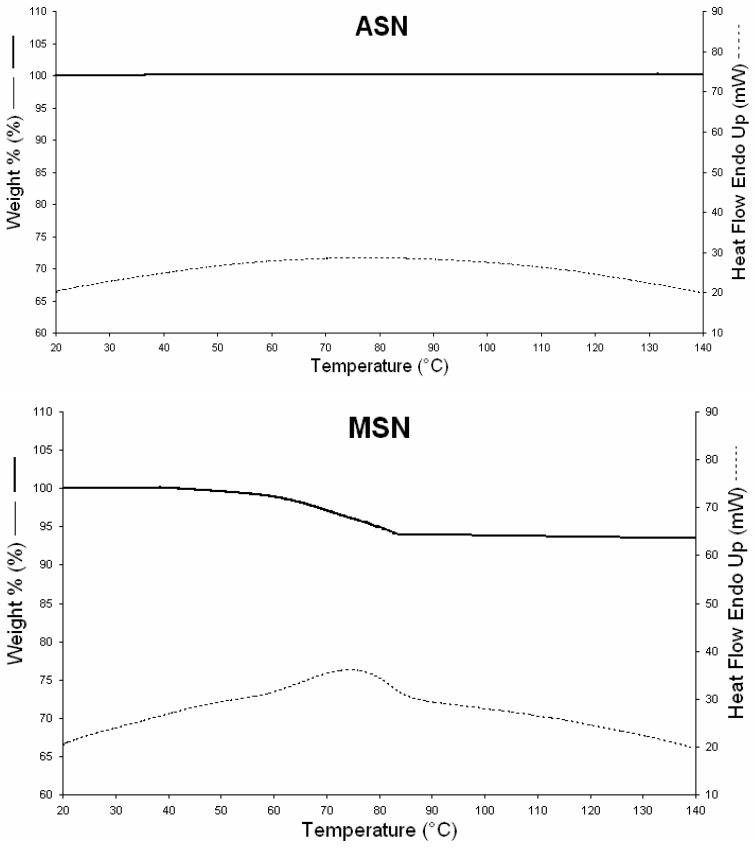

(Figure 5.1 follows next page)

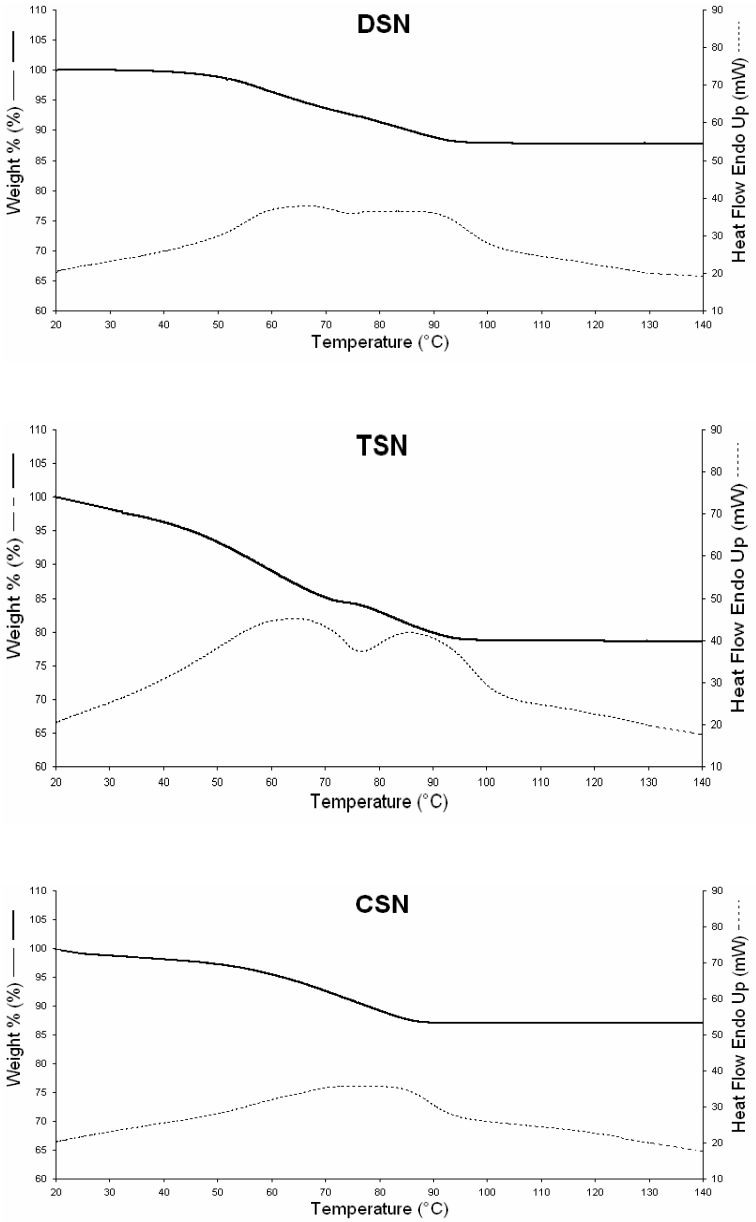

Figure 5.1

Thermograms of Simultaneous Thermal Analysis (STA) of the anhydrous and hydrated forms of sodium naproxen carried out at 10 K/min. Bolt line corresponds to the TGA-STA analysis; broken line corresponds to DSC-STA analysis. ASN: anhydrous sodium naproxen; MSN: monohydrate sodium naproxen; DSN: dihydrate sodium naproxen; TSN: tetrahydrate sodium naproxen; CSN: crystallized sodium naproxen.

.

In order to summarize some important physicochemical characteristics of these forms, theoretical and experimental water contents determined by TGA-STA are listed in Table 5.1 and also compared to values previously reported in the literature.

Table 5.1

Summary of water content determined by thermogravimetry (TGA-STA) of anhydrous and hydrated sodium naproxen forms. Experimental results are compared to those reported in literature.

		TGA-STA (% W/W)	
	Theoretical water content (%W)	**Data from literature**	**Data of the present work**
ASN	0.00	0.05 ± 0.01 [a] 0.39 ± 0.03 [b]	0.07 ± 0.02
MSN	6.66	6.83 ± 0.29 [a]	6.68 ± 0.02
DSN	12.49	12.90 ± 0.04 [b]	12.87 ± 0.24
TSN	22.21	20.68 ± 0.48 [b]	21.55 ± 0.13
CSN	12.49	12.96 ± 0.66 [a]	12.92 ± 0.31

[a] Kim and Rousseau.

[b] Di Martino et al.

Table 5.1 shows that samples produced for the present study are all in compliance with the expected values. In particular, it must be noted that two different dihydrate SN are mentioned, the crystallized sodium naproxen (CSN) obtained by crystallizing SN from water (Di Martino et al., 2001; Kim and Rousseau, 2004) and the dihydrate sodium

naproxen (DSN) obtained by exposing anhydrous SN powder to 55% RH (Di Martino et al., 2007).

X-ray powder diffraction analysis was first performed at the beginning of this study in order to check the crystallographic form of the powders being used. Patterns, given in Figure 5.2, were thus compared to those previously reported in the literature.

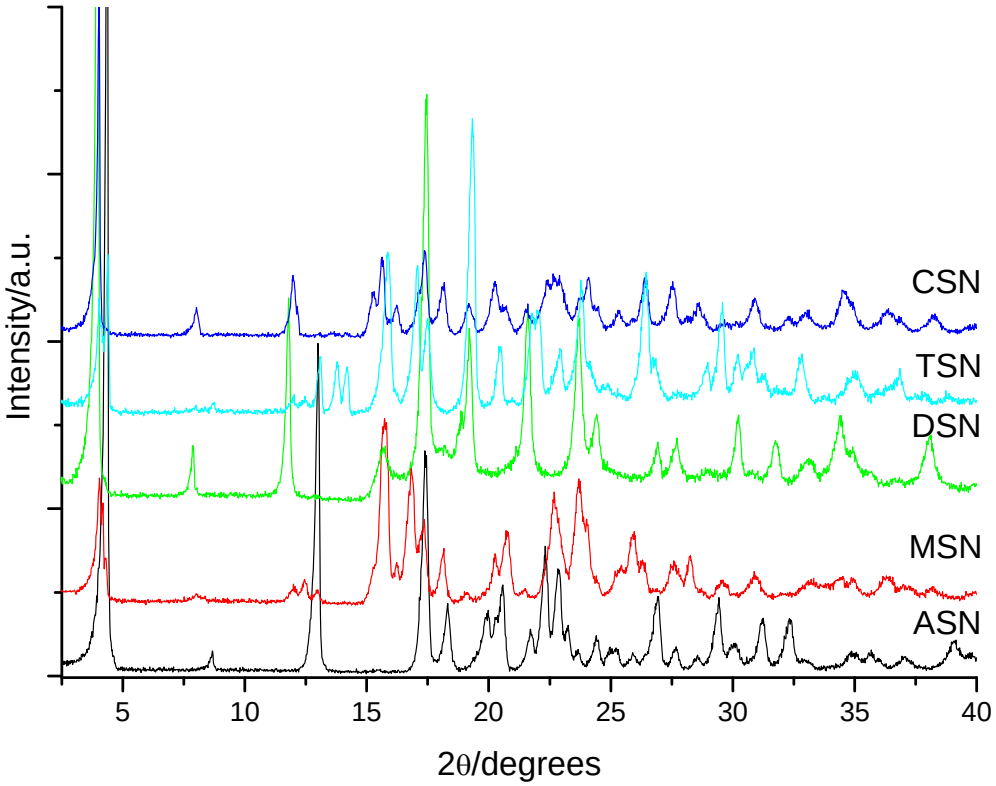

Figure 5.2

XRPD patterns of the anhydrous and hydrated forms of sodium naproxen. ASN: anhydrous sodium naproxen; MSN: monohydrate sodium naproxen; DSN: dihydrate sodium naproxen; TSN: tetrahydrate sodium naproxen; CSN: crystallized sodium naproxen.

The patterns of all the structures comply with those presented in previous papers: ASN and CSN comply with Kim and Rousseau (2004) and Di Martino et al. (2007); MSN complies with Kim and Rousseau (2004); and DSN and TSN comply with Di Martino et al. (2007). Of striking interest is the fact that the two hydrated forms, DSN and CSN, display

some differences in XRPD patterns, even though they have similar water content. In particular in the region of low angles, XRPD patterns of DSN and CSN show very high similarity, and all high intensity reflections of DSN are present in CSN, but slightly shifted to lower angles (3.8, 7.9, 11.8 2θ). This fact can probably reflect an expansion of the unit cell, indicating at the same time a high degree of structural similarity between the two dihydrates. In addition, several peaks of the two forms overlap (17.5, 19.2, 21.6, 23.7 2θ) and other peaks, typical of the CSN, are absent in the DSN (15.3, 16.3, 18.1, 20.2, 22.7, 24.1, 25.3 2θ).

As previously stated, this work also aims to describe differences between these two dihydrate forms and to ascertain whether they behave differently under dehydration. For this reason, these two dihydrate forms will be considered independently as different solids in the present chapter.

V.2 DEHYDRATION KINETICS

Detection of the dehydration process mechanism is based on the rate of water removal from crystal, which can be expressed as

$$\frac{d\alpha}{dt} = kf(\alpha) \tag{14}$$

where α is defined as the fraction of water removed at time *t*, that is,

$$\alpha = \frac{M_T - M}{M_T} \tag{15}$$

where M_T is the initial mass of water in the sample, and M is the mass of water in the sample at time *t*. The relationship between water content in a crystal sample (α) and time is embodied in the function $g(\alpha)$, which in turn depends on the mechanism of water removal.

Integration of equation (14) at constant temperature gives:

$$\int_0^1 \frac{d\alpha}{f(\alpha)} = g(\alpha) = \int_0^t k(T)\cdot dt = k(T)\cdot t \tag{16}$$

The rate constant *k(T)* may be considered as follows, based on Eyring's dependence on *T*:

$$k(T) = \frac{k_B T}{h} exp\left(\frac{\Delta S^*}{R}\right) exp\left(\frac{-\Delta H^*}{RT}\right) \tag{17}$$

where ΔS^* is the activation entropy change, ΔH^* is the activation enthalpy change, *R* is the gas constant, k_B is Boltzmann's constant and *h* is Planck's constant. Both ΔS^* and ΔH^* can be estimated from rate constant values determined by isothermal measurements (at several temperatures), provided $g(\alpha)$ is known. The kinetics of solid-state reactions can be classified into (a) diffusion controlled, (b) phase boundary controlled, and (c) nucleation and growth controlled reactions (Sharp et al., 1963). Table 4.1 represented in chapter IV gives selected expressions (Šesták, 1971; Dong et al., 2002) for $g(\alpha)$ corresponding to the most common solid-state processes. Plots were placed according to kinetic equations shown in Table 4.1 and their conformity assessed by the least-squares method. The function that best fitted the hydration data was selected, and the corresponding *k* values were determined. By fitting Eyring's expression to these values, the changes in enthalpy and entropy of the activation process could be determined.

In order to best support and explain the discussion of the kinetic results, a general premise is now given.

In a kinetic process involving the reaction A $\rightarrow$ B, an energy map may be supposed versus the reaction coordinate where it is possible to find a region of highest energy level.

This maximum energy level corresponds to the "activated complex". In an activated complex, the chemical bonds of A (or a part of them) are partially modified or excited.

In the present study, i.e. sodium naproxen dehydration, two different processes can be identified: the first one corresponding to the detachment of water molecules, the other corresponding to the diffusion of the detached water molecule.

The first process leads to the breakage of the naproxen – water bonds. It is possible to assume that in its active state (activated complex) the bond salt-water is weaken even if not entirely broken, and the relative constant strength lower. Therefore, one may expect that the vibration mode possesses smaller spacing between energetic levels (vibrational levels that convert towards translational levels). Therefore, one may expect positive ΔS^*.

On the contrary, all the values deduced from the Eyring's equation are negative, with the exception of only one (the first dehydration of TSN). This suggests that while the weakening of the salt-water bond occurs, the molecules are arranged more closely, fact that reduces the possibility of their movements. Summarizing, the analysis of enthalpic and entropic parameters of the activation process indicates that in the sodium naproxen dehydration two different phenomena are present: the weakness of the salt - water bond and the arrangement of the molecules. They play an opposed role, the first one giving a positive contribution to the ΔS^* and the other a negative one.

Kim and Rousseau (2004) have already described the dehydration model for MSN, showing that the MSN is formed by maintaining the dihydrate form crystallized from water (in the present work identified as CSN) in a desiccator at 0 % RH for 2 days. The water loss occurred in one step according to a three-dimensional diffusion model.

We repeated the Kim and Rousseau (2004) study of CSN dehydration kinetics under the same experimental conditions in order to compare the behaviour under dehydration of our two different dihydrated forms.

Figure 5.3a plots the percentage of the dehydrated fraction of CSN versus time, according to the isothermal temperature used during the experimental procedure.

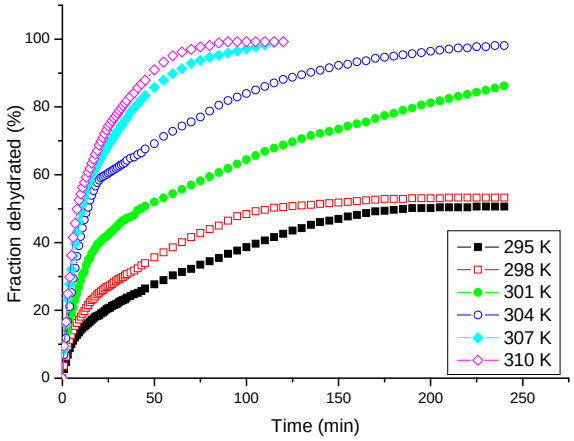

(a)

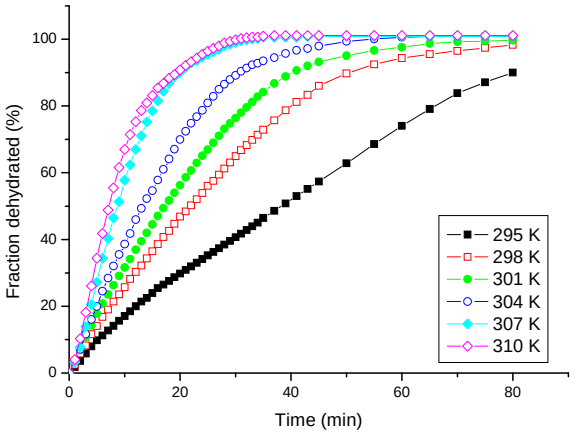

(b)

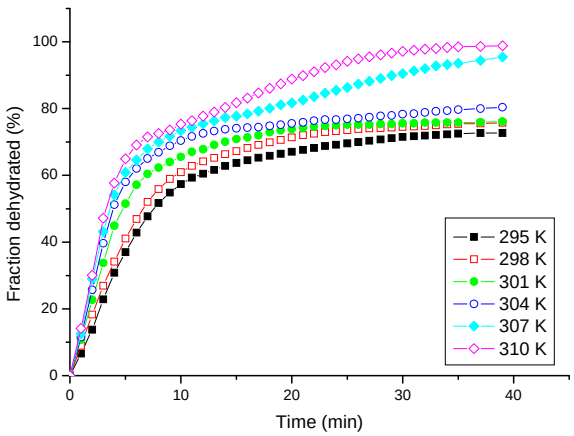

(c)

Figure 5.3

Plot of dehydration rate at different experimental temperatures expressed as weight decrease versus time. (a) CNS; (b) DSN; (c) TSN.

Table 5.2

Thermodynamic parameters for dehydration determined from TGA-STA measurements as a function of temperature

					Eyring plot			
Hydrated form	**Model**	**T (K)**	***k* (sec^{-1})**	***R*²**	**ΔH^* ($kJmol^{-1}$)**	**ΔS^* ($JK^{-1}mol^{-1}$)**	***r***	**$\Delta G°$ ($kJmol^{-1}$)**
CSN First dehydration	R2	295	1.523E-4	0.967	57.2	-15.0	0.9	61.7
		298	2.038E-4	0.981				
		301	1.923E-4	0.987				
		304	2.920E-4	0.988				
		307	3.250E-4	0.981				
		310	5.532E-4	0.991				
CSN Second dehydration	D3	295	0.375E-4	0.980	37.3	- 24.3	0.9	44.6
		298	0.557E-4	0.989				
		301	0.577E-4	0.967				
		304	0.649E-4	0.967				
		307	0.733E-4	0.995				
		310	0.932E-4	0.999				
DSN	R2	295	1.512E-4	0.994	56.7	-15.1	0.9	61.3
		298	2.035E-4	0.996				
		301	2.495E-4	0.988				
		304	3.018E-4	0.984				
		307	4.097E-4	0.990				
		310	5.073E-4	0.982				
TSN First dehydration	D3	295	0.827E-4	0.999	95.4	+0.1	0.9	95.4
		298	1.320E-4	0.998				
		301	2.120E-4	0.995				
		304	3.020E-4	0.988				
		307	4.337E-4	0.987				
		310	5.624E-4	0.987				
TSN Second dehydration	R1	295	1.510E-3	0.999	23.1	-26.6	0.9	31.0
		298	1.650E-3	0.995				
		301	1.870E-3	0.996				
		304	2.040E-3	0.996				
	D1	307	1.473E-2	0.999	-	-	-	-
		310	2.071E-2	0.998				
	D2	307	1.727E-2	0.996	-	-	-	-
		310	2.036E-2	0.996				

The dehydration proceeds exponentially with time and is a function of temperature, the dehydration rate increasing with temperature. During the period used in these experiments, 100% dehydration was achieved only at higher temperatures (304, 307, 310 K), while dehydration was incomplete at 295, 298, 301 K.

By plotting these data according to the equations given in Table 4.1, parameters for the dehydration process were calculated and reported in Table 5.2.

Curves did not fit any models reported in Table 4.1 and thus were split into two separate parts at their inflection point, where a decrease in dehydration rate was observed. The inflection point was located by calculating the first derivative thanks to the programme Origin® v. 7.0383 (1991-2002) (Northampton, MA, USA). Fitting was thus performed separately for the initial dehydration phase and the final dehydration phase, because it seemed that there were two different hydration steps. In fact, the present study shows that mechanisms for water removal of CSN are in compliance with those previously reported by Kim and Rousseau (2004) and that, in both studies, water was removed in two different steps. During the first one, water was removed according to a R2 model, i.e. a two-dimensional phase boundary reaction, a mechanism in which water is dissociated from the crystal lattice. During the second step, water was removed according to a D3 model, i.e. three-dimensional diffusion, a mechanism in which water moves through hydrophilic channels or defects in the crystal. The activation enthalpy for the first step is comparable and of the same order (57.17 kJ mol^{-1}) to that of the previous study (67.2 kJ mol^{-1}). By contrast, the activation energy of the second dehydration period reported in the present study (37.31 kJ mol^{-1}) is significantly lower than that of Kim's results (98.6 kJ mol^{-1}). In fact, sample preparation, surface area, bulk density, particle size, flow rate, and RH of the drying stream may affect dehydration rate, and thus it is not surprising that the rate constants obtained in this work do not agree with previous results, as also proven in other studies (Zhu et al., 2001). According to Taylor and York (1998), it is possible that activation energies are similar for the first dehydration phase because the dissociation of water from the crystal lattice is not affected by particle size, while the lower activation energies of the second dehydration phase can be explained by small particle size. In fact,

the second phase, in which water diffuses through the crystal channels, can be enhanced by the greater particle surface of the smaller particles (Agbada and York, 1994). Similarly, Sakata et al. (2004) showed that the activation energy for the dehydration of untreated creatine monohydrate was slightly higher than that of the pulverized form, but that the dehydration occurred with the same mechanism.

Dong et al. (2002) postulated that the dehydration of monohydrated neotame occurred in two steps: (a) dissociation of water with the breakage of bonds, and then (b) diffusion of water through channels in the crystal. Kim and Rousseau (2004) drew upon this same concept to describe the dehydration of CSN. So, the present results can be oriented towards the same conclusion.

In addition, this study also includes evaluation of activation of the process. The rate constant k was considered to be dependent on T according to Eyring's equation. One could expect a positive ΔS^* for the reasons previously discussed. Actually, the negative and the non-negligible ΔS^* means that the system moving from reactant area to product area, along the reaction coordinate, loses degrees of freedom. In this case, an alternative evaluation of the order degree as a consequence of water removal can be done. In both stages, the entropy change for the activation process is negative. According to Kim et al. (2005) the removal of water results in changes in physical and energetic environments in the unit cell. After dehydration, spaces previously occupied by water are vacated and sodium cations and naproxen anions rearrange themselves into a new lattice, as previously explained.

Different kinetics are involved during the dehydration of the dihydrate form obtained by hydration at 55% RH (DSN). In Figure 5.3b, the percentage of the dehydrated fraction of the DSN is plotted versus time, according to the isothermal temperature used during the experimental procedure. Profiles differ from those previously reported for CSN: in particular, complete dehydration is reached for most of the isothermal temperatures (298, 301, 304, 307 and 310 K) within 80 minutes and only at the lower temperature of 295 K dehydration was incomplete, the dehydrated fraction reaching 90%. Plotting these data with the equations in Table 4.1, parameters for the dehydration process were calculated (Table 5.2). In this case, good fits were obtained by plotting all the experimental data, meaning that the dehydration most likely occurs in only one step. This can indicate that all

the water molecules are lost simultaneously and there are no different resistances in controlling the removal rate of water molecules. Water molecules were removed in all cases according to the R2 model, i.e. the two-dimensional phase boundary reaction. This mechanism is thus the same described for the removal of water during the first dehydration step of CSN. This result implies that in the case of DSN as well, water is removed after the dissociation of water from the crystal lattice. Thus, only one activation value has been calculated (60.4 kJ mol^{-1}). This value is comparable to that calculated for the removal of water from CSN during the first dehydration period. Also in this case, the activation entropy change is slightly negative, meaning that the system loses degrees of freedom during the activation process. The explanation for this occurrence is the same as that previously described for CSN, related to the fact that solid-solid transition proceeds from a less ordered state towards a more ordered activated state. In the case of DSN, the diffusion phase of water molecules through the crystalline structure seems to be absent. In the author's opinion, this conclusion is not entirely true, as it does not comply with the thermograms obtained by conventional DSC analysis carried out at 10 K/min, where double peaks are clearly evident (Figure 5.4a). Prior to comment the results given in the Figure 5.4, a clarification is necessary. DSC-STA thermograms are clearly different from thermograms recorded by conventional DSC at same heating rate (10 K min^{-1}). Differences in environmental conditions such as changes in pressures may affect the water removal from solids (Di Martino et al., 2001). In this study, DSC-STA thermograms were carried out in open pans because only these conditions permit a correct quantitative evaluation, as was the objective of this analysis (Di Martino et al., 2001). On the contrary, conventional DSC was carried out in perforated pans to create a slight overpressure that enables to highlight that dehydration may proceed in different steps according to the hydrate under study and according to the heating rate, as it will be discussed later.

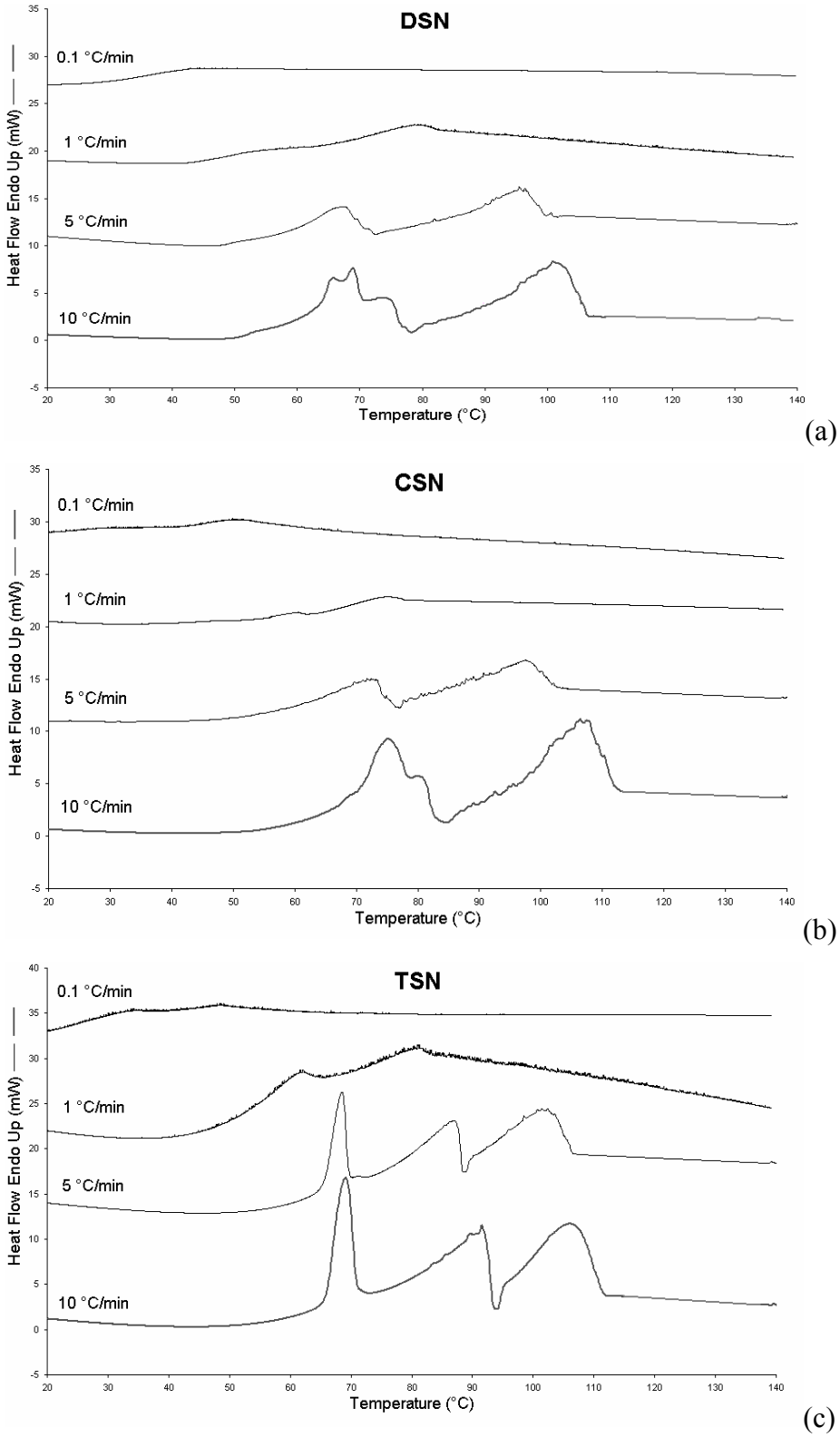

Figure 5.4

Conventional DSC scans of sodium naproxen hydrates at different heating rates. (a) DSN; (b) CSN; (c) TSN.

Thus, the presence of double peaks in conventional DSC thermograms can justify the suggestion that dehydration occurs in more than one step and that different energy changes are required to promote water removal. In fact, the two dehydration curves start at different temperatures, possibly due to the fact that conventional DSC thermograms are kinetically recovered, while dehydration experiments were carried out in isothermal conditions and at different temperatures, rather close to the room temperature.

To support this idea, authors repeated the conventional DSC of DSN at different heating rates (Figure 5.4a).

As long as the heating rate decreased, the two dehydration curves fused together, forming only one curve. On the contrary, the same analysis carried out on CSN revealed the presence of two different peaks even at the heating rate of 0.1 K min^{-1} (Figure 5.4b). It is the author's opinion that the limiting reaction step in DSN dehydration is the breakage of the hydrogen bonds between water and the SN molecule. The diffusion of water molecules and their escape from the crystal are facilitated by the fact that water molecules can pass through pre-existing channels. Thus, in isothermal conditions this phase can be masked by the previous, and most limiting, step. Some considerations can support this hypothesis. In the chapter IV of this thesis, the authors described the hydration kinetics of ASN when exposed to 55% of RH. This hydration process occurred in two steps: first, water molecules diffuse inside the anhydrous crystal, according to a one-dimensional diffusion mechanism. This means that water could access the crystal following only one direction, corresponding to hydrophilic planes present in the crystal. Second, once in contact with the SN molecule, water could react with SN, creating hydrogen bonds, a reaction that favours slight rearrangements of the crystallographic structure. The slight negative value of ΔS^* of the two-dimensional phase boundary reaction can be observed in the fact that dehydration does not cause much crystal rearrangement. In the present study, we can thus assume that, during the dehydration of DSN, water can easily move through the same channels through which it had access during hydration. The case is different for CSN, which is formed by dissolving and crystallizing SN from water. Since the lattice is formed by nucleation and progressive crystal growth, with water molecules included in the crystal structure, once the bonds between SN and water are broken during the first stage of dehydration, the water

molecules cannot pass through escape channels, but must diffuse through the hydrophilic sites of the crystals or through crystalline defects formed during the SN crystal growth.

Thus, there are different degrees of resistance to water escape from the crystal. This conclusion can be supported by the differences in the XRPD patterns of CSN and DSN. In addition, both dehydration phases are fundamental during CSN dehydration, a fact further supported by the DSC experiments: a very low heating rate (0.1 K min^{-1}) of CSN is unable to fuse the two phases, which remain clearly evident (Figure 5.4b).

In the present study, dehydration of the tetrahydrate form of SN was also studied. The dehydration profiles of TSN differ from those previously reported for the dihydrate forms (CSN and DSN), and vary according to the dehydration temperatures (Figure 5.3c). At lower temperatures (from 295 to 304 K), the dehydration proceeds exponentially in a very short time period, approaching a limiting value, which is in any case lower than 100% (approximately 70-80%). At higher temperatures (307 and 310 K), the first part of the dehydration curves is followed by an inflection point, which is in turn followed by a new increase in dehydration rate. In this case, the dehydration is complete during the experimental period, reaching a dehydrated fraction of 100%. Because integration of each whole curve did not fit with the expressions described in Table 4.1, we split each curve at the inflection point and considered dehydration as a multi-step process.

During the first dehydration phase, water was removed according to the (D3) model, i.e. three-dimensional diffusion (Jander's equation), which describes the diffusion of water through channels present in the crystal. This mechanism has been used to describe the loss of water from CSN during the second dehydration phase and to describe the loss of water from MSN (Kim and Rousseau, 2004). This model D3 means that the dissociation of water with the breakage of bonds between water and SN molecules does not precede the diffusion phase, as instead previously described for CSN. The reason can be found in the fact that TSN can be described as a channel hydrate: some water molecules form hydrogen bonds with the oxygen atoms of the carboxylic group and with the sodium ion of SN; the lattice is able to incorporate further water into presumably non-specific sites, and this excess of water molecules in their turn form hydrogen bonds with the other water molecules. This model is in accordance with Allen et al. (1978) who describe water

released at low temperatures because of very weak interactions with nearby molecules in the crystal lattice, as is the case with TSN (Di Martino et al., 2007). Probably the strength of bonds between water molecules is higher than the interaction between SN and water molecules. This can also explain the slight positive ΔS^*, which can be ascribed to the gain of freedom of water molecules during the activation process.

For the second dehydration phase, a good fit was calculated only for the experimental temperatures from 295 to 304 K, which comply with the R1 model, i.e. a one-dimensional phase boundary reaction (zero-order mechanism). This mechanism, in which the hydrogen bonds between SN and water are broken, is independent of the amount of species involved in the process. The negative value of ΔS^* may be explained as previously reported.

The points recovered at 307 and 310 K do not fit the same model, but rather both the D1 (one-dimensional diffusion) and D2 (two-dimensional diffusion) models, which are quite similar and indicate that water is released as a consequence of a diffusion process. The inability to fit all the temperatures with the same model is rare, but not inconsistent, and some examples have been given in the literature. Zhu et al. (2001) reported that fenoprofen calcium dihydrate followed different dehydration kinetics at low and high temperatures. Han and Suryanarayanan (1998) showed that carbamazepine dihydrate followed three-dimensional nucleation at lower temperatures, while a two-dimensional phase boundary mechanism controlled dehydration at higher temperatures. At 313 K, the dehydration of theophylline was found to be a two-step process, while at 320 K it was a single step process (Duddu et al., 1995).

In the case of SN, the result may depend on a discontinuity in the dehydration behaviour according to the temperatures. The dehydration curves of TSN indicate that dehydration behaviour at 307 and 310 K is clearly different from that at lower temperatures.

This means that at higher temperatures, water is involved more in a diffusion mechanism than in a breakage of hydrogen bonds. The higher amount of heat supplied to the system for dehydration facilitates this process. Because only two values for each mechanism have been calculated, ΔH^* and ΔS^* values were not taken into account. The

multi-step dehydration process of TSN is clearly evident in DSC thermograms carried out at different heating rates (Figure 5.4c).

ΔH^* and ΔS^* enabled the calculation of Gibbs free energy ($\Delta G°$) from the well known Gibbs equation. Results are given in Table 5.2 and they decrease in the order TSN first dehydration > CSN First dehydration > DSN dehydration > CSN second dehydration > TSN second dehydration. Less positive is the Gibbs free energy, easier is the formation of the activated state. In other words, more negative is this function, higher is the driving force of the reaction. According to the reported results, the highest driving force is observed for the TSN second dehydration.

V.3 X-RAY POWDER DIFFRACTION STUDY

In order to follow the structural changes that occur in DSN, TSN and CSN under dehydration, XRPD studies were carried out. Checks were performed on the powders exposed to the same temperatures used during the isothermal dehydration (295, 298, 301, 304, 307, and 310 K).

During dehydration, the evolution with time of each phase was assessed by collecting a series of XRPD patterns on different portions taken at several time intervals from the same sample (Di Martino et al., 2007). Each sample under study (DSN, TSN and CSN) was maintained in isothermal conditions at all the temperatures used for the dehydration kinetic experiments. The presence of typical diffraction peaks for each crystalline form was monitored in the patterns. Peaks were chosen in a region where no peaks for the other forms were present: 8.6° (2θ) for ASN; 14.7° (2θ) for MSN; 7.9° (2θ) for DSN; 13.8° (2θ) for TSN; and 18.1° (2θ) for CSN.

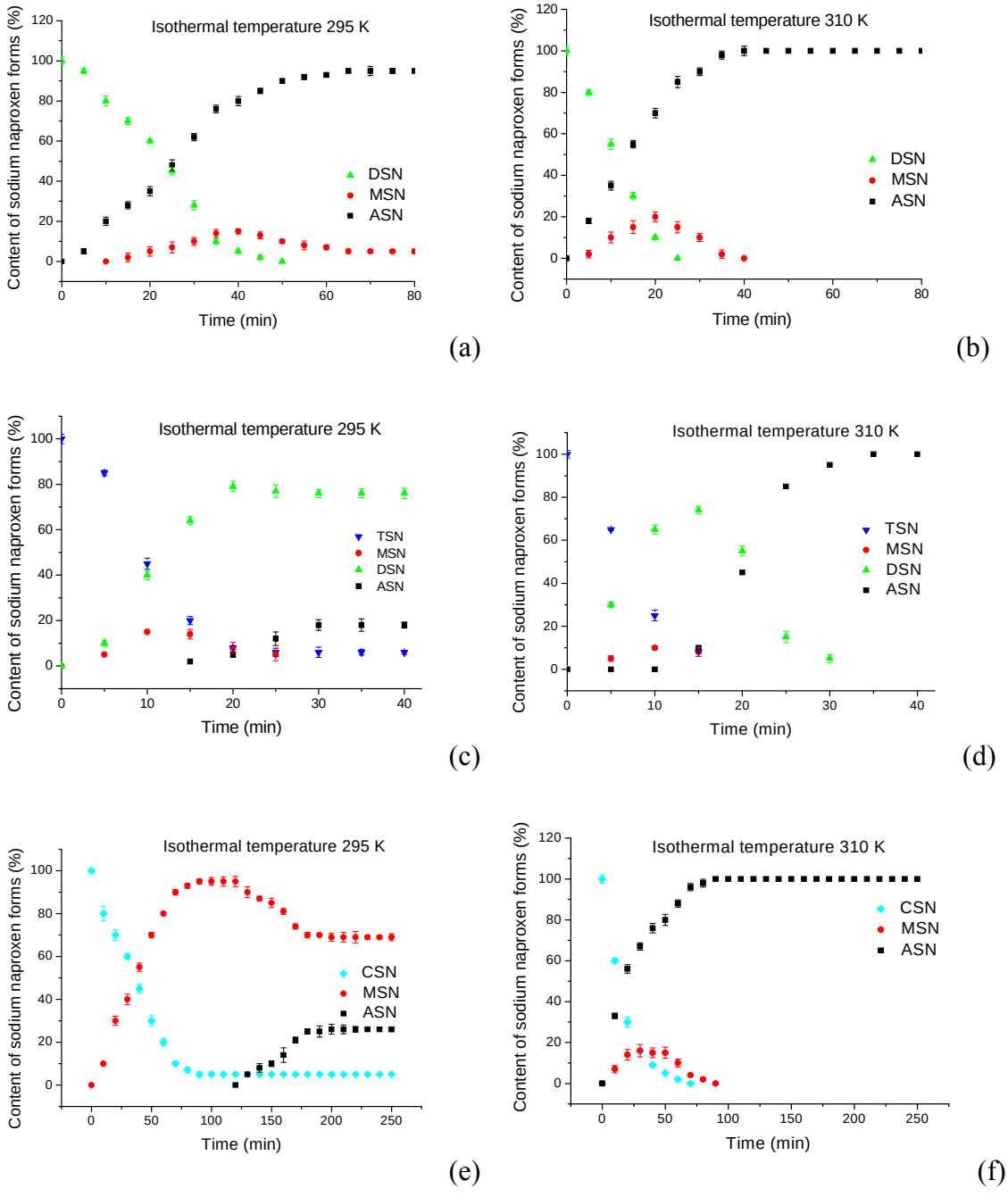

Figure 5.5

Plots' describing the phase conversions at different temperatures of sodium naproxen forms during the isothermal dehydration experiments. (a-b) DSN; (c-d) TSN; (e-f) CSN.

Peak intensities were evaluated and expressed as percentage with respect to the maximum intensity of the same peak when the form is pure. Figure 5.5 shows the results of the two extreme temperatures, the lower one, 295 K, and the highest one, 310 K.

During the dehydration of DSN, the ASN form immediately appears at the beginning of the reaction and progressively increases as long as the dehydration of the DSN occurs. Traces of MSN also appear. At the end of the dehydration experiment carried out at the lowest temperature, the SN is not completely dehydrated; rather, it is composed of a mixture of ASN with some traces of MSN. Similar behaviour is observed at the highest temperature, except that the dehydration is complete and the only form present at the end of the process is ASN. Intermediate temperatures exhibit intermediate behaviour.

At 295 K, TSN dehydrates while the DSN form progressively increases. Slight amounts of MSN also appear during the initial phases of dehydration. The dehydration proceeds with the appearance of ASN, and is not complete at the end of the experiment, with a mixture of ASN and DSN evident. At 310 K, the phases involved in the dehydration are the same, but the dehydration is complete at the end of the experiment. Intermediate results were observed for intermediate temperatures.

At 295 K, CSN progressively dehydrates by converting into MSN. As the dehydration proceeds, ASN also appears, but dehydration is not complete at the end of the experiment, when a mixture of CSN, MSN and ASN is present. At 310 K, the phases involved in the dehydration are the same, but the dehydration is complete.

VI. MECHANICAL PROPERTIES OF DIFFERENT ANHYDROUS AND HYDRATED FORMS OF SODIUM NAPROXEN

The aim of the study presented in this chapter is to investigate the technological and mechanical properties of several solid forms of sodium naproxen: the anhydrous form (ASN), one dihydrated form obtained after exposure at a relative humidity of 55% (DSN), one dihydrated form obtained by crystallization from water (CSN), the monohydrated form obtained by dehydration from DSN, the tetrahydrated form obtained by exposure at a relative humidity of 75% (TSN).

Any attempts have been made in order to reduce among the samples differences in crystal habit, particle size and distribution, amount of absorbed water, so that only the hydration degree and the crystalline structure might affect the technological behaviour of powders. Thus, the compression behaviour were determined by using an instrumented single punch tablet machine and evaluated through the tabletability, compressibility and compactibility analysis. The results showed that the compression ability was influenced by the hydration degree and the crystalline form, and in general the tabletability was mainly due to the ability of particles to close together by establish numerous bonds.

VI.1 PHYSICO-CHEMICAL CHARACTERIZATION OF SN FORMS

All the powders were first analyzed by XRPD to check their crystalline form by comparing their powder patterns with those of known forms. The analysis confirmed the compliance of all the powders with the crystalline forms previously characterized. In particular, the patterns of ASN and CSN comply with Kim and Rousseau (2004) and Di Martino et al. (2007); the patterns of MSN comply with Kim and Rousseau (2004), and those of DSN and TSN comply with Di Martino et al. (2007). Authors would emphasize that the two hydrated forms, DSN and CSN, possess different crystalline form, even though they have similar water content, as already proved in the chapter V of this Thesis.

The interaction of water with pharmaceutical powders is one of the most important factors affecting their tableting performance. Water can be present in powders in different physical forms: as adsorbed monolayers or multilayers on the surfaces of the particles, as condensed water on the surface, as physically absorbed water within the particles or as strongly bound water (Malamataris et al., 1991). The objective of this study is to evaluate the influence of the water bound in the crystalline structure of SN on the compression behaviour, regardless the effect exhibited by the water absorbed on the particle surface. For this, the 50-100 μm fractions of any sample under study were stored as a thin layer on an aluminum plate for 2 h under vacuum and at 298 ± 2 K. This treatment was intended to reduce the difference in surface moisture between the samples (Sun and Grant, 2004). As proven by X-ray powder diffractometry, the powders are stable in these conditions and the treatment leveled off the possible effect of absorbed water. The fact that only negligible differences in the amount of absorbed water among the samples is present is well proven by the results in Table 6.1, where the total water content determined by STA is given together to the theoretical water content.

The water content is always in compliance with the theoretical one, but it is always slightly higher than that expected (max 3.55%). So it is possible to assume that the excess of water is absorbed on the particle surface. This rough approximation is necessary because desolvation of hydrated forms of SN already occurs at temperatures near to room temperatures (Di Martino et al., 2001; Kim et al., 2005), so it is difficult to accurately

determine the amount of water that takes part of the crystalline structure of SN (bound water) and that simply absorbed into the crystal surface (unbound water).

Table 6.1

Formula and water content for the sodium naproxen forms.

Form	Formule	Molecular weight (Dalton)	Total water content (%) [(a)]	Theoretical water content (%)
ASN	$C_{14}H_{13}O_3Na$	252	0.066 ± 0.026	0.0
MSN	$C_{14}H_{13}O_3Na \cdot H_20$	270	6.68 ± 1.03	6.66
CSN	$C_{14}H_{13}O_3Na \cdot 2H_20$	288	12.95 ± 1.15	12.49
DSN	$C_{14}H_{13}O_3Na \cdot 2H_20$	288	12.86 ± 2.78	12.49
TSN	$C_{14}H_{13}O_3Na \cdot 4H_20$	324	21.79 ± 2.24	22.22

[(a)] *Determined by Simultaneous Thermal Analysis (STA)*

VI.2 DETERMINATION OF MICROMERITIC PROPERTIES

Another important factor that affects the technological behaviour of powders is represented by the initial particle size and shape, as it has been extensively demonstrated in previous works (Alderborn and Nyström, 1982; Sun and Grant, 2001a). As also previously mentioned, to assess the aim of this study it was important to level off all the parameters that might affect the compression behaviour, in the benefit to evaluate the degree of hydration and crystalline form as unique variables among the samples. For this scope, the same granulometric fraction was chosen for all the samples. In addition, it must be considered that the most part of the samples are prepared from the ASN thanks to a hydration process (MSN, DSN, and TSN) and as already proven previously, the hydration of original ASN particles does not affect neither particle size nor shape. Figure 6.1 shows SEM micrographs at constant resolution of SN samples.

Not significant differences are highlighted even between the CSN (produced by crystallization from water) and the other samples. In general, particles of all the samples appear like irregular crystals composed by large particles with quite rounded and smoothed edges in presence with irregular and smaller particles.

The similarity in particle morphology affects the granulometric particle distribution. As exhibited by the Figure 6.2, the particle size distribution is very similar for all the samples and non-statistically relevant differences can be highlighted.

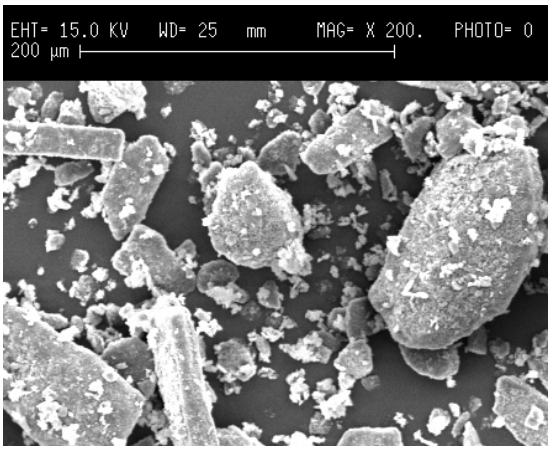

(a) ASN

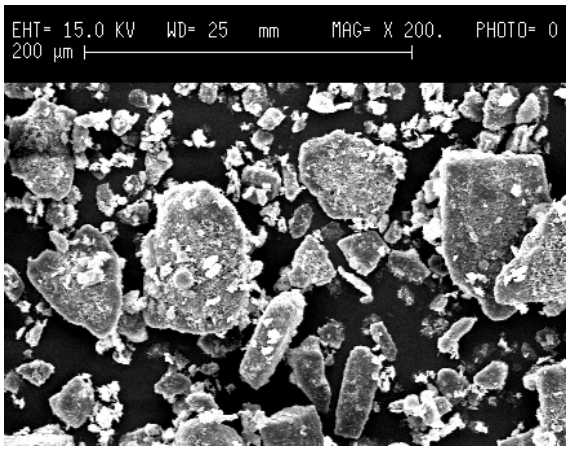

(b) MSN

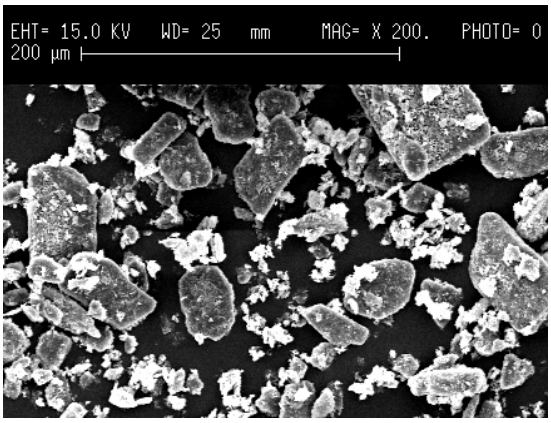

(c) DSN

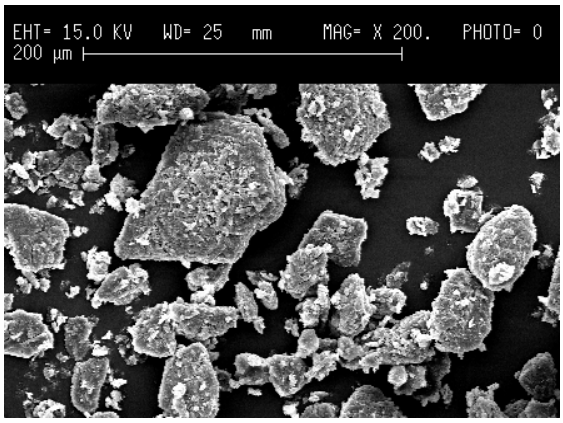

(d) TSN

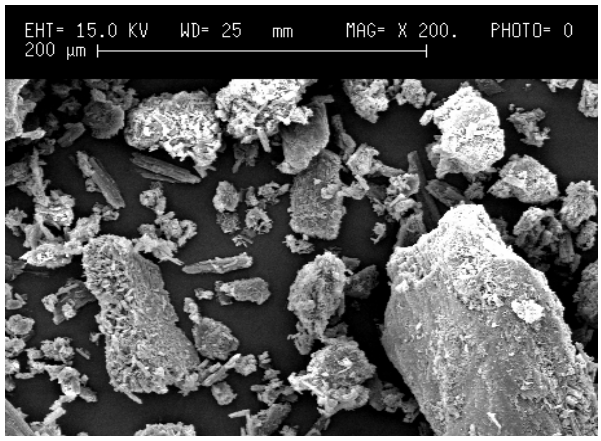

(e) CSN

Figure 6.1

SEM microphotographs (200x) of SN crystals. (a) ASN; (b) MSN; (c) DSN (55%RH); (d) TSN (76%RH); (e) CSN.

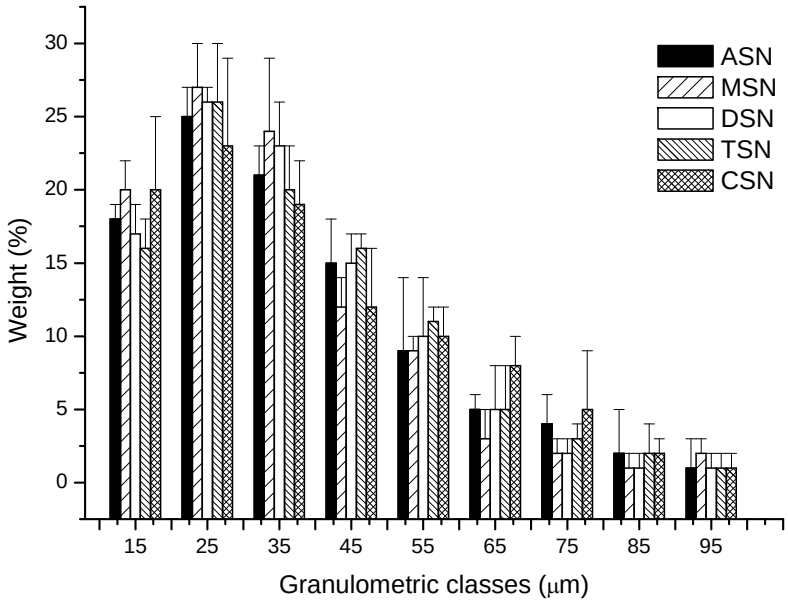

Figure 6.2

Particle size and particle distribution of sodium naproxen forms. ASN: anhydrous sodium naproxen; MSN: monohydrated sodium naproxen; DSN: dihydrated sodium naproxen; TSN: tetrahydrated sodium naproxen; CSN: crystallized sodium naproxen.

Other important micromeritic properties are given in Table 6.2.

The apparent particle densities were measured to evaluate the powder densification through the Heckel's equation. Apparent particle densities decrease in the order ASN>CSN>MSN>DSN>TSN, therefore, in general, they decrease by increasing the hydration degree. The only exception is given by the CSN. As it will be shown further, the CSN frequently will exhibit exceptions to the normal behaviour underlined for the other samples.

Table 6.2

Micromeritic properties and results of compactibility study of sodium naproxen anhydrous and hydrated forms

	ASN	MSN	CSN	DSN	TSN
Apparent particle density ($g\ cm^{-1}$)(a)	1.374±0.001	1.352±0.002	1.360±0.003	1.341±0.001	1.333±0.001
Bulk density ($g\ cm^{-1}$) (b)	0.506±0.004	0.523±0.005	0.500±0.024	0.554±0.002	0.570±0.003
Tapped density ($g\ cm^{-1}$) (c)	0.639±0.002	0.651±0.013	0.619±0.027	0.662±0.017	0.673±0.015
Carr's index (d)	20.94	18.29	19.97	16.27	15.30
σ_0 (MPa) (e)	2.05 ± 0.02	2.88 ± 0.03	3.50 ± 0.02	2.99 ± 0.01	3.47 ± 0.02
R (f)	-0.98	-0.99	-0.99	-0.98	-0.99

(a) Determined by helium pychnometry. Standard deviations are also indicated.
(b) Determined from the volume of 100 g of powder. Standard deviations are also indicated.
(c) Determined from the volume of 100 g of powder after 500 tapping to constant volume. Standard deviations are also indicated.
(d) Calculated from bulk and tapped densities.
(e) Tablet tensile strength extrapolated to zero porosity in Eq. (19). The 95% confidence intervals are indicated.
(f) Linear regression of the Eq. (19).

The hydration degree shows a clear repercussion also on bulk and tapped densities: they rank in the following order CSN<ASN<MSN<DSN<TSN, therefore bulk and tapped densities significantly increase with increasing the hydration degree. Again, the only exception is represented by the CSN, whose densities are the lowest one. Particle densities have repercussions on powder flowability, as proven by the Carr's indexes: Carr's index decreases, and thus flowability increases, with increasing in hydration degree and, again,

with the exception of the CSN, that exhibits similar value than ASN. The Carr's index, which indicates the ability of a powder to reduce in volume, as it will be explained later, affects the particle rearrangement at the initial stage of compression.

VI.3 DETERMINATION OF MECHANICAL PROPERTIES

Tabletability can be considered one of the most important mechanical characteristic of a solid material and it describes the effectiveness of a powder to give tablets of satisfactory tensile strength. In particular, tabletability describes the effectiveness of the applied pressure in increasing the tensile strength of the tablet and demonstrates the relationship between the cause, the compaction pressure, and the effect, the strength of the compact (Sun and Grant, 2001b). It has been defined as the capacity of a powder material to be transformed into a tablet of specified strength under the effect of compaction pressure (Joiris et al., 1998).

Tabletability of SN samples is reported in Figure 6.3a and follows the order TSN>CSN>>DSN>MSN>>ASN. The tabletability of TSN is always the highest one, even if at higher compaction pressures (over 170 MPa) tabletabilities of TSN and CSN get closer.

In fact, the tabletability curves of these two compounds appear quite linear in the range 20-120 MPa, where the tablet tensile strength proportionally increases with the compression pressure, but over this pressure the curve of the TSN gradually levels off, while that of CSN slightly continues to increase.

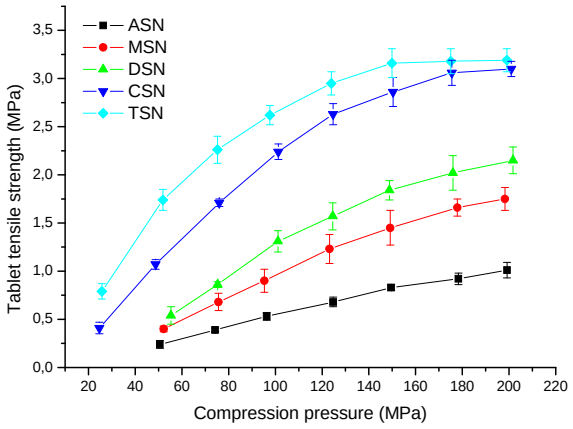

(a)

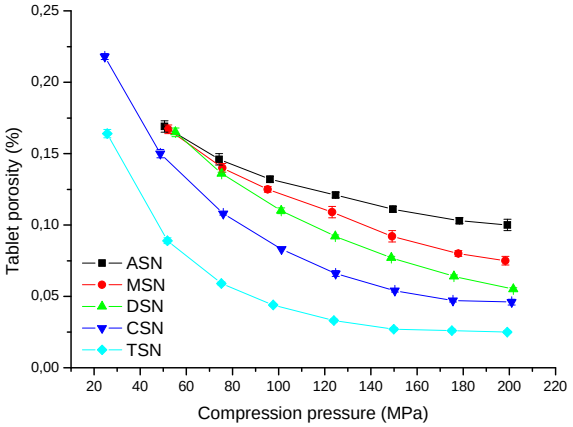

(b)

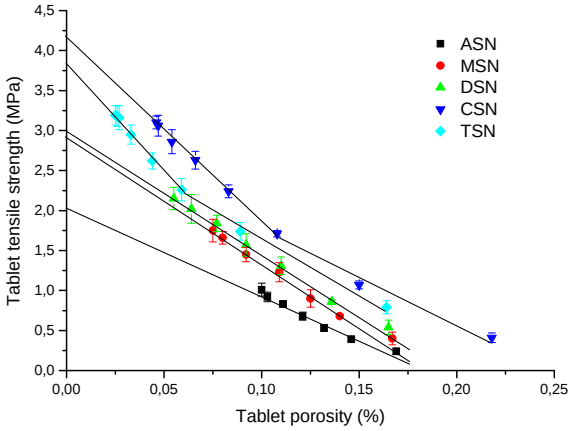

(c)

Figure 6.3

Tabletability, compressibility and compactibility of SN powders. Each point is representative of five acquisitions and 95% confidence intervals are indicated as error bars.

By taking into account only ASN, MSN, DSN and TSN powders, results of tabletability clearly suggest that the presence of water into the crystalline structure enhances the tabletability and that such an enhancement increases with increasing water content into the lattice. This result is in agreement with results reported in the chapter IV of this thesis, which demonstrated that the tablet tensile strength increased with increasing the water content of SN during its hydration. Anyway, if the hydration was the only parameter affecting the tabletability, one might expect that the tabletability behaviour of DSN and CSN were similar because of the same hydration degree. However, CSN tabletability is considerably higher than that of DSN and even approaches that of the TSN at higher compression pressures, as previously mentioned. Since, as previously proved, particle morphology, particle size, total water content of these two forms are very close and small differences cannot explain the substantial difference in tabletability, reasons for this behaviour must be researched in other factors. Certainly, the crystalline form must be taken into account to explain powder tabletability. As proved in the chapter V, in spite of the same number of water molecules implied in the bound with the SN molecule, CSN and DSN show some differences in the X-ray powder patterns. Probably the arrangement of the SN molecule and the position of the water molecule inside the crystalline structure are different. In fact, the CSN is formed by dissolving and crystallizing SN from water and thus the lattice is formed by nucleation and progressive crystal growth. Water molecules are then progressively included in the crystal structure, as long as the crystal growth occurs. On the contrary, in the case of the DSN, during the hydration process, water molecules access through some hydrophobic sites, mainly formed by the π cloud of the naphthalene rings, and they can then be easily accommodated between the SN molecules by forming hydrogen bonds with both Na and/or O atoms (Joiris et al., 2008). These differences can reflect differences in the arrangement of molecules in the crystals.

In particular, in the region of low angles, all high intensity reflections of DSN are present in CSN, but slightly shifted to lower angles (3.8, 7.9, 11.8 2θ). This fact can probably reflect an expansion of the unit cell, indicating at the same time a high degree of structural similarity between the two dihydrates.

Tabletability describes the relationship between compaction pressure and tablet strength, but does not provide a fundamental understanding of the relationship. Therefore, tabletability alone does not adequately describe the tabletability performance (Sun and Grant, 2001b).

In fact, the ability of a powder to give tablet of satisfactory tensile strength can be related either to the number of bonds (the bonding area) (compressibility) or to the strength of these bonds (compactibility).

As stated above, compressibility is the ability of a material to undergo a reduction in volume as a result of an applied pressure (Joiris et al., 1998). Thus, compressibility indicates the ease with which a powder bed undergoes volume reduction under compaction pressure and is represented by a plot showing the reduction of tablet porosity with increasing compaction pressure (Sun and Grant, 2001b) (Figure 6.3b). At the lowest compression pressure, the tablet porosity of ASN, MSN and DSN is the same. This means that, at the highest porosity, the small differences in tabletability cannot depend on the interparticulate bonding area. In addition, this same maximal porosity is exhibited at lower compression pressures by the TSN. Thus, again, differences in tabletability cannot depend on the interparticulate bonding area. It is also significant to observe that at the same minimal compression pressure, the TSN exhibits lower tablet porosity than CSN, and thus larger interparticulate bonding area can explain the better tabletability of TSN with the respect to the CSN at lower porosities.

By increasing compression pressure, the compressibility reflects the behaviour observed for the tabletability: curves are aligned from the ASN to the TSN with the same order previously observed for tabletability (TSN>CSN>DSN>MSN>ASN). In addition, by considering the initial and the final porosities, the total tablet porosity decreases by 41, 55, 67, 79 and 85% in the order ASN, MSN, DSN, CSN and TSN. Again, CSN shows different compressibility than that of DSN confirming that its higher tabletability can be related to their higher aptitude to densificate under the application of a compression pressure, even if porosities tend to be the same at the higher pressures.

It must be noted that at the highest compression pressure, the TSN can reach far lower porosity than CSN in spite the tablet tensile strength at this same pressure was the

same. Therefore, one may expect that the similar tensile strength of TSN and CSN at the higher pressure may depend on other reasons than compressibility factors. This will be argued later.

Any way, in general, it is possible to state that tabletability is affected by the ability of these materials to undergo a reduction in volume as a result of an applied pressure.

Compactibility is the ability of a material to produce tablets with sufficient strength under the effect of densification (Joiris et al., 1998). It shows the tensile strength of a tablets normalized by tablet porosity (Sun and Grant, 2001b) (Figure 6.3c). In many cases, the tensile strength of a tablet decreases exponentially with increasing porosity (Ryshkewitch, 1953). In this study, the compactibility of all the samples has been adequately described by the Ryshkewitch's equation (Ryshkewitch, 1953):

$$\sigma = \sigma_0 e^{-a\varepsilon} \tag{19}$$

where σ is the tensile strength of porous tablets, ε is the porosity, σ_0 is the tensile strength extrapolated to zero porosity, and a is a constant that may be linked to the pore distribution within a tablet. For all the powders, the tensile strength decreased exponentially with increasing porosity.

Several considerations arise from the compactibility study:

- The slope of the plot of ln(σ) versus porosity and the tensile strength extrapolated at zero porosity (σ_0) (Table 6.2) of ASN are the lowest one, indicating the worst ability to reduce in porosity giving strength tablets.
- The slope and the tensile strength extrapolated at zero porosity (σ_0) of MSN and DSN are practically the same, indicating similar distribution of pores in the tablets (corroborated by similar particle size and shape) and similar mechanism in reducing tablet porosity as long as the compression pressure increases.
- The slopes of the plots of the CSN and the TSN change with the compression pressures and they are similar between the two powders; similar slope change has been previously described by Sun and Grant (2004), who have assumed that the

change of slope of the monohydrated form of *p*-hydroxybenzoic acid might reflect a change of consolidation mechanism at higher pressures.

- In the case of both CSN and TSN, slopes are similar in the higher porosity range (lower compression pressures) indicating similar initial pore distribution, due to similar particle size and shape, as well as similar initial particle rearrangement and deformation. As long as the porosity decreases (higher compression pressure) the densification mechanism can be modified and probably the plastic deformation becomes the most predominantly densification mechanism, accompanied by very low elastic properties. The tensile strength extrapolated at zero porosity (σ_0) of the CSN is higher than that of TSN.
- For the same tablet porosity, the CSN always exhibits higher tensile strength than TSN, in spite that TSN always exhibited better tabletability. Therefore, the higher tabletability of TSN is a result of its greater interparticulate bonding area (compressibility) and not of its greater bonding strength (compactibility), and the greater bonding strength of CSN and interparticulate bonding area can explain its better tabletability with the respect to the DSN.

In order to better understand the mechanism responsible for porosity reduction, an evaluation of the densification under compression can be made through the Heckel's analysis, which, in the present study, has been carried out by the "in die" method. The Heckel's parameters are indicated in Table 6.3.

Table 6.3

Heckel's parameters obtained from a single compression cycle and total elastic recovery. Data are the mean of five acquisitions and 95% coefficient variation is indicated.

	ASN	**MSN**	**CSN**	**DSN**	**TSN**
D_0' (a 3.0 MPa)	0.663±0.003	0.602±0.003	0.639±0.009	0.618±0.004	0.631±0.009
D_A	0.814±0.001	0.728±0.002	0.747±0.001	0.733±0.001	0.794±0.003
D_B' ($D_A - D_0$')	0.151±0.002	0.126±0.01	0.108±0.010	0.114±0.004	0.163±0.004
P_Y (MPa)	124.5±1.4	99.8±2.4	85.3±0.3	97.3±0.8	59.0±2.2
Total elastic recovery (%) *(a)*	6.95±0.42	4.07±0.28	3.00±0.16	3.07±0.05	1.50±0.13

(a) Total elastic recovery

$$TER = \left[\left(\frac{t_2 - t_1}{t_1}\right)\right] \times 100$$

t_1 : Minimal tablet thickness, when the maximal pressure is applied (150 MPa).

t_2 : Tablet thickness.

D_0' takes into account the densification by particle slippage and rearrangement occurring at the initial stage of compression, when a pre-compression pressure of 3.0 MPa has been applied. In an earliest experiment (previous chapter), D_0' increased with increasing hydration degree. In this one, previous results are confirmed in part and D_0' increased in the order MSN<DSN<TSN<CSN<ASN. This means that unexpectedly ASN and CSN undergo higher densification during this compression stage. Taking into account their lowest bulk densities (Table 6.2), it is possible that the higher densification is just due to the lower bulk density of the powders. It is also interesting to note that D_0' decreased by

decreasing hydration degree for TSN, DSN and MSN, results that once more are in accordance with the bulk density.

D_B' takes into account the fragmentation tendency of the particles during the initial stage of compression. D_B' increased in the order CSN<DSN<MSN<ASN<TSN.

In the previous study (Joiris et al., 2008), D_B' decreased as long as the hydration proceeded and, at the end of hydration, it was higher for the TSN.

In this case it is difficult to find a relationship between the water amount and the fragmentation ability.

Thus, notwithstanding ASN has pronounced fragmentation propensity, its new surfaces are unable to form strong and resistant particles bonds: in other words, fragmentation and formation of new surfaces are not enough to create strength bonds. Such a result is not a trivial one, as it is often found that smaller particles lead to harder tablets (Eriksson and Alderborn, 1995; Di Martino et al., 2000).

The mean yield pressure, decreased in the order ASN>MSN>DSN>CSN>TSN. Thus, in general, it is possible to conclude that the plastic deformation increases with increasing the hydration. In addition, CSN shows higher plasticity than DSN that can explain its better tabletability.

The very high plastic deformability of TSN added to the very low elastic recovery can explain the very good tabletability of TSN. The elastic recovery decreased in the order ASN>MSN>DSN≈CSN>TSN.

VII. CONCLUSIONS

CONCLUSIONS

Drug substance exposure to water during several pharmaceutical operations or storage, is of great relevance because it can cause changes in the crystal lattice. The structural changes related to the hydration/dehydration process can strongly affect the technological performance, the bioavailability and the drug stability.

In light of this well-known evidence, structural changes associated with hydration/drying processes must be carefully evaluated during the preformulation and formulation studies.

Sodium naproxen (sodium salt of (S)-(+)-6-methoxy-α-methyl-2-naphtalenacetic acid) is a drug belonging to the class of aryl propionic acid derivatives (APADs) of non-steroidal anti-inflammatory drugs (NSAIDs).

Despite being a well-known drug, it has only recently been revealed that it can exist in several hydrated forms, when exposed to humid air. Sodium naproxen exists in one anhydrous form (ASN) and four hydrated ones: one monohydrate (MSN), two dehydrate (DSN; CSN) and one tetrahydrate (TSN).

ASN (the commercialised form) can be differently hydrated or dehydrated according to the vapour pressures during storage and pharmaceutical processing.

During this study, the influence of the solid state properties on the technological performance of sodium naproxen in its different hydrate forms was examined. It was observed that changes in the experimental procedures of technological processes or storage conditions may affect the physico-chemical stability of SN hydrate forms.

In conclusion:

- It was demonstrated that technological processes such as wet-granulation/drying procedures can strongly influence the crystallographic form of SN. In fact, when subjected to wet granulation in a high-shear mixer-granulator, ASN undergoes hydration to the tetrahydrated form. Subsequently, performing two different drying

procedures lead to granules in which SN has varying degrees of hydration, with significant consequences for granule characteristics and tableting performance.

- Differences in compression behaviour of SN forms were observed and have been ascribed to the hydration degree. The behaviour under compression revealed that one of the granules batches presented the best tabletability and compressibility. Therefore, the behaviour of the active raw material (granules) under compression has been examined at different hydration degrees. Compression behaviour increases with the degree of hydration, a phenomenon that could be attributed either to differences in the crystallographic structures of sodium naproxen, or to water content. This phenomenon was considered in depth by examining the behaviour under compression of different hydrated forms of sodium naproxen.

- It was clearly shown that, the hydration degree considerably changes the compression behaviour of SN. The insertion of the water molecule into the crystal modifies the tabletability, compressibility and compactibility of SN. However, the effect is not always proportional to water content. The complex evolution of tabletability, which is the main property for the industrial production of tablets, has been explained by considering the evolution of both compressibility and compactibility. It has been supposed that water penetration into the crystal is localised in the periphery. The kinetic study, explaining how water enters into the crystal, offers a better understanding of why the hydrated forms of SN show better tabletability than the anhydrous one.

- Models for the hydration kinetics of ASN at 55% and 86% RH, corresponding to the formation of the dihydrated and tetrahydrated forms respectively, were evaluated assuming Eyring's dependence on temperature. Kinetic data is consistent with a model where water molecules enter the crystal preferentially along hydrophilic tunnels existing in the crystal structure and corresponding to the propionate side chain. Water inclusion perturbs the crystallographic structure,

causing slight structural changes according to the amount and associated to an increase in entropy. The interposition of water molecules between SN molecules weakens intermolecular bonds, and these sites can behave like sliding planes under compression. Such structural changes may explain the improved compression behaviour and modified densification propensity mechanism. Kinetic data, describing the water hydration mechanism of ASN, explain in an original way the improved tableting and densification properties under hydration.

- The isothermal dehydration of some of SN hydrates was observed by thermogravimetry at several temperatures and it was clarified the dehydration mechanism. Multi-step mechanisms for the dehydration process are proposed for all the hydrated forms analyzed. Different models are identified to describe the dehydration process, indicating either diffusion or boundary reaction mechanisms, according to the lattice structure and the translational freedom degrees of the water molecules. SN dehydration promotes changes in the crystallographic structures of the samples, as proven by XRPD, and transitions from the hydrated phases to the dehydrated ones, depending on the experimental temperatures.

- The technological and mechanical properties of several solid forms of SN were investigated. Particular attention has been made in order to reduce differences, among the samples, in crystal habit, particle size and distribution, amount of absorbed water, so that only the hydration degree and the crystalline structure might affect the technological behaviour of powders. Thus, the compression behaviours were determined by using an instrumented single punch tablet machine and evaluated through the tabletability, compressibility and compactibility analysis. The results showed that the compression ability was influenced by the hydration degree and the crystalline form, and in general the tabletability was mainly due to the ability of particles to close up by establishing numerous bonds. Also, it was reported the effect of water inclusion in the crystal lattice and the effect of crystalline structure on the compression behaviour of sodium naproxen.

- MSN, DSN and TSN have been considered as tunnel hydrates. These tunnel hydrates are characterized by the presence of an increased water amount that fills the tunnel. In these structures, it is possible to assume the presence of some water molecules directly bound to the SN molecule through hydrogen bonds. These water molecules are rather strongly bound to the SN molecule, fact that limits their mobility. As far as the water content increases, further water molecules penetrate into the tunnel establishing new hydrogen bonds with neighboring water molecules. Since these latest water molecules are more distant from the SN molecule, they are more mobile and create quite movable layers. This behaviour has been proposed to explain the improvement in tabletability when the water content increases from the MSN up to TSN. The movable layers filled by the water molecules are more and more deformable as water molecules increase behaving as sliding planes.

- Several considerations have emerged concerning the CSN. In particular, it is necessary to highlight the very good tabletability of CSN with respect to the DSN. As previously explained, while the DSN can be considered as a tunnel hydrate because it is formed during a progressive inclusion of water molecules inside the crystals, the CSN crystallizes from water and SN crystal grows up while it includes and bounds in the crystalline structure the water molecules. It is possible to assume that this mechanism gives rise to a structure completely different from that described for the tunnel hydrate.

Finally, it should be kept in mind that water exposure during storage or pharmaceutical processing can cause changes in the crystal lattice of the SN starting material and the hydration state of SN may strongly influence its physico-chemical and technological properties and consequently its bioavailability and its stability.

Therefore, a complete understanding and characterisation of SN solid state and phase transitions throughout storage or processing are important in predicting and defining its technological performance. In depth knowledge of hydrated forms and their stability

under different experimental conditions are essential to the development of successful drug products.

From an industrial point of view, changes in process variables (equipment, excipient characteristics and their amount, and process parameters) must be carefully evaluated, in order to validate the processes in use and reduce risks of lot-to-lot variability.

The results of this work are relevant to industrial practice as they can orient choice towards the most appropriate form of sodium naproxen as a raw material for industrial tablet production and support the preparation of tablets by direct compression at lower cost and with improvements in biopharmaceutical properties.

ACKNOWLEDGEMENTS

I am sincerely grateful to my supervisor, Prof. Piera Di Martino, for her invaluable guidance, help and support throughout the course of this study. Thank you for the dedicated time, patience and enthusiasm. Without your continuous encouragement this work would not have been possible. Thank you for inviting me to this interesting journey into the study of pharmaceutical technology and helping me along the way.

I wish to express my warmest gratitude for our late colleague, Prof. Etienne Joiris. I will miss our long talks. His valuable comments and great experience helped me during the part of the study carried out at the University of Lille, France.

I want to appreciate the friendship over the last years of all the colleagues and friends of the Chemical Sciences Department (University of Camerino) that made me feel always at home.

Special thanks belong to my colleagues at the Department of Pharmacy, University of Tirana for supporting and encouraging me towards the fulfilment of the PhD studies. I wish to thank in particular Prof. Besnik Jucja for his positive view on all aspects of life and for his friendship.

I would like to thank the staff at the Department of Galenic and Hospital Pharmacy, University of Lille, for welcoming me to the Department and to France. Special gratitude belongs to Prof. Christine Barthélémy and to Prof. Pascal Odou.

MURST (Ministero dell'Università e della Ricerca Scientifica e Tecnologica, Italy) and MASH (Ministry of Education of Albania) are acknowledged for their financial support.

I would like to express particular gratitude to Prof. Gianfrancesco Berchiesi for his kind help in the discussion of the results.

Mrs Sheila Beatty (University of Camerino, Italy) and Mrs Alexandra Tavernier (M.A. University of Glasgow, University of Lille, France) are gratefully thanked for their help in revising the English manuscript.

Many thanks go to Prof. Stavros Malamataris, Head of the Department of Pharmaceutical Technology, School of Pharmacy, Aristotle University of Thessaloniki for having accepted with pleasure to join my thesis presentation and to be part of the final examination commission.

My warmest thanks belong to my beloved parents and brother for their loving support and encouragement. The warm support of my family-in-law is heartily acknowledged, as well.

Finally, I want to thank my dear wife and son. Ela and Anri, thank you for always being there for me and for bringing so much joy into my life.

LIST OF FIGURES

LIST OF TABLES

REFERENCES

1. Adeyeye CM; Rowley J; Madu D; Javadi M; Sabnis SS. **1995**. Evaluation of crystallinity and drug release stability of directly compressed theophylline hydrophilic matrix tablets stored under varied moisture conditions. Int. J. Pharm. 116**,** 65-75.

2. Agbada CO; York P. **1994.** Dehydration of theophylline monohydrate powder-effects of particles size and. sample weight. Int. J. Pharm. 106, 33-40.

3. Airaksinen S; Luukkonen P; Jørgensen A; Karjalainen M; Rantanen J; Yliruusi J. **2003.** Effects of excipients on hydrate formation in wet masses containing theophylline. J. Pharm. Sci. 92(3), 516-528.

4. Airaksinen S; Karjalainen M; Räsänen E; Rantanen J; Yliruusi J. **2004**. Comparison of the effect of two drying methods on polymorphism of theophylline. Int. J. Pharm. 276, 129-141.

5. Airaksinen S; Karjalainen M; Shevchenko A; Westermarck S; Leppänen E; Rantanen J; Yliruusi J. **2005.** Role of water in the physical stability of solid dosage formulations. J. Pharm. Sci. 94, 2147-2165.

6. Alderborn G; Nyström C. **1982**. Studies on direct compression of tablets. IV. The effect of particle size on the mechanical strength of tablets. Acta Pharm. Suec. 19, 381-390.

7. Allen PV; Rahn PD; Sarapu AC; Vanderwielen AJ. **1978.** Physical characterization of erythromycin: anhydrate, monohydrate and dihydrate crystalline solids. J. Pharm. Sci. 67, 1087-1093.

8. Ando H; Ishii M; Kayano M; Ozawa. **1992.** Effect of moisture on crystallization of theophylline in tablets. Drug Dev. Ind. Pharm. 18(4), 453-467.

9. Armstrong NA; Haines-Nutt RF. **1974**. Elastic recovery and surface area changes in compacted powder systems. Powder Technol. 9, 287-290.

10. Bechtloff B; Nordhoff S; Ulrich J. **2001.** Pseudopolymorphs in industrial use. Cryst. Res. Technol. 36, 1315–1328.

11. Betz G; Bürgin PJ; Leuenberger H. **2003**. Power consumption profile analysis and tensile strength measurments during moist agglomeration. Int. J. Pharm. 252, 11-25.

12. Borka L; Haleblian JK. **1990**. Crystal polymorphism of pharmaceuticals. Acta Pharm. Jugosl. 40, 71–94.

13. Byrn SR. **1982.** Solid-State Chemistry of Drugs, Academic Press, New York.

14. Byrn SR; Pfeiffer RR; Stowell JG. **1999.** Solid-State Chemistry of Drugs, SSCI, West Lafayette, IN.

15. Cabri W; Ghetti P; Alpegiani M; Pozzi G; Justo-Erbez A; Pérez-Martínez JI; Villalón-Rubio R; Monedero-Perales MC; Munoz-Ruiz A. **2006**. Cefdinir: a comparative study of anhydrous vs. monohydrate form. Microstructure and tableting behaviour. Eur. J. Pharm. Biopharm. 64, 212-221.

16. Carr RL. **1965a**. Evaluating flow properties of solids. Chem. Eng. 72, 163-168.

17. Carr RL. **1965b**. Classifying flow properties of solids. Chem.Eng. 72, 69-72.

18. Carstensen JT; Morris T. **1993.** Chemical stability of indomethacin in the solid amorphous and molten states. J. Pharm. Sci. 82, 657 – 659.

19. Cox J S G; Woodard GD; McCrone WC. **1971.** Solid-state chemistry of cromolyn sodium (disodium cromoglycate). J.Pharm. Sci. 60(10), 1458-1465.

20. Cui Y. **2007.** A material science perspective of pharmaceutical solids. Int. Journal of Pharm. 339, 3-18.

21. Dawoodbhai S; Rhodes CT. **1989**. The effect of moisture on powder flow and on compaction and physical stability of tablets. Drug Dev. Ind. Pharm. 15, 1577-1600.

22. Di Martino P; Di Cristofaro R; Barthélémy C; Joiris E; Palmieri GF; Martelli S. **2000.** Improved compression properties of propyphenazone spherical crystals. Int. J. Pharm. 197, 95-106.

23. Di Martino P; Barthélémy C; Palmieri GF; Martelli S. **2001**. Physical characterization of naproxen sodium hydrate and anhydrate forms. Eur. J. Pharm. Sci. 14, 293-300.

24. Di Martino P; Barthélémy C; Joiris E; Capsoni D; Masic A; Massarotti V; Gobetto R; Martelli S; Bini M. **2007**. A new tetrahydrated form of sodium naproxen. J. Pharm. Sci. 96, 156-167.

25. Di Martino P; Censi R; Barthélémy C; Gobetto R; Joiris E; Masic A; Odou P; Martelli S. **2007**. Characterization and compaction behaviour of nimesulide crystal forms. Int. J. Pharm. 342, 137-144.

26. Doelker E. **1994**. Assessment of powder compaction. In: Chulia D; Deleuil M; Pourcelot Y. (Eds.) Powder technology and pharmaceutical process. Elsevier, Amsterdam. 403-471.

27. Dong Z; Salsbury JS; Zhou D; Munson EJ; Schroeder SA; Prakash I; Vyazovkin S; Wight CA; Grant DJW. **2002.** Dehydration kinetics of neotame monohydrate. J. Pharm. Sci. 91, 1423-1431.

28. Dreu R; Širca J; Pinte-Hodi K; Burjan T; Planinšek O; Srčič S. **2005**. Physicochemical properties of granulating liquids and their influence on microcrystalline cellulose pellets obtained by extrusion-spheronisation technology. Int. J. Pharm. 291, 99-111.

29. Duddu SP; Das NG; Kelly TP; Sokoloski TD. **1995.** Microcalorimetric investigation of phase transitions: I. Is water desorption from theophylline HOH a single-step process? Int. J. Pharm. 114, 247-256.

30. Dzidic I; Kebarle P. **1970.** Hydration of Alkali Ions In Gas Phase - Enthalpies and Entropies of Reactions $M+(H_2O)N-1+H_2O = M+(H_2O)N$. Journal of Physical Chemistry. 74(7), 1466.

31. Ebube NK; Hikal AH; Wyandt CM; Beer DC; Miller LG; Jones AB. **1997**. Effect of drug, formulation and process variables on granulation and compaction characteristics of heterogeneous matrices. Part 1: HPMC and HPC systems. Int. J. Pharm. 156, 49-57.

32. European Pharmacopoeia 5^{th} Edition. **2006.** Supplement 5.3

33. Falk M; Knop O. **1973.** Water, A Comprehensive Treatise. Plenum Press, New York. 2, 55-113.

34. Fell JT; Newton JM. **1970**. Determination of tablet strength by the diametral-compression test. J. Pharm. Sci. 5, 688-691.

35. Florey K. **1973.** Cephradine. In Analytical Profiles of Drug Substances, Florey, K., Ed. Academic Press: New York. 2, 1-62.

36. Gandhi R; Pillai O; Thilagavathi R; Gopalakrishnan B; Kaul CL; Panchagnula R. **2002.** Characterization of Azithromycin hydrates. Eur. J. Pharm. Sci. 16(3), 175-184.

37. Giron D. **1995.** Thermal analysis and calorimetric methods in the characterization of polymorphs and solvates. Thermochim. Acta. 248, 1–59.

38. Guillory KJ. **1999.** Generation of polymorphs, hydrates, solvates, and amorphous solids, in: Brittain H.G. (Ed.), Polymorphism in Pharmaceutical Solids, Marcel Dekker, New York. 95, 183–226.

39. Haleblian J; McCrone W. **1969.** Pharmaceutical applications of polymorphism. J. Pharm. Sci. 58, 911-929.

40. Haleblian JJ. **1975.** Characterization of habits and crystalline modification of solids and their pharmaceutical applications. Pharm. Sci. 64, 1269-1288.

41. Han J; Suryanarayanan R. **1998.** Influence of environmental conditions on the kinetics and mechanism of dehydration of carbamazepine dihydrate. Pharm. Dev. Technol. 3, 587-596.

42. Harrington PJ; Lodewijk E. **1997.** Twenty years and naproxen technology. Org. Proc. Res. & Dev. 1, 72-76.

43. Hausman DS, Thomas Cambron R, Sakr A. **2005**. Application of on-line Raman spectroscopy for characterizing relationship between drug hydration state and tablet physical stability. Int. J. Pharm. 299, 19-33.

44. Heckel RW. **1961**. Density-pressure relationships in powder compaction. Trans. Metall. Soc. AIME. 221, 661-675.

45. Herman J; Remon JP; Visavarungroj N; Schwartz JB; Klinger GH. **1988.** Formation of thephylline monohydrate during the pelletisation of microcrystalline cellulose-anhydrous theophylline blends. Int. J. Pharm. 42, 15-18.

46. Herman J; Visavarungroj N; Remon JP. **1989.** Instability of drug release from anhydrous theophylline-microcrystalline cellulose formulations. Int. J. Pharm. 55, 143-146.

47. Holm P. **1997**. High shear mixer granulators. In: Parikh DM, editor. Handbook of pharmaceutical granulation technology. New York: Marcel Dekker. 151-204.

48. Joiris E; Di Martino P; Berneron C; Guyot-Hermann A-M; Guyot, JC. **1998**. Compression behaviour of orthorhombic paracetamol. Pharm. Res. 15, 1122-1130.

49. Jørgensen A; Rantanen J; Karjalainen M; Khriachtchev L; Räsänen E; Yliruusi, J. **2002.** Hydrate formation during wet granulation studied by spectroscopic methods and multivariate analysis. Pharm. Res. 19, 1285-1291.

50. Juslin MJ; Paronen TP. **1980**. On the accuracy of displacement measurements by instrumented single-punch machine. J. Pharm. Pharmacol. 32, 796-798.

51. Khankari RH; Grant DJW. **1995**. Pharmaceutical hydrates. Thermochim. Acta. 248, 61-79.

52. Khankari R; Chen L; Grant DJW. **1998.** Physical characterization of nedocromil sodium hydrates. J. Pharm. Sci. 87, 1052–1061.

53. Kim YB; Song HJ; Park IY. **1987**. Refinement of the structure of (+)-6-methoxy-a-methyl-2-naphtalenecetic acid. Arch. Pharm. Res. 10, 232.

54. Kim YB; Park IY; Lah WR. **1990**. The crystal structure of naproxen sodium, ($C_{14}H_{13}O_3Na$), a Non-Steroidal Antiinflammatory Agent. Arch. Pharm. Res. 13, 166-173.

55. Kim YS; Rousseau RW. **2004**. Characterization and solid-state transformations of the pseudopolymorphic forms of sodium naproxen. Crystal Growth and Design. 4, 1211-1216.

56. Kim YS; VanDerveer D; Wilkinson AP; Rousseau RW. **2004**. Anhydrous sodium naproxen, Acta Crystallogr. 60, 419-420.

57. Kim YS; Paskow HS; Rousseau RW. **2005**. Propagation of solid-state transformations by dehydration and stabilization of pseudopolymorphic crystals of sodium naproxen. Crystal Growth Des. 5, 1623 – 1632.

58. Kim YS. **2005**. Crystallization and solid-state transformations of the pseudopolymorphic forms of sodium naproxen, Ph.D. Thesis, Georgia Institute of Technology, Atlanta.

59. Kojima T; Onoue S; Katoh F; Teraoka R; Matsuda Y; Kitagawa Sh; Tsuhako M. **2007.** Effect of spectroscopic properties on photostability of tamoxifen citrate polymorphs. Int. J. Pharm. 336(2), 346-351.

60. Kojima T; Yamauchi Y; Onoue S; Tsuda Y. **2008.** Evaluation of hydrate formation of a pharmaceutical solid by using diffuse reflectance infrared Fourier-transform spectroscopy. J. Pharm. Biomed. Anal. 46(4), 788-791.

61. Kojima T; Katoh F; Matsuda Y; Teraoka R; Kitagawa S. **2008.** Physicochemical properties of tamoxifen hemicitrate sesquihydrate. Int. J. Pharm. 352, 146-151.

62. Kontny MJ; Zografi G. **1995**. Sorption of water by solids, in: H.G. Brittain (Ed.), Physical characterization of pharmaceutical solids, Marcel Dekker, New York. 387-418.

63. Kuhnert-Brandstatter M. **1971.** Thermomicroscopy in the Analysis of Pharmaceuticals, Pergamon, Oxford.

64. Lazghab M; Saleh K; Pezron I; Guigon P; Komunjer L. **2005**. Wettability assessment of finely divided solids. Powder technol. 157, 79-91.

65. Lerk CF; Zuurman K; Kussendrager K. **1983.** Effect of dehydration on the binding capacity of particulate hydrates, J. Pharm. Pharmacol. 36, 399.

66. Leuenberger H. **1982**. Granulation, new techniques. Pharma Acta Helv. 57, 72-82.

67. Malamataris S; Goidas P; Dimitriou A. **1991**. Moisture sorption and tensile strength of some tableted direct compression excipients. Int. J. Pharm. 68, 51-60.

68. Martindale. **2005**. The complete drug reference. The Pharmaceutical Press.

69. Morris KR; Rodriguez-Hornado N. **1993.** Hydrates, in Encyclopedia of Pharmaceutical Technology, Marcel Dekker, New York. Vol. 7.

70. Morris KR. **1999.** Structural Aspects of Hydrates and Solvates. Polymorphism in Pharmaceutical Solids. H. G. Brittain. New York, Marcel Dekker, Inc. 95, 126-179.

71. Morris KR; Griesser UJ; Eckardt CJ; Stowell JG. **2001.** Theoretical approaches to physical transformations of active pharmaceutical ingredients during manufacturing processes. Adv. Drug Dev. Rev. 48, 91-114.

72. Newitt DM; Conway-Jones JM. **1958**. A contribution to the theory and practise of granulation. Trans Inst. Chem. Eng. 36, 422-442.

73. Nyström C; Karehill PG. **1996**. The importance of intermolecular bonding forces and the concept of bonding surface area. In: Alderborn G; Nyström C. (Eds.) Pharmaceutical powder compaction technology. Marcel Dekker, New York. 17-53.

74. Oberholtzer ER; Brenner GS. **1979.** Cefoxitin sodium: solution and solid-state chemical stability studies. J. Pharm. Sci. 68, 863 – 866.

75. Otsuka M; Teraoka R; Matsuda Y. **1991.** Physicochemical stability of nitrofurantoin anhydrate and monohydrate under various temperature and humidity conditions. Pharm. Res. 8(8), 1066-1068.

76. Otsuka M; Matsumoto T; Higuchi S; Otsuka K; Kaneniwa N. **1995.** Effects of compression temperature on the consolidation mechanism of chlorpropamide polymorphs. J. Pharm. Sci. 84, 614-618.

77. Otsuka M; Hasegawa H; Matsuda Y. **1997**. Effect of polymorphic transformation during the extrusion-granulation process on the pharmaceutical properties of carbamazepine granules. Chem. Pharm. Bull. 45, 894-898.

78. Otsuka M; Hasegawa H; Matsuda Y. **1999.** Effect of polymorphic forms of bulk powders on pharmaceutical properties of carbamazepine granules. Chem. Pharm. Bull. 47(6), 852-856.

79. Paronen P; Ilkka J. **1996**. Porosity-pressure functions. In: Alderborn G; Nyström C. (Eds.) Pharmaceutical powder compaction technology. Marcel Dekker, New York. 55-75.

80. Pont V; Saleh K; Steinmetz D; Hémati M. **2001**. Influence of the physicochemical properties on the growth of solid particles by granulation in fluidized bed. Powder Technol. 120, 97-104.

81. Ravikumar K; Rajan SS; Pattabhi V. **1985**. Structure of naproxen, $C_{14}H_{14}O_3$, Acta Cryst. 41, 280-282.

82. Rodrıguez-Hornedo N; Lechuga-Ballesteros D; Wu HJ. **1992.** Phase transition and heterogeneous/epitaxial nucleation of hydrated and anhydrous theophylline crystals. Int. J. Pharm. 85, 149–162.

83. Rondeau X ; Affolter C ; Komunjer L ; Clausse D; Guigon P. **2003**. Experimental determination of capillary forces by crushing strength measurements. Powder Technol. 130, 124-131.

84. Ryshkewitch E. **1953**. Compression strength of porous sintered aluminia and zirconia. J. Am. Cer. Soc. 36, 65-68.

85. Sakata Y; Shiraishi S; Otsuka M. **2004.** Characterization of dehydration behavior of untreated and pulverized creatine monohydrate powders. Colloids and Surfaces B: Biointerfaces. 35, 185-191.

86. Saleh K; Vialatte L; Guigon P. **2005**. Wet granulation in a batch high shear mixer. Chem. Eng. Sci. 60, 3763-3775.

87. Šesták J; Gunnar B. **1971**. Kinetics of the mechanism of solid-state reactions at increasing temperature. Thermochim. Acta. 3, 1-12.

88. Shalaev EY; Shalaeva M; Byrn SR; Zografi G. **1997.** Effects of processing on the solid-state methyl transfer of tetraglycine methyl ester. Int. J. Pharm. 152, 75 – 88.

89. Sharp JH; Brindley GW; Achar BNN. **1963.** Numerical data for some commonly used solids-state reaction equations. J. Am. Ceram. Soc. 52, 781-791.

90. Shefter E; Highuchi T. **1963.** Dissolution behavior of crystalline solvated and non-solvated forms of some pharmaceuticals. J. Pharm. Sci. 52(8), 781-791.

91. Sheng J; Venkatesh GM; Duddu SP; Grant DJW. **1999.** Dehydration behavior of eprosartan mesylate dehydrate. J. Pharm. Sci. 88, 1021–1029.

92. Simons SJR; Rossetti D; Pagliai P; Ward R; Fitzpatrick S. **2004**. Predicting the performance of granulation binders through micro-mechanistic observations. Powder Technol. 140, 280-289.

93. Stahl HP. **1980.** The Problems of Drug Interactions with Excipients. In: Braimar, D.D. (Ed.), Towards Better Safety of Drugs and Pharmaceutical Products. Biomedical press, Elsevier/North Holland. 265–280.

94. Sukenik CN; Bonapace JAP; Mandel NS; Bergman RG; Lau; Wood G. **1975.** Enhancement of a chemical reaction rate by proper orientation of reacting molecules in the solid state. Am. Chem. Soc. 97, 5290 – 5291.

95. Sun C; Grant DJW. **2001a**. Effects of initial particle size on the tableting properties of L-lysine monohydrochloride dihydrate powder. Int. J. Pharm. 215, 221-228.

96. Sun C; Grant DJW. **2001b**. Influence of crystal structure on the tableting properties of sulfamerazine polymorphs. Pharm. Res. 18, 274-280.

97. Sun C; Grant DJW. **2004**. Improved tableting properties of p-hydroxybenzoic acid by water of crystallization: a molecular insight. Pharm. Res. 21, 382-286.

98. Taylor LS; York P. **1998.** Effect of particle size and temperature on the dehydration kinetics of trehalose dehydrate. Int. J. Pharm. 167, 215-221.

99. Threlfall TL. **1995.** Analysis of organic polymorphs- a review. Analyst. 120, 2435-2460.

100. United States Pharmacopeia 27th Edition. **2004.**

101. Wong DYT; Wright P; Aulton ME. **1988**. The deformation of alpha-lactose monohydrate and anhydrous alpha-lactose monocrystals. Drug Dev. Ind. Pharm. 14, 2109-2126.

102. Wöstheinrich K and Schmidt PC. **2001.** Polymorphic changes of thiamine hydrochloride during granulation and tableting. Drug Dev. Ind. Pharm. 27(6), 481-489.

103. Zhang D; Flory JH; Panmai S; Batra U; Kaufman MJ. **2002**. Wettability of pharmaceutical solids: its measurement and influence on wet granulation. Colloids and Surfaces. 206, 547-554.

104. Zhu H; Yuen C; Grant DJW. **1996.** Influence of water activity in organic solvent + water mixtures on the nature of the crystallizing drug phase. 1. Theophylline. Int. J. Pharm. 135, 151-160.

105. Zhu H; Padden BE; Munson EJ; Grant DJW. **1997.** Physiochemical characterization of nedocromil bivalent metal salt hydrates. 2. Nedocromil Zinc. J. Pharm. Sci. 86, 418-428.

106. Zhu H; Grant DJW. **2001.** Dehydration behavior of nedocromil magnesium pentahydrate. Int. J. Pharm. 215(1-2), 251-262.

107. Zhu H; Jia X; Peter V; Stacey L; Chris K. **2001.** Dehydration, hydration behavior, and structural analysis of fenoprofen calcium. J. Pharm. Sci. 90(7), 845-859.

108. Zografi G. **1988**. States of water associated with solids. Drug Dev. Ind. Pharm. 14, 1905-1926.

LIST OF ORIGINAL PUBLICATIONS (JANUARY 2006-JANUARY 2009)

PUBLICATIONS RELATED TO THE STUDY OF SODIUM NAPROXEN

Joiris E; Di Martino P; **Malaj L;** Censi R; Barthélémy C; Odou P. **2008.** Influence of crystal hydration on the mechanical properties of sodium naproxen. Eur. J. Pharm. Biopharm. 70 (1), 345-356.

Di Martino P; **Malaj L;** Censi R; Martelli S. **2008.** Physico-chemical and technological properties of sodium naproxen granules prepared in a high-shear mixer-granulator. J. Pharm. Sci. 97 (12), 1-11.

Malaj L; Di Martino P. **2007.** Technological analysis of naproxen sodium crystals. UNIEL Bul. Shk. 2007/1. XI(4), 59-74.

Joiris E †; **Malaj L;** Delaruelle O; Barthélémy C; Odou P; Censi R; Di Martino P. **2008.** Effect of water uptake on compression behaviour of sodium naproxen. In Proceeding: 6th World Meeting on Pharmaceutics Biopharmaceutics and Pharmaceutical Technology Barcelona, Spain.

Di Martino P; **Malaj L;** Barthelemy C; Martelli S. **2006.** Hydration of anhydrous naproxen sodium: a new tetrahydrated form. In Proceeding: 5th Word Meeting. P.B.P.T., Geneva.

Di Martino P; **Malaj L;** Martelli S. 2006. Effect on technological properties as a consequence of the change in crystalline structure of anhydrous naproxen sodium subjected to the liquid granulation. In Proceeding: 5th Word Meeting. P.B.P.T.,Geneva.

Di Martino P; **Malaj L;** Barthelemy C; Joiris E; Capsoni D; Massarotti V; Bini D; Martelli S. 2006. Dehydration of naproxen sodium. In Proceeding: 5th Word Meeting. P.B.P.T., Geneva.

OTHER PUBLICATIONS

Di Martino P; **Malaj L;** Joiris E; Cespi R; Barthélémy C; Martelli S. **2007.** The role of several L-HPCs in preventing tablet capping during direct compression of metronidazole. Drug Dev. Ind. Pharm. 33(12), 1308 – 1317.

Hoti E; Censi R; Ricciutelli R; **Malaj L;** Barboni L; Martelli S; Valleri M; Di Martino P. **2008.** Validation of an HPLC-MS method for rociverine tablet dissolution analysis. J. Pharm. Biomed. Anal. 47, 422-428.

Di Martino P; Censi R; **Malaj L;** Capsoni D; Massarotti V; Martelli S. **2007.** Influence of solvent and crystallization method on the crystal habit of metronidazole. Crystal Res. Tech. 42(8), 800-806.

Di Martino P; Cespi R; **Malaj L;** Joiris E; Barthélémy C; Martelli S. **2007.** Influence of metronidazole particle properties on granules prepared in a high shear mixer-granulator. Drug Dev. Ind. Pharm. 33, 121-131.

Malaj L; Censi R; Di Martino P. **2008.** Stability prediction of nicergoline and cabergoline amorphous forms by calculation of the mean relaxation time constant. In Proceeding: 6th World Meeting on Pharmaceutics Biopharmaceutics and Pharmaceutical Technology Barcelona, Spain.

Malaj L; Clementi S; Di Martino P. **2008.** Study of the feasibility of protein release systems: analysis of the influence of swelling mechanism on dissolution profile. In Proceeding: 6th World Meeting on Pharmaceutics Biopharmaceutics and Pharmaceutical Technology Barcelona.

Malaj L; Censi R; Di Martino P. **2008**. Evaluation of physical dispersions of cabergoline and nicergoline in poly(vinylpyrrolidone). In Proceeding: 6th World Meeting on Pharmaceutics Biopharmaceutics and Pharmaceutical Technology Barcelona, Spain.

Censi R; **Malaj L;** Di Martino P. **2008.** Effect effect of several amorphous polymers on nimesulide amorphous form stability. In Proceeding: 6th World Meeting on Pharmaceutics Biopharmaceutics and Pharmaceutical Technology Barcelona, Spain.

Censi R; **Malaj L;** Di Martino P. **2008.** Comparison of properties of ketoprofen and flurbiprofen at their amorphous state. In Proceeding: 6th World Meeting on Pharmaceutics Biopharmaceutics and Pharmaceutical Technology Barcelona, Spain.

Hoti E; Censi R; Ricciutelli M; **Malaj L;** Barboni L; Valleri M; Di Martino P. **2008.** Development and validation of a RP-HPLC/ESI-MS method for rociverine tablet dissolution analysis. In Proceeding: 6th World Meeting on Pharmaceutics Biopharmaceutics and Pharmaceutical Technology Barcelona, Spain.

Anniballi E; **Malaj L;** Censi R; Valleri M; Di Martino P. **2008.** A new formulation for the industrial direct compression of a high dosage active ingredient. In Proceeding: 6th World Meeting on Pharmaceutics Biopharmaceutics and Pharmaceutical Technology Barcelona, Spain.